Construction and Post-Construction Deformation Analysis of an MSE Wall using Terrestrial Laser Scanning and Finite Element Modelling

by

Devon Joseph Adamson

A Thesis submitted to the Faculty of Graduate Studies of

The University of Manitoba

In partial fulfillment of the requirements of the degree of

Master of Science

Department of Civil Engineering

University of Manitoba

Winnipeg, Manitoba

Abstract

Terrestrial Laser Scanning (TLS) is a new technology surveying tool that can collect highly accurate cartesian coordinates of data points surrounding the scanner in a 360° field of view. This technology can be useful in the field of monitoring heavy civil structures, in the case of this research, the settlement of bride interchange abutments.

Two bridge abutments were monitored with TLS, designed with Cast-In-Place (CIP) belled piles and Mechanically-Stabilized Earth (MSE) retaining walls with a segmented precast concrete panel facing system. The foundation was further reinforced with vibration-compacted rockfill columns supporting the approach embankments, which increased the stiffness of the soil and acted as drains to dissipate pore water pressure. The wall facing panels had discernable edges that could easily be identified by the scanner, allowing for a total wall survey rather than the limited discrete location surveying used by traditional methods. Multiple scan surveys were taken along each wall face and were registered together to create a larger Project Point Cloud (PPC). Once PPCs were collected for successive survey dates, point clouds were aligned in the same coordinate system and relative movement was measured. These measurements were then compared against the surveying performed on site by the contractor to observe discrepancies in measured readings.

Once surveying was completed, numerical models were developed with site investigation information and laboratory testing results to compute pore water pressure behaviour and predict foundation settlement using Finite Element Method (FEM) and 3-Dimensional (3D) vertical settlement analysis. Since 2D modelling software was used for FEM to analyze a 3-Dimensional site, discontinuous materials were treated as equivalent material walls using converted plane strain parameters. The 3D vertical settlement analysis retained axisymmetric parameters but required the foundation soil and rockfill columns reinforcement to combine into a single material layer of equivalent stiffness within the reinforced soil zones.

Both surveying and numerical modelling observed the abutments to settle more outside the extents of the bridge deck where there were less columns. The laser scanner had some small deviations in relation to the surveying performed on site and the computed settlements from FEM. It is recommended when using TLS for future research and design projects to include more scans during baseline readings and to include more settlement instrumentation near the end of the reinforcement strips to measure differential settlement effects

Acknowledgements

I would first like to thank my advisor Dr. Marolo Alfaro for his leadership and guidance in conducting my research. Providing all the necessary resources and allowing independent decision making was key to my understanding and growth as a graduate researcher. Not only encouraging our geotech student group to present our research at different conferences but you have also encouraged my study experience in Japan which was a once-in-a-lifetime opportunity. I would also like to thank the rest of my thesis committee Dr. James Blatz and Dr. Sri Ranjan for their contributions and feedback.

I would also like to thank Mr. Kent Bannister from TREK Geotechnical Inc. as he was the lead engineer on the foundation design. He would always find time to answer my inquiries when I had questions on the consulting side. Himself and Dr. Blatz have also been co-authours for my conference publications on my research and their efforts to provide meaningful feedback have been appreciated.

I would like to acknowledge that research was conducted on PCL Contractors' construction site and their cooperation with safety training and communicating schedule updates allowed myself a great opportunity to work on an active construction site.

I would like to thank university's Civil Technical Staff Kerry Lynch for he was instrumental in teaching me how to use the surveying equipment and helping to prepare for every site visit. My site work would not be as successful as it was without this prep work.

Thanks Earl Marvin DeGuzman for all that you have done; assisting my site surveying, bringing awareness to different research aspects, and engaging in different friendly cinema debates. I would like to thank Joash Adajar and Cole Adamson as well for the site monitoring assistance. Dylan Stafford, thanks for listening to me vent about frustrations with laser scanning and the

occasional sauna chat. I would like to thank Irene Ubay, Alitking Anongphouth, and the rest of the geotech gang for sharing laughs and good banter to take breaks from research.

This project was funded through NSERC by the Engage grant to help support the expenses incurred from project and student expenses. The combined efforts from Dr. Alfaro and Mr. Bannister to submit the necessary documents have made this possible. Thank you to all involved.

I would like to thank my parents Jay and Sherri Adamson, and brothers Matthew and Cole Adamson for encouraging myself to pursue graduate studies and providing the support I needed away from the office, even if it was another two years of living in the basement and paying for my groceries.

Thank you to my partner Megan Peterson for she has been there for the good days and bad days that come with research, letting me know that it is worth it in the long run.

Table of Contents

List of Tables

List of Figures

List of Copyrighted Material for Which Permission was obtained

Figure 3-2 – VW Piezometer Install Locations (TREK Geotechnical Inc., 2019)

Figure 3-3 – North Abutment Monitoring Report (TREK Geotechnical Inc., 2019)

Figure 3-4 – South Abutment Monitoring Report (TREK Geotechnical Inc., 2019)

Figure 7-1 – Rod and Level Survey North Abutment Cross-Section Settlement (TREK Geotechnical Inc., 2019)

Figure 7-2 – Rod and Level Survey South Abutment Cross-Section Settlement (TREK Geotechnical Inc., 2019)

Figure 7-3 – Rod and Level Survey North Abutment Settlement Rate Plot (TREK Geotechnical Inc., 2019)

Figure 7-4 – Rod and Level Survey South Abutment Settlement Rate Plot (TREK Geotechnical Inc., 2019)

List of Symbols and Acronyms

TLS	Terrestrial Laser Scanning
CIP	Cast-In-Place
MSE	Mechanically-Stabilized Earth
PPC	Project Point Cloud
FEM	Finite Element Method
RL	Rod and Level
VW	Vibrating Wire
1D/2D/3D	One, Two, or Three Dimensional
TS	Total Station
LiDAR	Light Detection and Ranging
EDM	Electronic Distance Measurement
ARR	Area Replacement Ratio
DISZ	Drain Influenced Soil Zone
PVD	Perforated Vertical Drains
BP	Before Present
ToF	Time of Flight
PS	Phase Shift
TVR	Top View Registration
TR	Target Registration

C2C	Cloud-to-Cloud Registration
UTM	Universal Transverse Meridian
GPS	Global Positioning System
RTK	Real-Time Kinematics
PWP	Pore Water Pressure
E’	Effective Stiffness
V	Poisson’s Ratio
γ’	Effective Unit Weight
SPT	Standard Penetration Test
MCC	Modified Cam Clay
C_c and C_r	Compression Coefficients
κ	Gradient of Swelling Line
λ	Gradient of Compression Line
ESA	Effective Stress Analysis
e	Void Ratio
OCR	Over-Consolidation Ratio
I	Moment of Inertia
k	Hydraulic Conductivity
SCF	Stress Concentration Factor
SRF	Stress Reduction Factor

1 Introduction

1.1 Significance of Deformation Analysis on Bridge Abutments

Mechanically-Stabilized Earth (MSE) retaining walls have become common practice for use in civil construction projects for their versatility in different design applications, in particular for this research in bridge abutments (Federal Highway Administration, 2009). A key contributor to their popularity is a more cost-effective alternative to the reinforced-concrete retaining as cost savings can amount up to 50% of total project cost due to avoiding additional foundation strengthening methods. However cost-savings does not always mean better design as site conditions, drainage, and construction execution can result in greater settlement and deflection of the wall (Harpstead, et al., 2010; MacIntosh & Rrokaj, 2018). This leads to a greater dependence on monitoring during and post-construction wall deformation to ensure performance design criteria is met.

Rod and Level (RL) surveying is the traditional method of measuring MSE wall deformations for its accuracy in measurements and avoiding risk of damage during construction as it is not installed on site. The main drawback with this method is that it measures in discrete locations where an MSE wall can be 100m long, creating gaps in the settlement profile that can otherwise provide important information on the performance of the structure (Oleksuik & Sankey, 2014; Staiger, 2011). TLS has been growing in this field of study as a result.

1.2 Research Hypotheses

The following hypotheses were made for both the surveying and modelling components

1. The laser scanner will scan the walls to measure settlement during and post-construction with a fluctuation tolerance within ±10mm. Most of the errors will come from the post-processing and alignment of the point clouds within a 3D coordinate space. Other contributors will include environmental conditions such as sunlight and traffic, and bounce back error from the laser reflecting off the concrete surface.

2. The surveying performed by TLS will compare with the measurements obtained by the RL to a precision of ±20mm. The RL surveying accuracy is controlled by human error while the TLS has additional errors during post-processing that can be mitigated but not prevented. However, more points collected by the TLS can assist with determining the trend or direction of settlement on between surveyed locations by the RL.

3. The finite element modelling of site conditions can replicate the behaviour or shape of the settlement measured by the performed surveying. However, the 2D modelling will have some discrepancies with the surveying as the abutment is more of a 3D problem. Careful consideration of the assumptions and justification for implementing them will be crucial for interpreting the results.

1.3 Research Objectives

To understand the performance of the MSE wall during construction and post-construction, the following objectives were developed:

1. Determine the measurement performance of TLS and RL during construction and post construction of the MSE wall.

2. Using FEM, develop a model replicating site conditions and determine the theoretical movements associated with each lift of reinforced soil and compare to the TLS results.

The listed objectives will be completed by the following methodologies, explained in further detail within the subsequent chapters.

1. Completed site visits to measure wall deformations during and post construction of the wall using TLS, beginning with the first row of panels and ending the following year. Two scans were performed during construction of the wall, two during the same summer, and two more scans during the following year for post-construction analysis.

2. Determined relative movements of the wall between each successive point cloud. Using FARO Scene point cloud registration software and 3D Reshaper point cloud meshing and manipulation software, point clouds are created and imported into the same 3D coordinate space.

3. Developed FEM numerical models using SIGMA/W component of GeoStudio 2019 will simulate the theoretical movements of the wall.

4. Determined site condition parameters for deformation analysis. Material properties and strength characteristics were found in the TREK Design Report (TREK Geotechnical Inc., 2017). Hydraulic properties were back calculated from hydraulic head graphs obtained in the Monitoring Report (TREK Geotechnical Inc., 2019), measured on site from installed Vibrating-Wire (VW) piezometers.

5. Compare FEM computed results with the 3D vertical settlement analysis. The settlement analysis was carried out using RocScience's Settle3 software for its application of 1D consolidation analysis over an entire site area; computing the each layer's settlement in the 3D model space.

1.4 Organization of Thesis

Chapter 1 outlines the background information on why this research is needed and what questions this research helps to answer. Methodologies were given to provide more clarity on how the main objectives were accomplished. Chapter 2 provides the literature required to understand what research has been done and the different approaches that can be made for this thesis. Literature provided covers background information on MSE walls and how additional foundation reinforcement can influence the settlement behaviour, the different field applications for TLS and why further research is needed for MSE wall monitoring, and how FEM has been applied to numerous civil construction projects and how it can simulate the site conditions into a simplified model.

Chapter 3 contains the necessary information on the site-specific conditions. A summary of the bridge interchange project along with a thorough investigation into the soil conditions on site are given in subsections. Information on the foundation design and installed instrumentation are also presented. Chapter 4 outlines the two different surveying methods used in this research. This chapter details background information on each method, the machine surveying specifications, and how each method will determine the deformations of the wall.

Chapter 5 provides information about FEM and the Geostudio software. Background information on the use of FEM in deformation analysis, the software assumptions for the model, the model parameters obtained from the design report, and the boundary conditions assigned are outlined. Chapter 6 details the setup and parameters used for the 1D consolidation analysis using Settle3. The sections included outline the material properties, geometry of the different soil layers, and the methodology on how the analysis was carried out.

Chapter 7 contains the results of the deformation analysis from both surveying and modelling. Discussion will follow on the differences between surveying methods along with the effective drained conditions (long-term settlement) and the Coupled/Pore Water Pressure (PWP) conditions (settlement with respect to time) from FEM analysis. It will also include the comparison between 1D consolidation analysis with the FEM results. Chapter 8 has concluding remarks and recommendations about future research work in the field of TLS in civil construction projects and how modelling can aid in understanding structure performance.

References and appendices are attached at the end of the thesis.

2 Literature Review

The literature review completed in this chapter will cover previous research related to monitoring of retaining wall structures, the use of TLS in civil engineering and other applications, and the use of FEM for embankment and earth retaining wall structures, primarily converting into a 2D model for simpler analysis.

2.1 Retaining Wall Structure Instrumentation and Monitoring

MSE retaining walls, Figure 2-1, have been used in various applications for structural and geotechnical engineering. These wall structures have become increasingly popular in roadway construction design, specifically highway bridge interchanges, for their ability to withstand large deformations without structural distress. However, deformations have to be determined to check if the structures satisfy serviceability requirements. The advantages also include quick and efficient construction, cost-effectiveness, applicability when space is limited, either Right-of-Way (ROW) constraints from neighbourhood development in the area or existing roadway infrastructure, and over cut slopes (Elias & Christopher, 2001; Hutchinson, 2011).

Settlement is inevitable and can only be reduced, however more cost is added to the project budget when more design alternatives are implemented to reduce settlement. This is especially the case when the structure is built on a soft foundation. Embankment construction on soft clay foundations pose a risk to bridge abutments as too high of total and differential settlements can compromise the integrity of the whole bridge structures. There are insufficient guidelines on allowable settlements for MSE walls as additional foundation improvement is commonly included to limit the settlement (Sankey, et al., 2011).

Bridge abutment monitoring is essential to ensure foundation designs perform to expectations, including settlement, hydraulic, and/or temperature monitoring to name a few (Vankavelarr & Leshchinsky, 2002). Settlement monitoring instrumentation can either be installed on site to

collect continuous data and remain during service life or be installed as reference targets for surveying; used for orientation of the surveying equipment or the measurement point to observe structure settlement. These monitoring equipment can include inclinometers, Vibrating-Wire (VW) piezometers, strain gauges, extensometers, settlement plates, survey level, and total station (Elias & Christopher, 2001; Jiang, et al., 2015; Stuedlein, et al., 2010).

Inclinometer monitoring consists of a plastic casing installed into the MSE walls, close to the back facing wall, and a probe is sent down the pipe taking positional readings every 0.5m on its way down and back up, see Figure 2-2. Baseline measurements are established when the casing is first installed, when it should be standing straight up without pressure on it. Relative movement readings are performed as the wall is built up and once completed, measuring the flex in the casing from lateral earth pressures. Both the top and bottom of the probe measure its tilt at each position in the pipe, down the pipe for readings and up the pipe for correction. This method is popular as it measures the horizontal displacement of the reinforced backfill that can be used to calculate shear band strains, and only requires one person for monitoring (Koerner & Koerner, 2011). However, damage from construction machinery can occur before meaningful data is collected and if lateral earth pressures are too great, the casing can break, requiring replacement.

VW piezometers are an instrument used on site to monitor the pore water pressure changes within the foundation soil or backfill material during construction as seen in Figure 2-3. A tensioned wire within a cable is encased with a porous end to allow water flow access to the wire (Encardo-rite Group, 2020). The tension in the wire relaxes and tightens with the change in pore water pressure, which can then either be downloaded continuously from a data logger or accessed from a readout box. The data collected can provide calibration of foundation hydraulic parameters when pump tests were performed on site (Haggerty & Contreras, 2020). Damage to the equipment is possible, however it is possible to repair and replace if needed.

Settlement plates are a popular displacement monitoring instrument, measuring relative settlements from the foundation surface (Koerner & Koerner, 2011). Plates are installed at a desired monitoring elevation and a steel rod is attached extending up as shown in Figure 2-4. A baseline survey on the top of the pipe is measured and documented for subsequent relative surveys. Fill material is built up and compacted around the pipe, generating adhesive forces between the two materials so they move together when settlement occurs. Routine surveys using the same benchmark are recorded to document the settlement behaviour at the user specified frequency. Many locations can be installed with these plates and does not require expensive or complex technology to measure settlements, however the instrument cannot be replaced if damaged. The errors incurred from surveying, referenced in the total station paragraph, and weak adhesive forces from poor compaction can affect measurement reliability.

Total Station (TS) is a surveying tool that uses lasers to determine a target's cartesian coordinates. Targets can either be a reflective prism placed on a rod or stuck on the structure, or a non-reflective planar surface. This is very similar to the RL method, also a standard tool for surveying, although the TS can determine the 3D coordinates while the former only measures the vertical alignment. Their long range capacity and ability to assemble and demobilize around site allow for minimal interruptions during the construction process. Single target surveys produce smaller data sets and do not require specific knowledge on data processing, resulting in simpler and quicker data processing (Oleksuik & Sankey, 2014). However, when the survey site becomes too large or too complex, additional survey shots and setups can increase errors in measurement. Additional setups incur more orientation error as the survey instrument will reorient itself every relocation, adding millimeters of error to each subsequent survey. Larger survey areas will require the surveyor to provide more detailed illustrations or legends of where each survey was taken, contributing to human error. Redundant surveys are also scarce due to discrete targets and

quality control for each survey is minimal; additional surveys in each area will also double survey duration so priority will govern.

2.2 Terrestrial Laser Scanning

TLS in the field of surveying has been an updated version of the TS as the scanner collects millions of data points in a single survey rather than discrete shots (Oleksuik & Sankey, 2014; Staiger, 2011). It is a relatively new technology that was developed only in 1997 when the first models made available on the market were from United States and Australia based companies, the CYRAX 2200 and the LMS Z210 respectively (Calders, et al., 2015; Staiger, 2011). These scanners are considered part of the “first generation” models where they first had their power externally supplied and could only collect data points at a rate ranging from 1 to 5Hz. Fast forward to the current “fourth generation” models like the FARO Focus X 330 and the Leica RTC360 where they have internal batteries, data point collection rates ranging from 500,000pts/sec to 2,000,000pts/sec, and can measure up to 330m (FARO Technologies Inc., 2013; Leica Geosystems, 2018). The increased collection rates and additional capabilities of these models provide the user with a better understanding of site characteristics to make better informed decisions on future projects.

The colourization of the 3D point space allows for more quality control as the user can explore within the site point cloud, as shown in Figure 2-5. This will decrease the human error associated with mistakes in labelling survey locations, redundancy of target measurements, and possible mishandlings on back-sight measurements for TS orientation. These added benefits do not go without consequence as the user will be required to have a good understanding of the more complex technology to post process and analyze the abundance of data. Surveying with the TS requires one user to direct the machine to the specified target, press the “measure” prompt, and write down the cartesian coordinates in their field book. Using a terrestrial laser scanner requires the user to set up targets around site in an arrangement that will allow the scanner to determine

where it is in space, scan its surroundings, import into the accompanying software, process and register the data, and then the user can analyze the processed data to determine coordinates (FARO Technologies Inc, 2019; Knaak, 2017). The pros and cons of using the TLS for surveying tasks will need to be carefully examined to assess its feasibility for different project situations (Guo, et al., 2019; Laefer & Lennon, 2008). This assessment can be based on a variety of criteria, including but not limited to time, cost, and quality.

Previous literature in the use of TLS has expanded across many different applications since its first introduction in the late 90's. TLS is most effective when a large area of interest is to be surveyed and requires a high level of accuracy in its measurements. Building structure renovations requires scanning internally or externally, picking up dimension detail accurately and the developed 3D point cloud allows the user to walk through the scans to visual the existing structure (Abdul Shukar, et al., 2015; Borodinecs, et al., 2018). This can replace taking a tape measure and/or Electronic Distance Measurement (EDM) to measure dimensions and avoid the human error as previously explained with documentation. The ability to identify precursors and prevent rockfalls is also made possible by routine TLS along high traffic roadways and nearby communities (Fanti, et al., 2013; Kromer, et al., 2015; Kromer, 2017; Kromer, et al., 2017; Lato, et al., 2017). The high level of accuracy in coordinate measurement along with long ranging capabilities allows for TLS to pinpoint critical sections of possible rockfalls along a wide area with successive scan surveys.

TLS can also observe the degradation and deformation of existing structures (Knaak, 2017; Lopez, et al., 2014; McGuire, et al., 2017; Truong-Hong & Laefer, 2014; Yang, et al., 2016). Attention to fine detail and the ability to geo-reference scans for subsequent deformation surveying (less movement expected than rockfall movement) will provide design engineers more information on in-situ performance to better calibrate preliminary project modelling parameters. This technology is not just for the engineering field as crime scene investigators can make use of

its ability to measure objects without disturbing the placement or its orientation (Alhasan, et al., 2016; Barazzetti, et al., 2012; Little, 2018).

In similar projects pertaining to analyzing deformations of MSE wall panels, test parameters were either used in a controlled, non-construction setup or a reduced number of scans were performed. McGuire et. al (2017) performed scanning test on three different wall setups; a lab tested mini-wall, a fully constructed segmented retaining wall, and a fully constructed large block MSE wall. The mini wall setup was a calibration test to determine accuracy of measurements as the wall is manipulated in displacements and tilts. Through sliding, settlement, and lean, the laser scanner was able to accurately measure how the wall was moved, errors given as 0.064in, 0.065in, and 0.22deg respectively. They compared TLS to fitting functions and least squares regression techniques using the full scale walls but only used one or two scans for each wall.

Scotland et. al (2014) had performed scanning programs on two different full-scale geogrid reinforced structures. These structures were both wrapped facing retaining walls and performed one scan during construction of backfill lifts and another one month post-construction. Scanned surveys calculated the amount of horizontal displacement between scan dates. Results found movement around the toe was zero, but gradually got larger displacements as wall height increased, maximum deformations observed to be 0.08m and 0.12m from each wall. The author recommends additional scans in my research site to monitor structure performance and provide more support for measurement accuracy.

Alhasan et al (2016) applied laser scanning to measure deformations of geosynthetic-reinforced soil as part of an integrated bridge system. Deformations from both the east and west abutments were monitored with two different scan dates, the first was after the abutments were constructed, and the other was after the superstructure was constructed but the bridge deck pouring was not completed. Using the initial and final scans, vertical and horizontal deformations were determined in a planar view. Each abutment settled at least 25mm and laterally displaced 7mm, with the west

abutment bulging more in the top half of the wall with a maximum of 9mm. The author concludes by suggesting research be done in to develop an algorithm that can allow the deformation software to identify identical features in paired point clouds at different times. This would automate the deformation process and be more efficient for large sets of point clouds.

2.3 Finite Element Modelling

Numerical modelling of MSE walls are a heavily researched area for their growing use in civil project applications. The ability to model site conditions and calibrate in-situ material index and strength properties, finite element numerical modelling can estimate stress and strain behaviour from embankment construction, and estimate the pore water pressure dissipation over time as each lift of backfill is placed and compacted. In the case of MSE retaining walls for bridge abutments, analyses become complex as the model dimensions are no longer continuous along the embankment and therefore, will be treated as a 3D problem. Furthermore, it may be difficult to analyze complex, 3D oriented foundation reinforcement such as rockfill columns or wick drains. The increased computation time and the complexity of soil-reinforcement interactions may not be as efficient as simplifying the model into a 2D analysis; in some cases the software can only compute in 2D. Several studies were done to determine the method that best translates 3D axisymmetric behaviour into 2D plane strain behaviour in the ground with foundation treatments. Figure 2-6 outlines the unit cells of an axisymmetric drain and the converted plane-strain drain per 1m in depth. Outlined below are different approaches researchers have developed.

2.3.1 Plane Strain Column Thickness Conversion

The theory on converting wall thickness is taking individual columns within the foundation soil and is transformed into an equivalent soil-column wall. Bergado and Long (1994) developed an equation that uses the Area Replacement Ratio (ARR) to account for the area of column in relation to the total amount of soil used for the equivalent wall. The derived equation is as follows:

$$a_S = \frac{A_P}{A_E} = \frac{t_{eq} \times s_y}{s_x \times s_y}$$ Eq. 2-1

Where: a_S = area replacement ratio; A_P = area of pile; A_E = area of soil and column; t_{eq} = equivalent thickness of soil-column wall; s_x = spacing in x-direction; and s_y = spacing in y-direction.

This method involves the amount of soil the column will influence in relation to the rest of the columns whereas the method used by Yapage (2014) as cited in Ariyarathne (2013) compares the area of column to the total area of soil within a strip perpendicular to the embankment seen below:

$$D' = \frac{\pi D^2}{4d}$$ Eq. 2-2

Where D' = equivalent thickness of soil-column wall; D = diameter of columns; d = centre-to-centre spacing in the direction parallel to the embankment.

2.3.2 Plane Strain Strength Conversion

Like the equation developed by Bergado and Long to use the ARR of the influenced soil zone around a column to determine the equivalent thickness of a soil-column wall, that theory can also be applied to determine strength properties of the equivalent wall. Huang et. al (2009) developed an equation to determine the stiffness of the equivalent soil-column wall:

$$E_{eq} = E_c a_s + E_s(1 - a_s)$$ Eq. 2-3

$$c_{eq} = c_c a_s + c_s(1 - a_s)$$ Eq. 2-4

Where: E_{eq}, c_{eq} = equivalent stiffness, cohesion of the soil-column wall; E_c, c_c = stiffness, cohesion of the column; E_s, c_s = stiffness, cohesion of the soil; and a_S = area replacement ratio.

Chan and Poon (2012) have used a similar approach like Ariyarathne (2013) to use a strip of area parallel to the embankment for incorporating the ARR but have applied it to plane strain strength parameters for the stiffness, cohesion, and friction angle. Determining the equivalent friction angle

requires prior knowledge of the stress concentration factor for the columns compared to the surrounding soil. Both equations are provided below:

$$E_{eq}(or\ c_{eq}) = \frac{E_{soil}(or\ c_{soil})A_{soil} + E_{column}(or\ c_{column})A_{column}}{A_{soil} + A_{column}} \quad \text{Eq. 2-5}$$

$$\tan(\varphi_{eq}) = \frac{A_{soil}\tan(\varphi_{soil}) + nA_{column}\tan(\varphi_{column})}{A_{soil} + nA_{column}} \quad \text{Eq. 2-6}$$

where n = stress concentration factor of the column.

Illustrations of the derivation of these equations are provided from Ariyarathne (2013) and is labelled as Figure 2-7 in this document.

One step further, Stewart (1993) determines the proportion of soil to column equivalency by adjusting these parameters using the column's and soil's moment of inertia within the strip of area. This application is best used on a flexible pile/column like rockfill or sand so deep cement mixed columns are not recommended in using this transformation. The equation is given below:

$$E_w = \frac{E_p I_p + E_s I_s}{I_w} \quad \text{Eq. 2-7}$$

Where E_p, I_p = parameters for piles; E_w, I_w = parameters for equivalent wall.

The aforementioned equations were developed for rectangularly spaced columns. Columns spaced triangularly are recommended by Ariyarathne (2013) to be modified, possibly by altering thickness and strength parameters.

2.3.3 Plane Strain Hydraulic Conductivity Conversion

Correctly representing the column influence on foundation soil's hydraulic conductivity in plane strain is decisive for an effective model. Bypassing solid testing of this parameter relies on previous regional testing and may not be accurate for site specific outliers, misrepresenting site conditions. Each transformation is derived from assumptions and depending on the conditions,

can be applicable or not and thus, due diligence must be performed to determine which method applies to the specific site.

Tan and Oo (2005) have developed a method that requires a thorough understanding on soil behaviour of the site. A key assumption made is that the axisymmetric hydraulic conductivity in the vertical direction will remain unchanged when converted to plane strain conditions, as the consolidation rate is mainly influenced by the radial or horizontal dissipation of pore water pressure ($k_{v,pl} = k_{v,ax}$).

$$\frac{k_{h,pl}}{k_{h,ax}} = \frac{F(N)_{pl}}{F(N)_{ax}} \left[\frac{m_{vs}m_{vc}(1-a_s)}{m_{vc}(1-a_s)+ m_{vs}a_s}\right]_{pl} \left[\frac{m_{vc}(1-a_s)+ m_{vs}a_s}{m_{vs}m_{vc}(1-a_s)}\right]_{ax} \frac{B^2}{R^2} \qquad \text{Eq. 2-8}$$

where $F(N) = [N^2/(N^2 – 1)]\ln(N) – (3N^2 – 1)/(4N^2)$; $N = R/r_c$ for axisymmetric conditions, $N = B/b$ for plane strain conditions; m_{vc}, m_{vs} = coefficient of volume compressibility in the vertical direction for both column and soil.

Indraratna and Redana (1997) and Hird et. al (1992) have used the same approach that considers the effect of well resistance and smearing. By using Barron's equation for determining the Drain Influenced Soil Zone (DISZ) diameter (1948), this method has been proposed to alter the hydraulic properties of the soil, rather than adjusting the spacing of the columns to observe the desired behaviour. The equation is provided below for both rectangular spaced and triangular spaced pile formations with Figure 2-8 providing the visuals of theoretical diameters for DISZ.

$$D_{rec} = 1.13S \text{ and } D_{tri} = 1.05S \qquad \text{Eq.2-9}$$

where D = Drain Influenced Soil Zone diameter (D = 2R from Figure 2-6) and S = column spacing

Although hydraulic properties will not be consistent throughout the length of the drain, the accuracy in representing general conditions is observed to not exceed 11%. The general equation is given as:

$$k_{pl} = \frac{2k_{ax}}{3\left[ln\left(\frac{n}{s}\right) + \left(\frac{k_{ax}}{k_s}\right)ln(s) - 0.75\right]} \quad \text{Eq. 2-10}$$

where n = ratio of effective drainage radius to radius of drain, k_s = hydraulic conductivity of smear zone in soil.

If effects of well resistance and smearing are negligible or will not be considered, the equation can be simplified to

$$k_{pl} = \frac{0.67k_h}{[ln(n) - 0.75]} \quad \text{Eq. 2-11}$$

Using the method from Hird (1992), Chai et al. (2001) developed a numerical model that replaced the columns and soil with a homogenous composite that has the improved hydraulic parameters. Constant pressure with depth boundary conditions are applied to the centreline of each column location, depicting horizontal pore water pressure movement towards the columns and are dissipated to the drainage outlets. Van Helden (2008) applied this theory in his numerical model using Canadian soils as the Prefabricated Vertical Drains (PVD) and sand drains provide negligible improvement to the foundation stiffness, allowing the equivalent improved soil block to be used for estimating pore water pressure movement.

2.4 Summary of Literature Review

MSE walls are a popular civil structure for use in transportation projects for their cost-effectiveness and durability with large deformations. A proficient monitoring program should be implemented during the construction phase and after completion to ensure design tolerances are not exceeded. Standard monitoring tools include slope inclinometer, settlement plate, vibrating-wire piezometer, and total station; However, they collect data in discrete locations and installed instrumentation are susceptible to damage.

Terrestrial laser scanning is a surveying tool that collects data points surrounding the scanner to create point clouds. Multiple point clouds taken at different times of the same object/area can be

compared against a baseline survey to determine deformations. Additional abilities like snapping pictures to identify objects on site and altering point collection density to suit the project requirements help to reduce human error associated with surveying. The high level of accuracy and large data set collections are great for monitoring MSE walls for bridge abutments. However, previous research either surveyed controlled walls for theory purposes or did not collect enough scans to properly assess deformation behaviour.

Numerical modelling using finite element method is a great tool to predict the behaviour of settlement and pore water pressure change during construction. The use of 2D analysis for 3D arranged columns within the site foundation is a heavily researched area as conversion methods were developed to alter the geometry, stiffness, and hydraulic parameters of the reinforcement and soil materials. Assumptions and limitations of using the conversion methods require thorough due diligence to determine if the conversion technique is applicable for your analysis. Thus, accurate knowledge of site conditions is needed from lab testing and a proficient site investigation.

Figure 2-1 – Mechanically-Stabilized Earth Retaining Wall Structure

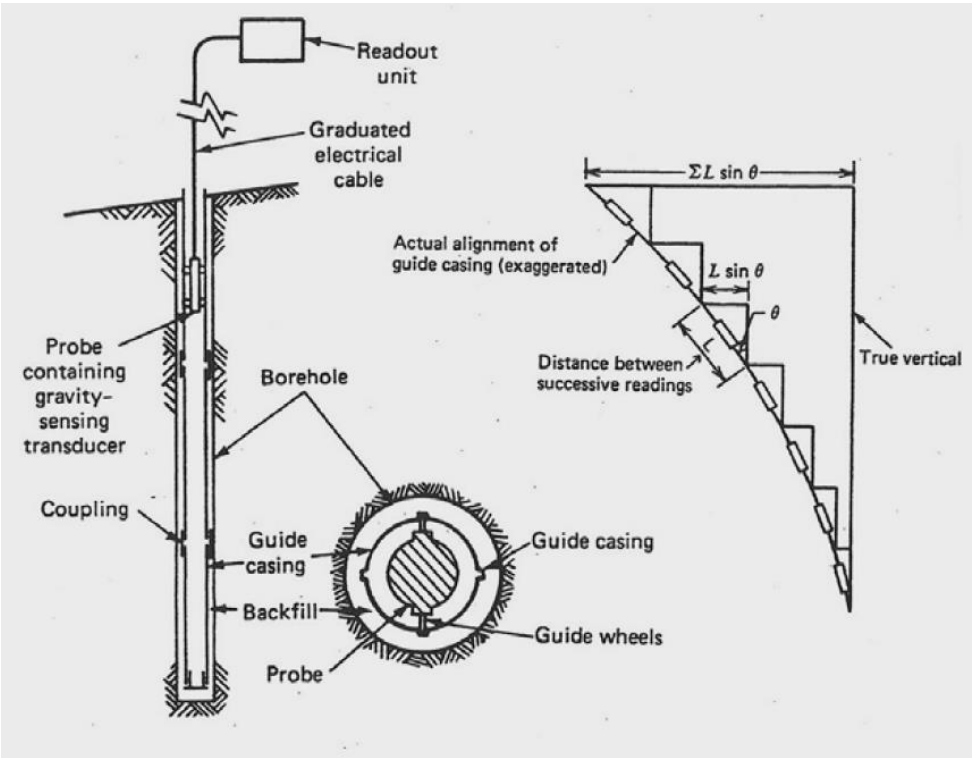

Figure 2-2 – Slope Inclinometer (Machan & Bennett, 2008)

Figure 2-3 – Vibrating Wire Piezometer (Envco Global, 2020)

Figure 2-4 – Settlement Plate (GEOKON, 2020)

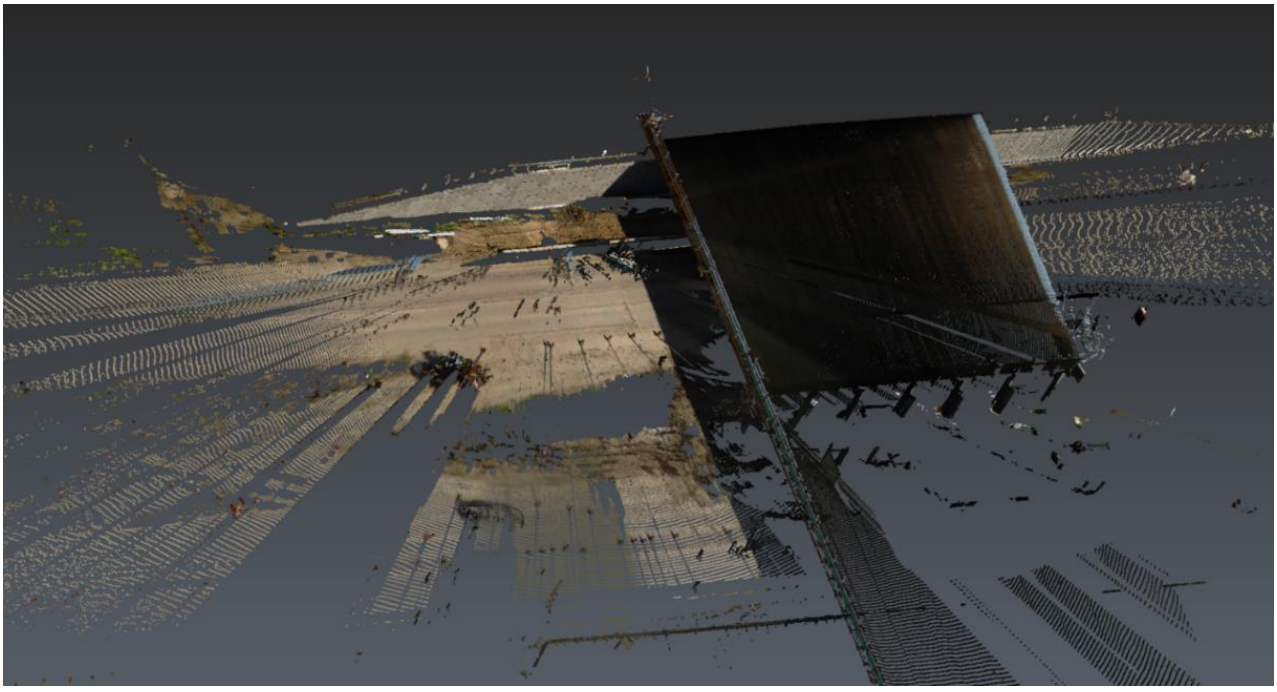

Figure 2-5 – Scan Point Cloud

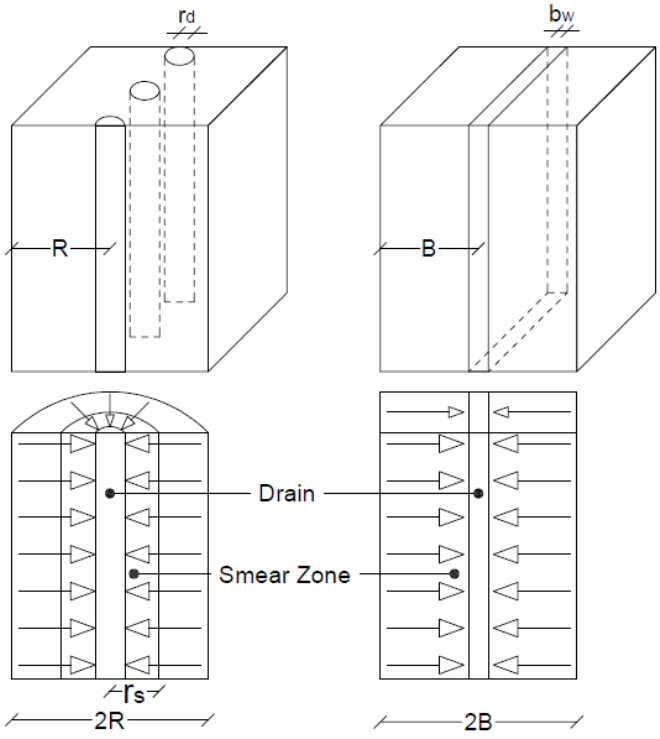

Figure 2-6 – Unit Cell of an Axisymmetric Column and Plane Strain Column (Van Helden, 2008)

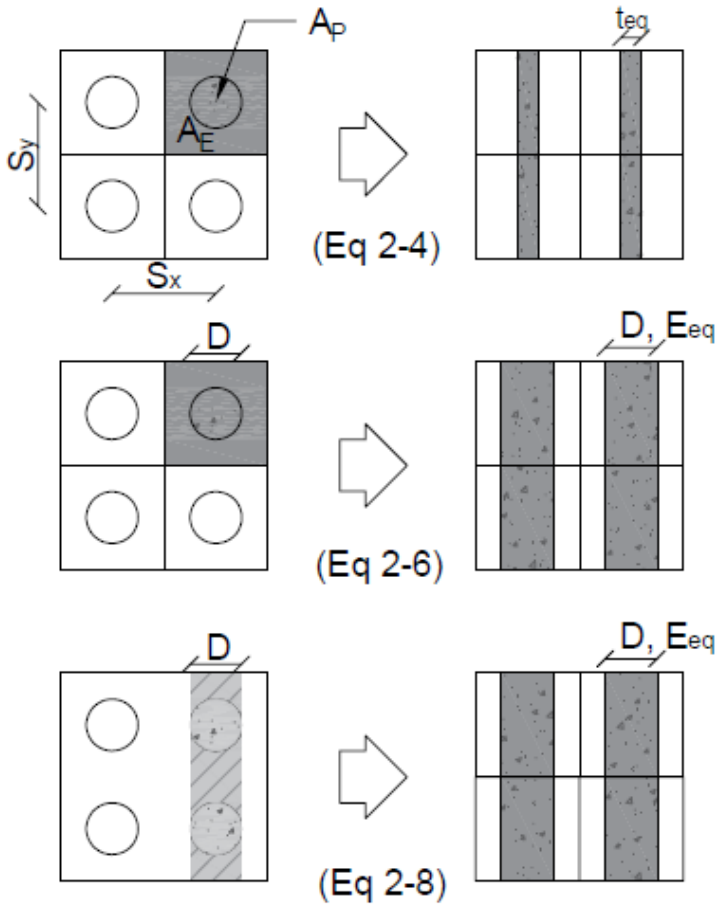

Figure 2-7 – Idealized Methods of Converting Axisymmetric Conditions to Plane Strain Conditions (Ariyarathne, et al., 2013)

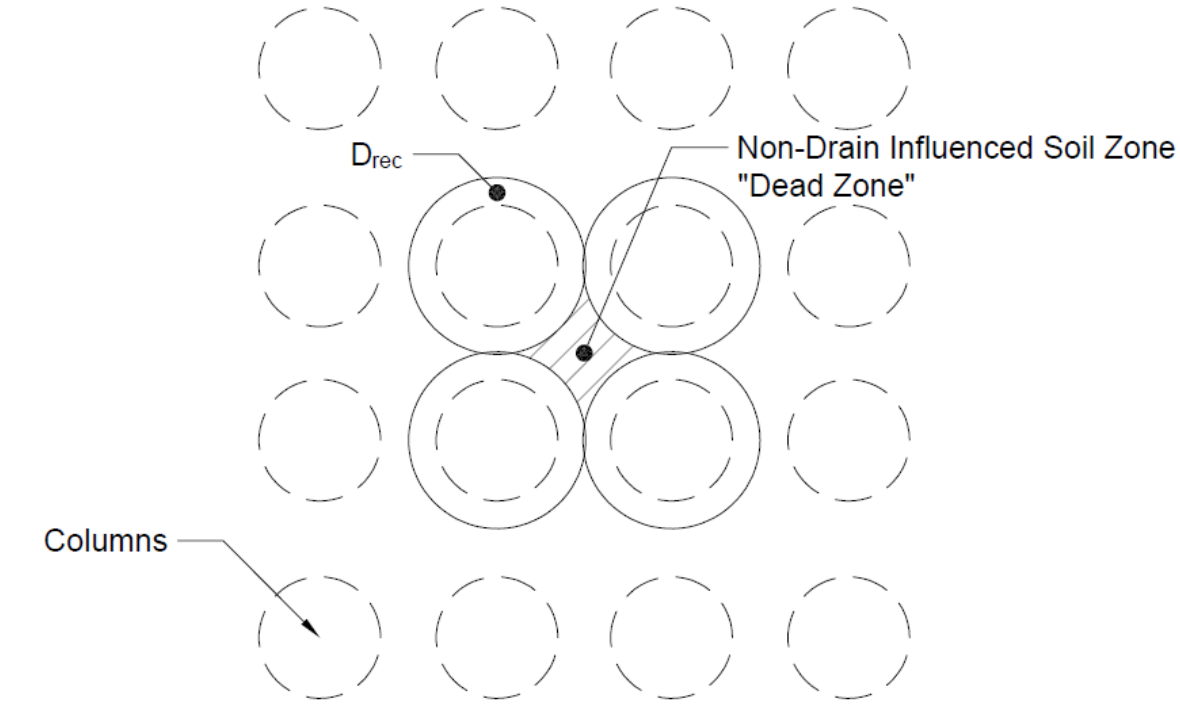

a)

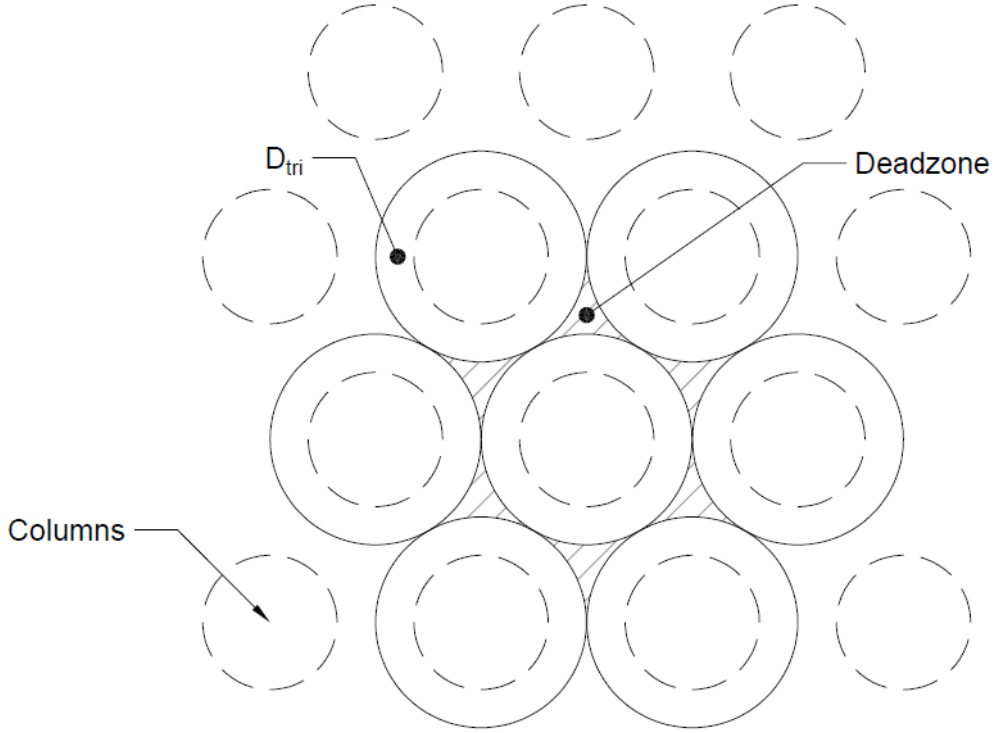

b)

Figure 2-8 – Diameters of DISZ for Columns Spaced a) Square pattern, and b) Triangular pattern

3 Site Specific Information

3.1 Introduction

The objective of this chapter is to describe the conditions at the site and how the design structures were selected. Beginning with the project site background, Saskatoon's geomorphology and local soil stratigraphy outline the soil properties and layer thicknesses. Then, the foundation and retaining structure design outline the interactions with the soil conditions and the field instrumentation monitoring program and results provide the pore water pressure before, during, and after construction. Understanding soil behaviour and identifying possible discrepancies in deformation analysis methods can be developed from that information.

3.2 Project Site Background

The McOrmond/College Drive bridge interchange was one of two different bride interchanges the City of Saskatoon proposed for construction in 2017 (City of Saskatoon, 2017). Traffic in the area has increased over the years with neighbourhood communities settling north of the 80km/hr speed limit highway. Development of new housing communities and shopping centres undergone construction south of the highway, heightening safety and environmental concerns due to a higher influx of traffic increasing the already dense commuting route.

Construction of the bridge interchange began in the Summer of 2017 and opened to the public in the Fall of 2018. The new bridge interchange has increased the number of lanes northbound-southbound, from 2 to 4, and installed traffic light-controlled intersections at both ends of the bridge to manage the high-speed commuters merging from the highway. The highway retained its existing conditions.

3.3 Geological History of Saskatoon

3.3.1 Geomorphology and Local Geology

Saskatchewan's geomorphology began 17,000 years ago when retreating glaciers by down-melting started to develop what is now the province's soil stratigraphy (Christiansen, 1979). De-glaciation of the land progressed to the north until nunataks emerged and forced the glaciers to separate, receding east and west into more frozen territory. It was not until 12,000 Before Present (BP) that Lake Saskatchewan was formed over what is now Saskatoon. River water pushed from continental glaciers, known as extraglacial rivers, created a large delta south of Saskatoon and a readvanced glacier clogged the west side of the Wakaw Spillway with moraine. When the glacier retreated westward, water from Lake Saskatchewan gushed back up through the Wakaw Spillway and eventually into Lake Agassiz, bypassing and thus resulted in the extinction of the Ou' Appelle Spillway. Both the North Saskatchewan Spillway and South Saskatchewan River continued to flow water through Lake Saskatchewan, forming large deltas south of Prince Albert. Lake Saskatchewan was quickly drained with the glaciers retreating north-east towards Manitoba and no longer contained water around 11,000 BP.

As the glaciers retreated northward along the South Saskatchewan River, deposits of lacustrine clay accumulated along the bottom of Lake Saskatchewan with extraglacial river flow interbedded silt and deltaic fine sands. A side effect of the extraglacial rivers depositing silts and sands into the lake, the quicker flow and debris in the water rapidly eroded away the channel walls to create the river valley evident in the Saskatoon area (Clifton, 2018).

Christiansen (1992) categorized the different till layers by carbonate content, weathering zones, and intertill stratified drift. The two main groups of till were named the Sutherland and Saskatchewan Groups; a third in the Empress Group was added in the update.

The deepest and oldest sediment group is the Empress Group as it lies between the bedrock and the oldest till layers. This sediment group is divided into a lower preglacial unit and an upper preglacial unit. The preglacial unit generally consists of quartzite and chert gravel; whereas the proglacial unit is a combined mixture of igneous, metamorphic, and carbonate clasts.

The next deepest sediment group is the Sutherland Group. Sutherland is a subdivision of Saskatoon where some of the rock deposits from this layer are found on the East side of the South Saskatchewan River, on the campus of the University of Saskatchewan (Christiansen, 1968). This stratified drift consists of dense till that has sections of oxidized areas and is generally less resistive than the next group, the Saskatoon Group.

The Saskatoon Group is composed of till and stratified drift and is found underneath the clay layer that is found at the present day. This group is found to be more sandy and less clayey than the Sutherland Group. This layer can be further divided into two formation layers: The Floral Formation and Battleford Formation. The Floral Formation is a more dense till than its counterpart and has little to no weathering. The Battleford Formation is a friable, soft till that is interbedded with sand and gravel.

3.3.2 Site Stratigraphy

The soil stratigraphy of site conditions were obtained and characterized from borehole logs that were produced beginning from boreholes drilled in 2015 by Golder Associates, 2016 by Golder Associates, and 2017 by TREK Geotechnical Inc (TREK Geotechnical Inc., 2017). These borehole logs provided the elevation of each soil layer, characterization of each soil material (distribution of particle sizes, colour, plasticity, surface hardness), sample types and names, water contents, undrained shear strengths, and selected laboratory tests on specific test samples.

From the mentioned borehole logs, they generally observed silty clay overlying clay till with instances of silt and/or weak clay within the transitioning zone between layers. Silty clay extended

11.5m and 9.5m below the surface of the north and south abutments, and the weak clay area was 0.5m and 1.5m in thickness where clay till was observed until the end of each borehole. Laboratory results determined the water contents of the silty clay ranging from 20% to 40% and the clay till ranging from 10% to 38%. Undrained shear strengths of test samples were determined in the field using torvane and pocket penetrometer instruments, and unconfined compression tests were completed from laboratory tests. Shear strengths of the silty clay were found to be ranging from 25kPa to 110kPa, the silt/weak layer ranging from 20kPa or less, and the clay till ranging from 60kPa to 180kPa. The silty clay was generally found to be firm to stiff and highly plastic, and clay till was stiff to very stiff and low in plasticity.

3.4 Geotechnical Design

The geotechnical design for the McOrmond/College Drive interchange consisted of three main components: Mechanically-Stabilized Earth (MSE) retaining walls with metallic strip reinforcement, vibration-compacted rockfill columns, and Cast-in-Place (CIP) belled piles. The MSE walls were constructed using segmented precast-concrete panels to a height of 6-7m and a width of 100m. Both walls were built to the same height but the south side of the bridge was at a lower elevation than the North side and therefore embankments required more backfilled material. This resulted in greater loads induced on the foundation and would cause the south abutment to settle more than its counterpart. Segmented panels were a great facing system as they could absorb large amounts of settlement and were flexible when differential settlement occurred (MacIntosh & Rrokaj, 2018; Sankey, et al., 2011). Metallic reinforcement was chosen as it reduced the amount of lateral movement from earth pressures. Since seismic activity is not prevalent in the Saskatoon area, the more rigid structure would not be subjected to large horizontal dynamic forces and not be more susceptible to failure. The reinforced backfill consisted of granular fill, as per Schedule 9-2, Article 5 of the project agreement, compacted to 100% density in 150mm lifts until design elevation. A big reason MSE walls settle too much or fail is because of drainage

difficulties within fine grained backfill, particularly during rainfall (Harpstead, et al., 2010; Scarborough, 2005). Granular fill allowed for the mitigation of water, as well as pore water pressure dissipation to avoid frost-jacking forces, and reduced corrosion of metallic reinforcement (DiFiore & Strohman, 2012). It was also determined to be a better material for backfill to reduce displacement of facing panels (Hossain, et al., 2012).

Vibration-compacted rockfill columns, also referred to as stone columns, were drilled 1m within the clay till at two specified diameters: 1.8m and 2.1m. 1.8m diameter columns were drilled within the bridge deck extents in two rows with a spacing of 2.6m and the last two rows of columns at the end of the reinforced zone, shown in Figure 3-1. The 2.1m diameter columns were installed everywhere else with spacings ranging of 3.0-3.3m (TREK Geotechnical Inc., 2017). Rockfill columns were introduced for the foundation design to improve the global stabilities of the embankment, reduce the magnitudes of both long-term and final settlements, and increase the settlement rate (Hutchinson, 2011; Mohamedzein & Al-Shibani, 2010). To note, underground sewer and storm water pipes run north and south, located on top of the clay till layer. The shaded columns that were installed in that area indicate short columns were drilled to 500m elevation. Embankment loading cannot be transferred from the columns to the clay till in this area, causing more stress within the weaker clay soil and theoretically more settlement. A 1m bridging layer of the same granular material overlaid the rockfill columns to allow pore water pressure dissipation from the columns to enter this layer and away from the foundation and increase the strength of the base directly underneath the concrete wall panels (TREK Geotechnical Inc., 2017). A high strength geogrid was placed overtop the bridging layer to distribute embankment loading across the reinforced zone through the stone columns. The inclusion of the rockfill columns and geogrid was expected to limit the differential settlements below a design tolerance of 1% for the wall facing panels.

CIP belled piles were proposed to support the bridge deck structure, drilled 15m -16m below ground surface and end-bearing into the clay till. The CIP belled piles had an unfactored end-bearing capacity of 900 kPa and were considered the more attractive option because they did not have complications with installation concerning boulders. Each pile group under the abutments and pier were expected to settle 15mm under an estimated service load of 330 kPa, not considering elastic compression of the piles.

3.5 Field Instrumentation

Field instrumentation was installed within the approach embankments for both the north and south abutments. Vibrating-Wire (VW) piezometers were chosen to monitor the pore water pressure changes within the foundation, both the influence of the embankment buildup in unreinforced clay and the influence of compacted granular fill buildup behind the wall. The settlement sensors measure the consolidation settlement and provide an alternative method to surveying the structure's performance. Due to damage sustained from construction, the sensors did not provide meaningful data and were not used for settlement comparison. A summary of the VW piezometers installed on site are provided in Table 3-1. Locations of piezometer installation are given in Figure 3-2. The monitoring results were used to calibrate the numerical models that are developed in this research.

3.5.1 North Abutment

A total of three piezometers were installed within the native clay layer on November 11, 2017 after construction of the stone columns was completed. Piezometer 1702974 was installed within the centre of the approach embankment area (TH17-03) at an elevation of 499.99m, while piezometers 1702976 and 1702977 were installed at the centre of the reinforced backfill zone (TH17-04) at elevations of 499.97m and 503.63m respectively. Data from TH17-03 was collected until April 18, 2018 when damage sustained from construction discontinued monitoring. TH17-04 piezometers were also damaged and stopped recording data on June 16, 2018 but were repaired

and reinstalled on August 11, 2018, and no complications have occurred since. Additional VW piezometers were installed on August 11, 2018 to replace the damaged piezometer within the reinforced soil area. Piezometers 1802410 and 1802411 were installed underneath the eastbound traffic lane (TH18-01) at elevations of 500.00m and 503.00m respectively within the native clay layer.

3.5.2 South Abutment

A total of four VW piezometers were installed within the native clay layer on November 3, 2011 at the same time as the north abutment. Piezometers 1702970 and 1702971 were installed outside of the stone columns, along the centreline of the embankment (TH17-01) at elevations 499.56m and 503.22m respectively. Piezometers 1702972 and 1702973 were installed along the centreline between the fourth and fifth rows of stone columns (TH17-02) at elevations 499.77m and 502.82m respectively. Data was collected at date of installation and continued monitoring pore water pressure response until completion of construction.

3.6 Field Instrumentation Monitoring Results

Piezometer monitoring results are provided separately in Figure 3-3 and Figure 3-4. Readings are given in Piezometric and Fill Elevation (Y-Axis) with respect to time (X-Axis).

3.6.1 North Abutment

Figure 3-3 provides the initial piezometric head readings for the approach embankment and within the stone columns began at 507m and 502m, before decreasing to 506m and 501m prior to embankment fill buildup, respectively. The lower water pressure between the piezometers was suspected to come from the installed columns acting as drains, drawing down the water table. A 1.8m rise in piezometric head (17.7kPa water pressure) under the embankment resulted from an added fill height of 2.5m (45 kPa vertical stress) before it was damaged, generating a B-Bar response of 0.4. The B-Bar response represents the ratio of increased excess pore water

pressure given an increased vertical pressure. This is used in short-term stability analysis to observe the impact of rapid loading in construction and determine when each backfill lift should be applied. Once piezometer operations resumed, the piezometric heads for both outside and inside the columns reached equilibrium at 507m elevation; the initial water table elevation monitored in TH17-03. This indicated that excess pore water pressure had almost entirely dissipated and final soil consolidation was nearly complete. Readings collected from the piezometers installed within the unreinforced soil area were observed to be identical, indicating accurate measurements.

3.6.2 South Abutment

Figure 3-4 shows the initial piezometric head readings for both outside and inside the columns were 505m and 503m, then decreasing to 504m and 502m prior to backfill loading, respectively. Piezometer 1702973 observed to flatline after surveying fill elevation on November 10, 2017, most likely a connection in the piezometer was disturbed and unable to accurately measure hydraulic pressures within the clay. The piezometric response within the stone columns was very small as the stone columns acted as drains to alleviate excess pore water pressures quickly (maximum observed pore water pressure change was 10.7kPa). The response outside the stone columns observed a piezometric head increase of 6.3m (61.8kPa water pressure) from an embankment fill height increase of 8.0m (144kPa vertical stress). This resulted in a B-Bar response of 0.43 which is very similar to the observed result in the north abutment clay section. After completion of fill heights and wall construction, the piezometric head elevations converged to approximately 506.0m with unreinforced zone piezometers measuring 505.6m and 504.8m respectively. The 0.05m discrepancy in piezometric convergence is not a concern but the 0.05m difference between piezometer readings in the same location is more indicative of a calibration error in hydraulic measurements. Since the final readings equalized to initial measurement elevations, the data collected was adequate in monitoring field hydraulic conditions.

3.7 Summary of Site Specific Information

The bridge interchange is in Saskatoon, Saskatchewan over the existing McOrmond/College Drive. Construction of the bridge intersection began in the Summer of 2017 and was opened to the public in the Fall of 2018. The soil stratigraphy in the construction area was characterized from boreholes, generally observed to have firm to stiff silty clay overlying soft to very stiff clay till with some soft clay and silt imbedded within the transition between clay and till. The lacustrine clay was deposited from Lake Saskatchewan with glacial alluvial deposits of sand and silt imbedded within the clay layer. The clay till consisted of two different formations: Battleford and Floral. Battleford formation clay till resides directly under the clay layer and is a soft and friable till whereas the Floral formation till is stiff to very dense.

The bridge interchange foundation design consisted of three main components: MSE wall reinforced with metallic strips, CIP belled piles, and vibration-compacted rockfill columns. The MSE wall was selected for its flexibility to absorb large deformations without failure and the metallic strips are stiffer than geosynthetic material, resisting more lateral deformations. The CIP belled piles have a large bearing capacity to minimize bridge deck settlements and reduce damage to the superstructure. The rockfill columns were selected to strengthen the silty clay to reduce settlements, and act as drains to dissipate pore water pressures during staged construction loading.

VW piezometers were installed within and outside of the reinforced area at the north and south abutments prior to construction to monitor pore water pressure responses during construction. Piezometers installed in the north abutment were damaged during construction and therefore, only data collected from the south abutment was used to observe the pore water pressure response. The initial water tables for both the north and south abutment were observed at 506m and 505m respectively. Outside of the reinforced area, the piezometric head increased by a maximum of 6.3m (excess pore water pressure of 61.8kPa) compared to a vertical stress increase

of 144kPa. This resulted in a B-Bar value of 0.43. The pore pressures did not surpass 10.7kPa within the reinforced area as the rockfill columns provided the pore water to escape.

Table 3-1 - Summary of Field Instrumentation Installed on Site (TREK Geotechnical Inc., 2019)

Abutment	VW Piezometer	Location	Elevation	Status
North	S/N 1702974	TH17-03	499.99m	Installed 3/11/2017, Damaged 18/04/2018
	S/N 1702976	TH17-04	499.97m	Installed 3/11/2017, Damaged 16/06/2018, Repaired 11/08/2018
	S/N 1702977	TH17-04	503.63m	Installed 3/11/2017, Damaged 16/06/2018, Repaired 11/08/2018
	S/N 1802410	TH18-01	500.00m	Installed 11/08/2018
	S/N 1802411	TH18-01	503.00m	Installed 11/08/2018
South	S/N 1702970	TH17-01	499.56m	Installed 3/11/2017
	S/N 1702971	TH17-01	503.22m	Installed 3/11/2017
	S/N 1702972	TH17-02	499.77m	Installed 3/11/2017
	S/N 1702973	TH17-02	502.82m	Installed 3/11/2017

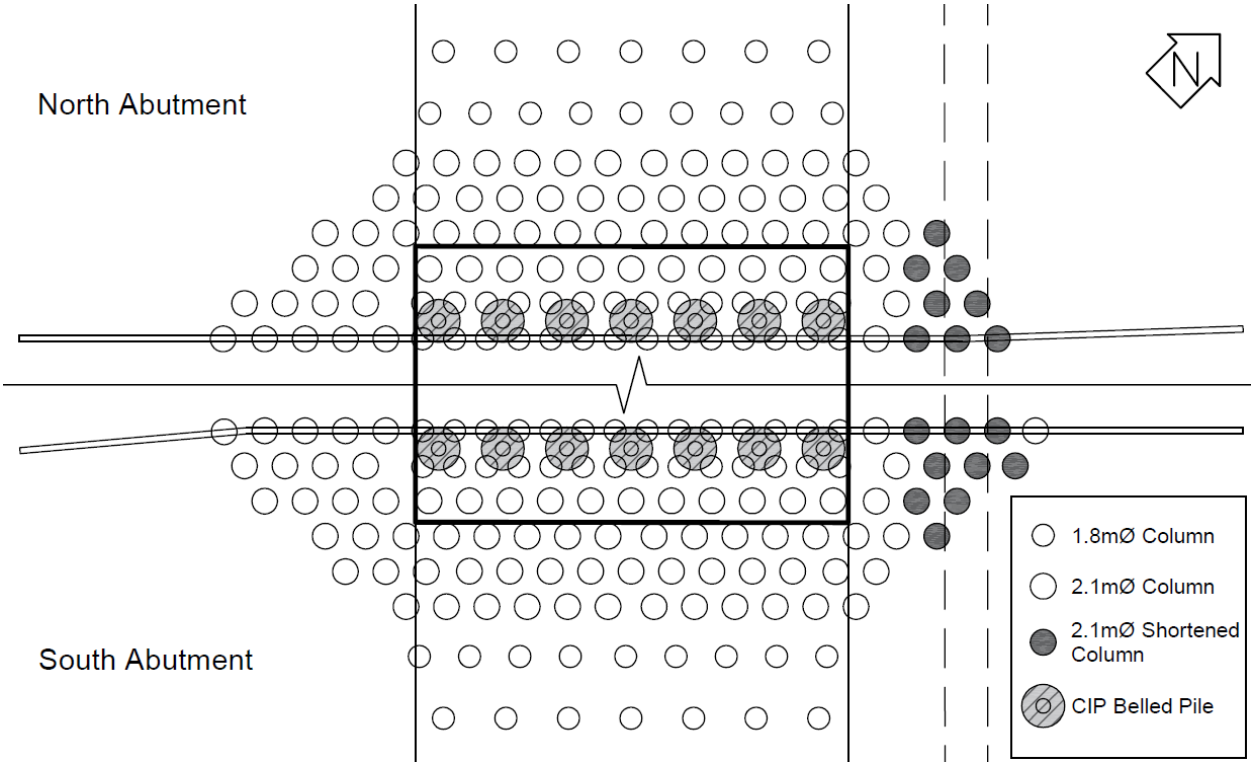

Figure 3-1 – Foundation Design Layout (TREK Geotechnical Inc., 2017)

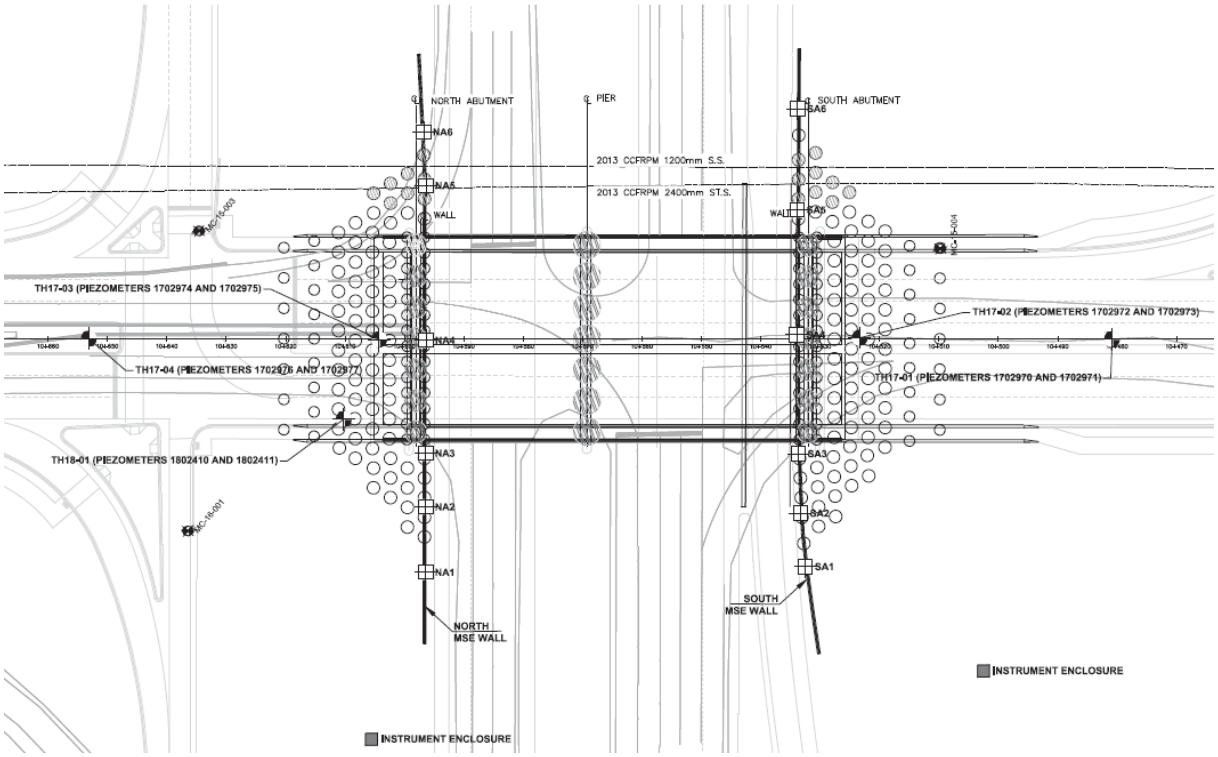

Figure 3-2 – VW Piezometer Install Locations (TREK Geotechnical Inc., 2019)

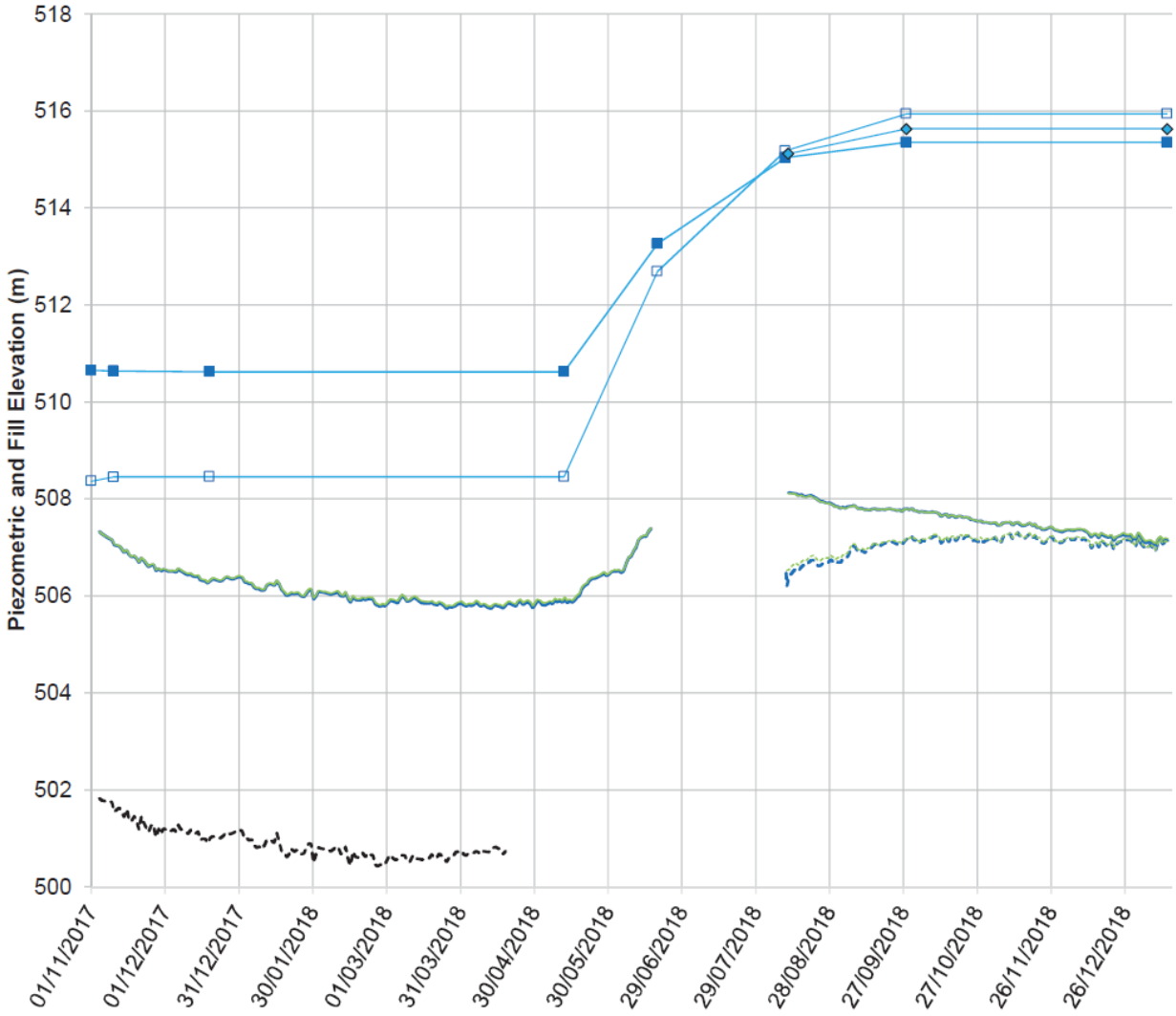

Figure 3-3 – North Abutment Monitoring Report (TREK Geotechnical Inc., 2019)

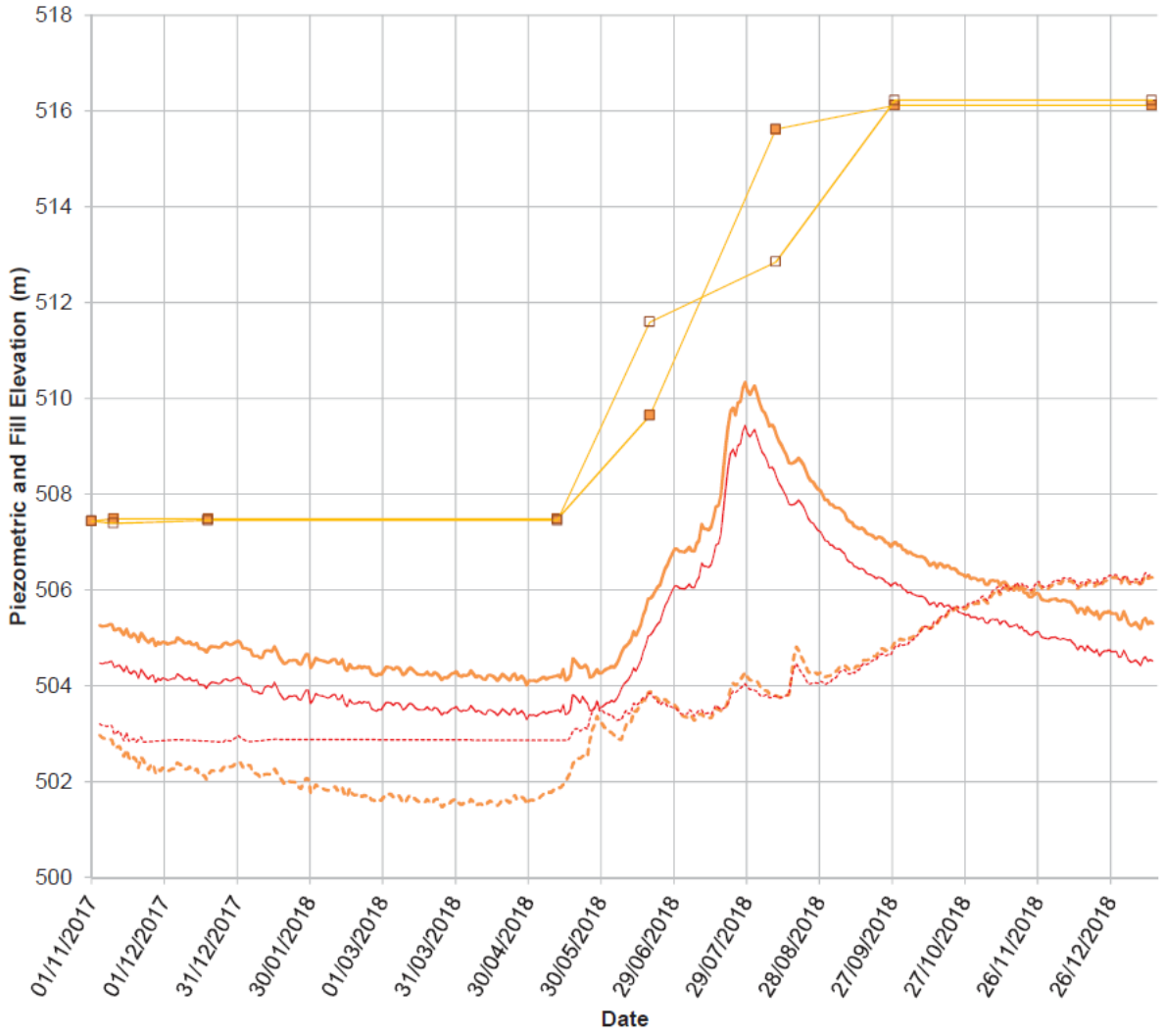

Figure 3-4 – South Abutment Monitoring Report (TREK Geotechnical Inc., 2019)

4 Deformation Surveying Techniques

4.1 Introduction

This chapter goes over the surveying methods, Rod and Level (RL) and Terrestrial Laser Scanner (TLS). The surveying specifications will indicate how each survey equipment measure their targets, the accuracy in which the coordinates are determined, possible errors associated with the measurements, and any other information that is pertinent to this research. The methodology chapters will discuss how the data was collected and can be used for deformation analysis. The first main objective is dependent on this chapter to interpret the results from the analysis and will provide the reasoning for discussion.

4.2 Rod and Level

4.2.1 Surveying Specifications

The RL measurements were provided by the contractor on site. Measurements were surveyed using the Leica NA720 for its ability to survey in all weather conditions and suppress vibrations from heavy machinery for accurate measurements (Leica Geosystems, 2015). The errors incurred with each survey can be split up into user errors and instrument errors. User errors are a result of poor practice, taking shortcuts, and/or lack of knowledge to name a few. Examples of these can be poor instrumentation setup leaving a slight tilt in the level, misreading the target measurements, and/or documenting measurements incorrectly (Washington State Department of Transportation, 2005). These errors are preventable with proper training and a second observer for measurements. Instrument errors are associated with the machine characteristics and can either be prevented or accepted. Situations such as the compensator not functioning properly, this compensates for the vertical axis tilt of the machine, and level bubble not properly calibrated can be prevented with proper inspection and maintenance. The instrument error that is accepted is the accuracy of height measurements. According to Leica's user manual, the accepted error at 30m is 1.5mm and was considered when reviewing measurements. Another accepted error that

was introduced was the use of rebar as a benchmark. The bridge interchange was not close to an established benchmark and thus temporary benchmarks were formed using rebar. During seasonal change, frost heave may alter rebar positioning within the ground and therefore cause inaccuracies in relative movement measurement. The amount of error is unknown but discrepancies will be apparent from the summer surveys (May-September) compared to the Fall/Winter surveys (October-January). Since the contractor was responsible for the measurements, it was assumed that the survey instrument had been properly maintained and only the instrument errors will be considered unless greater discrepancies were found.

4.2.2 Methodology

RL surveys were completed at the beginning of wall construction and continuous surveys once the reinforced backfill material was compacted on each of the reinforcement strips. Measurements were selected at 6 points along each north and south wall, denoted as NA1-6 and SA1-6. Targets 1, 2, and 3 were taken on the west side, Target 4 was selected at the centre, and targets 5 and 6 were taken on the east side of each wall; these locations are provided in Figure 4-1. The baseline survey was established on May 5, 2018 at the base of the wall panels, placing a rod on the levelling pad to determine the starting elevation. This was completed again for the next survey measurement taken on July 5, 2018 but target locations were moved after settlement was recorded. The target locations were moved 2m up from the levelling pad onto the wall facing panels as later in construction backfill was placed 1m high along the first row of panels and the pad could not be accessed. The following surveys were taken two weeks apart (July 19 and August 2), six weeks apart (September 13), five weeks apart (October 18), and two months apart (January 16, 2018). These surveys only determined the amount of settlement post-construction of the wall and will be used to compare against the TLS for its applicability in structure performance.

4.3 Terrestrial Laser Scanner

4.3.1 Survey Data Collection

TLS is an advanced surveying method that determines object positioning around the scanner by reflecting a continuous stream of lasers into a rotating mirror, collecting data points in a vertical range of 360° and horizontal range of 300°, creating an explosion of points in 3D space called a point cloud (FARO Technologies Inc., 2016). The scanner calculates the cartesian coordinates of its data point's position in 3D space by measuring the horizontal and vertical angles of the laser orientation. However, the laser scanner does not only use triangulation for its calculation of coordinates, but can measure the data point distances either through triangulation, Time-of-Flight (ToF), or Phase-Shift (PS) (Garcia-Ferandez, 2016). Triangulation measures distance using known locations of laser origin and object position, then calculates the coordinates based off the angle of mirror reflection and orientation of the scanner on its base. ToF method determines the flight path duration from laser emittance to object position and back to scanner. The flight path distance can be calculated with the known speed of light. PS is similar to ToF using duration of flight path, however it measures the "phase of emittance" and compares it against the bounce back phase or "phase of reflected" for a more precise measurement. The accuracy or precision of these point measurements can be tailored to project specific requirements by modifying the resolution and quality parameters (FARO Technologies Inc., 2016). Scanner resolution specifies the point spacing between data points and the quality parameter dictates the amount of additional points required for measuring a certain location or the amount of noise compression. Increasing the resolution and quality will densify the point cloud with more precise data point positions but will increase the duration of surveying on site and post-processing. Also to be considered are the environmental conditions; indoor vs outdoor, open space vs line of sight issues, sunny vs cloudy, etc. (FARO, 2019) Increasing quality to reduce noise error from light refraction on a sunny day, lowering resolution to reduce the time on site from additional survey positions due to poor line of

sight of the project area, etc. Pictures are then taken from the scanner's internal camera which are overlain onto the point cloud to colourize and distinguish targets used for registration of scans.

Depending on the accuracy threshold required from the scans, altering the amount of data points collected will have a positive and negative affect on other project constraints. Adjusting the resolution will dictate the number of data points that are collected in its full revolution and the adjustment of the quality changes the speed of the scanner's rotation (FARO 2019). Increasing rotation speed will help to reduce scan durations when project schedule is sensitive and/or if the accuracy tolerance is low. Decreasing rotation speed will help increase the accuracy of measurements when environmental conditions are not ideal. Depending on scanning environmental conditions such as scanning indoors, outdoors with overcast, and outdoors with sunny skies, the resolution and quality should adjust to accommodate the ability for the scanner to detect target coordinates in the point cloud.

The targets used for registration can either be cooperative targets like spheres and placards that the scanner can determine coordinates based on sphere diameter and color contrast on the placard, or identifiable targets like corners, edges, and planes of existing structures (Knaak 2017).

Surveying larger areas and surfaces require multiple scans to be performed and each point cloud is aligned together by targets that are identical in each scan. These aligned point clouds create a larger Project Point Cloud (PPC) which can be compared to successive point clouds for applications in deformation analysis, structure degradation, and site investigations (Truong-Hong and Laefer 2014).

4.3.2 Survey Data Processing

The scanner used in this research is the FARO Focus X330 with the accompanying FARO Scene software to process the data and create the project point clouds. FARO Scene has registration tools to either align the point clouds by Top View Registration (TVR), Target Registration (TR)

and/or Cloud-to-Cloud Registration (C2C). TVR is the simplest form of registration as the software aligns the point clouds through a plan view (XY plane). TR orients the point clouds together based on the selected identical targets in each scan view. FARO Scene requires at least three targets to allow for registration of two point clouds to confirm the X, Y, and Z coordinates. C2C is a micro registration tool which uses the software's algorithm to best fit the point clouds together from user input parameters that determine the scope of registration; number of iterations, search distance, and subsampling size. These parameters adjust to serve the requirements of the project, whether it is accuracy, outdoor project, and/or efficiency. The term 'micro' refers to its inability to align clouds that are distanced away from each other in the 3D space. Therefore, a TVR or TR is required before performing the C2C. Once a registration tool is completed, a report is produced outlining the success of the registration in terms of the maximum and mean point error, and the percentage of minimum point overlap. If satisfied, errors are noted for measurement accuracy and either the next point cloud can be measured, or the project point cloud can be used for its intended purpose. If the errors were outside of the project tolerance, re-registering the point clouds would be required. This would entail either registering with a new arrangement of targets, using a different registration tool, or a combination of the two.

4.3.3 Methodology

Laser scanning occurred during construction and post-construction of the bridge to measure wall displacements as the backfill material was built up in lifts. Displacements of the wall would be recorded as relative movement, referenced to the placement of the first row of concrete panels.

The scanning schedule was recommended to be performed after each row of panels were erected and monthly after wall completion to observe the influence of compacting backfill behind the wall during construction (Scotland, 2014). However, due to budgetary and location constraints for this project, residence is in Winnipeg and location site is in Saskatoon, only two scans were performed during construction; completion of the first row of concrete panel facings and completion of the

last row (May 9 and June 2). The post-construction scanning schedule began when backfilling was completed (one month later) and then another two months later (July 5 and August 28) during the summer of 2018, with two additional scans completed in the summer of 2019, each were separated by 3 months (May 7 and August 13). These additional scans were completed to observe the influence of ground thaw and service traffic loading, if any were observed.

The laser scanning performed on site varied for each survey date to accommodate site conditions during surveying and growing experience in point cloud processing, but the parameters used for data collection were generally a ¼ resolution (44MPts) and a quality of 4x. The 2019 surveys for the north abutment (May 7 and August 13) required a resolution of ½ as traffic was no longer rerouted and thus the scanner had to be placed farther away from the wall. The south abutment section had a safe space between the existing traffic lanes and the newly constructed turnoff lane and therefore, could remain with the ¼ resolution. Reference targets brought to site included six 0.23m diameter spheres and six 2m x 2m placards. Surface planes and corner points along the bridge deck and wall panels were also used for point cloud alignment. Target layouts used for each scan survey varied with each survey as the construction of the bridge interchange would require traffic to be rerouted from the existing roadway lanes, resulting in north wall scans to be restricted in a confined space with the south abutment scans free with space, and vice versa. A typical survey layout is provided in Figure 4-2, outlining the location of the scanner in relation to the spheres and placards. Each scan was required to have at least three targets to provide orientation of the scanner in the X, Y, and Z planes (Knaak, 2017; Laefer & Lennon, 2008). These targets were also placed close enough for each scan and surrounding the scanner in each 90° quadrant. This was to ensure target tensions secured the scanner in its correct orientation for either registering with subsequent point clouds or converting local coordinates into a Universal Transverse Meridian (UTM) global coordinate system (Tice, 2017). The target tensions for laser scanning is similar to Global Positioning System (GPS) where it requires satellite signals to

communicate all around the receiver's position to accurately determine its location; satellites in only two quadrants will not give the receiver information on its position with respect to the other two quadrants and therefore cannot determine its exact cartesian coordinates. An example to better visualize this effect involves a man with 3 bungee cords tied around his waist in Figure 4-3. First, the three cords are pulled under tension on only the Eastside of his body (180°). His position is quite secure in the north-south plane with minimal movement allowed in the cords. However, he has a tensile force pulling him east with no resistive cord in the other direction, resulting in the man being pulled out of position and the eastern cord relaxes. Now the man can move more in the east-west plane, resulting in more deviation from his original position. If the cords were evenly distributed, his position is resisted proportionally well in all directions, restricting less displacement from his original position. Adding more bungee cords will add more resistive tension to the man's movement and therefore secure his current location (more satellites/targets will allow the GPS receiver/scanner to determine its global cartesian coordinates more accurately).

Deformation analysis was performed using a baseline or reference point cloud and compared to subsequent point clouds orientated in the same coordinate system. Creating project point clouds for each survey date was found to create large discrepancies in wall deformation observed in preliminary measurements. Each successive point cloud registration would compound the registration errors and with more scans, the potential for a larger compounded error was greater. Take for example, four scans are each registered with a 3mm mean point error. The potential compounded registration error of these three scan registrations from initial scan to the final scan would be ±9mm. Misclosure loop is determined by performing additional surveys towards your initial survey location from the final survey, creating a loop to measure the difference in orientation between beginning coordinates to the final looped measurement; a visual aid is provided in Figure 4-4. Then with this coordinate deviation value, each scan can be slightly adjusted in the user's software to bring the surveyed coordinate measurement back to the original starting position. The

FARO Scene software used to create the PPC combines the individual point clouds into a larger point cloud, but does not allow the last point cloud registered to align with the first point cloud. Because of this, the loop misclosure cannot be calculated and each registration cannot be adjusted. Instead, deformation analysis was carried out with a reference PPC and subsequent survey dates will use single scan point clouds for relative movement. This alternative allowed the author to avoid compounding error from multiple point cloud registrations and could determine if actual wall deformations were heavily influenced by misalignments.

The June 2, 2018 scan was considered the reference cloud for both abutments as the first row of wall panels was covered with either backfilled sand or concrete poured along the face of the wall, rendering the first scan (May 9, 2018) ineligible for observing all surveys. Scan point clouds used for analysis were chosen on the east and west side of the wall, close enough to the centre of the wall to minimize as best the impact of bounce back error from scanning panel faces at too sharp of angles. The selection of scans on either side of the bridge deck also allowed a rotation comparison of the aligned clouds. Target registration aligned a best fit of the target for each cloud, including rotation of the non-reference cloud. Manual translations and rotations were required to make fine adjustments to counteract this misalignment that the software algorithm could not fix. The fine adjustments were made in relation to the bridge deck in each survey date as the long beams and girders provided good references for rotation adjustment in the X and Y axes. The bridge deck may be presumed as an unsuitable reference object for aligning point clouds together as it settled from its massive weight but that was not the case in this project. The bridge deck was built on CIP belled piles drilled into the till layer, a permeable material to dissipate pore water pressure buildup and from analysis done by TREK Geotechnical Inc., they predicted final settlements of the structure to be 15mm (excluding elastic compression). Most of the 15mm settlement, if not all, would have occurred in the six months leading up to the start of the MSE wall surveying as the structure was completed by October 2016. To put that error into perspective,

Real-Time Kinematics (RTK) surveying uses satellites to determine its global position. A proficient number of satellites communicating coordinate positioning (7+ satellites) and is held static for a proficient amount of time (30+sec) would result in errors for the horizontal and vertical directions to be ±3mm and ±5mm respectively (3D error is ±6mm). TLS requires three targets and therefore three points will need to be determined, each with the same errors. However, each of these targets using RTK coordinates are independent of each other so when the point cloud tries to align itself using those coordinates, the positioning errors are compounded, like the problems surveying without loop misclosure, and the registered point cloud global position may be off by more than 18mm (±6mm x 3 targets = 18mm). After review, the possible error incurred from the settling bridge deck was accepted to be used as reference.

To determine wall movements, Figure 4-5 shows cross-sections were developed in 0.5m intervals along the wall and measurements were taken at least every 1.5m to provide a continuous profile. 3D Reshaper's meshing tool can generate smooth surfaces along the planes created by the point clouds. This is beneficial to fill in gaps of missing data points along the wall surface from line of sight obstructions such as vehicle traffic or signs. It can also smooth out surfaces that may have a rough or scattered surface, such as carpet, grass, and/or scaled concrete. Measurements were determined from manual point-to-point comparison of opposing point clouds separation. This was selected as judgement of actual wall movement through manual inspection would reduce error incurred from the software's measurement algorithm, as it computes the distance between planes where the point of reference was the edge of each wall panel as shown in Figure 4-6.

As previously stated, the reference PPC was the June 2 survey. Therefore, the deformations observed after this date were to be added onto the deformations observed from May 9-June 2. This created a dependency on the accuracy of this analysis and discrepancies in final observations could be referenced to this method.

4.4 Summary of Surveying Techniques

The two surveying techniques used to observe deformations were the rod and level, and terrestrial laser scanner.

Rod and level surveying was used by the contractor to determine the structure's vertical settlement. This is a simple measuring method that has small machine ranging error (±1.5mm @30m) and with limited user error, can measure settlements accurate to the millimetre. The monitoring schedule developed began with the baseline survey taken on May 5, 2018, and deformation surveys performed from July 5, 2018 to January 16, 2019. Settlements were observed in seven different locations along the MSE wall, three spots on each the east and west locations, and one in the centre of the wall.

The terrestrial laser scanner collects data points in a 360° view around the scanner, creating a web or mesh of coordinates called scan point clouds. Using accompanying point cloud software, individual scan point clouds was aligned within the same coordinate system using like targets within the field of view in each scan, creating larger sets of data called project point clouds. Once multiple surveys were performed on the monitored structure and the project point clouds are developed, the clouds can be imported into the same coordinate system and analyzed for deformations. The scanning schedule developed for the bridge structure consisted of two scans during construction (May 9 and June 2, 2018), two post-construction scans during the same summer (July 5 and August 28, 2018), and two additional scans the following year (May 7 and August 13, 2019). Since the laser scanner is able to collect more data points than the rod and level, deformations of the wall can be determined along the entire face of the wall and predetermined survey locations were not required. Deformations using the point cloud software was obtained using manual point-to-point measurement.

a)

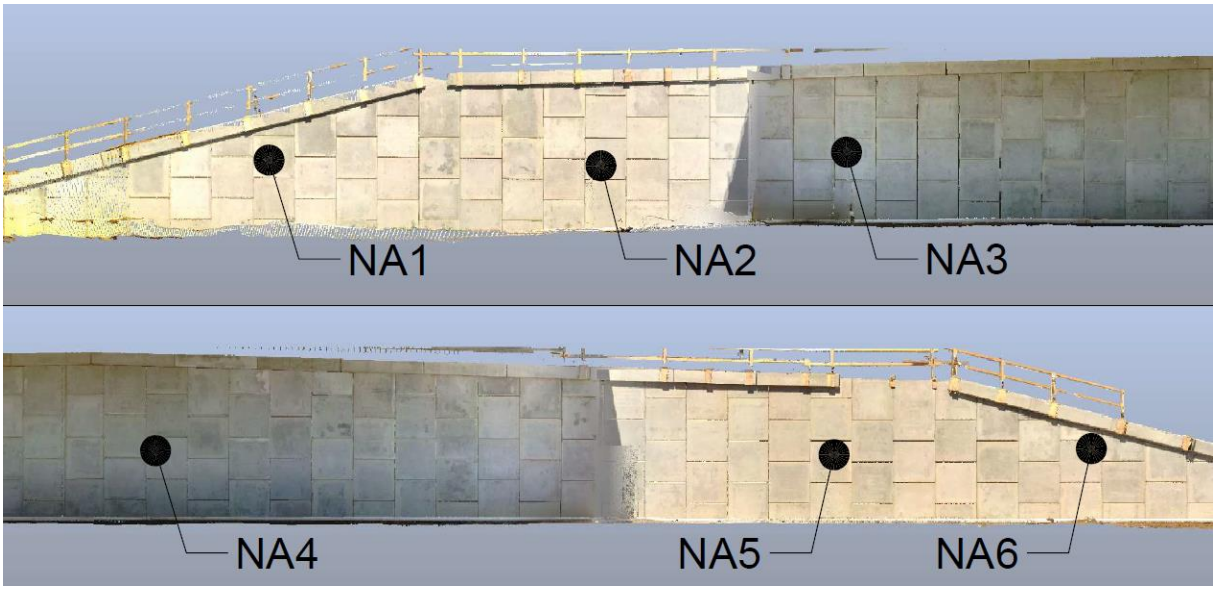

b)

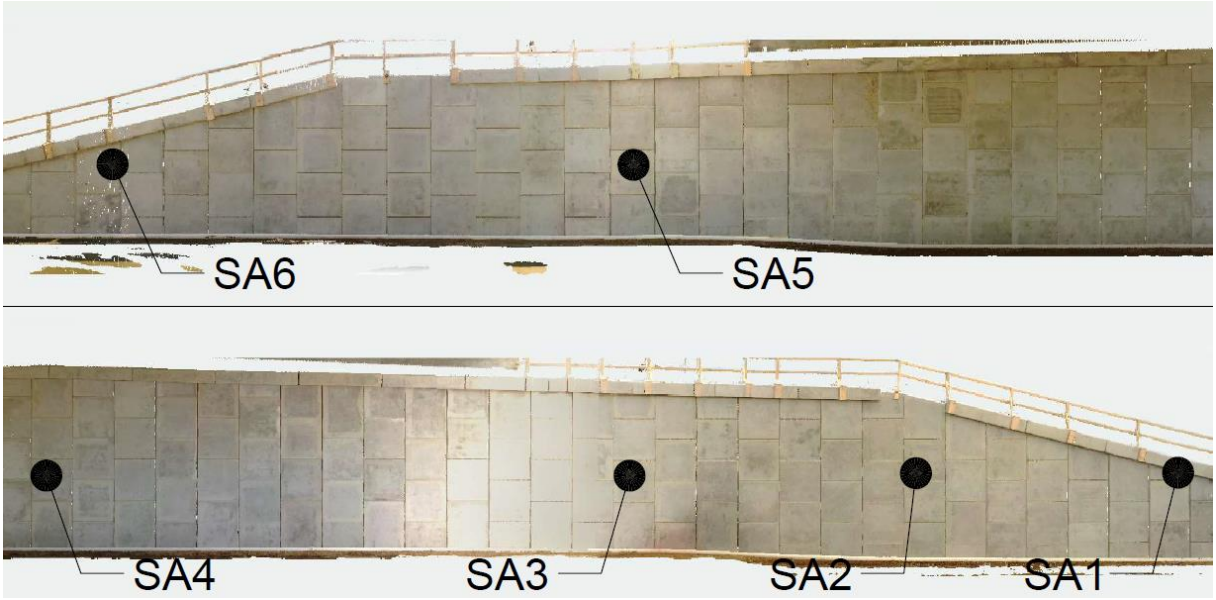

Figure 4-1 – Rod and Level Surveying Locations for a) North Abutment, and b) South Abutment

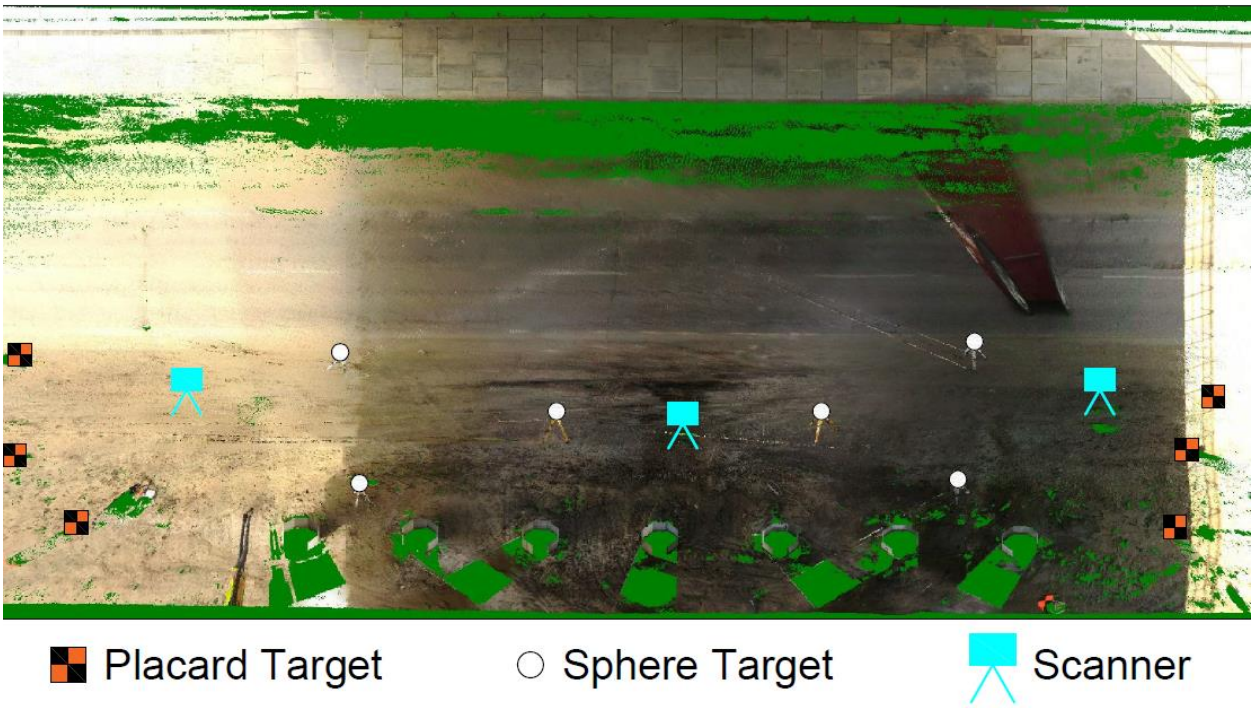

Figure 4-2 – Scan and Target Layout used for North Abutment 190813

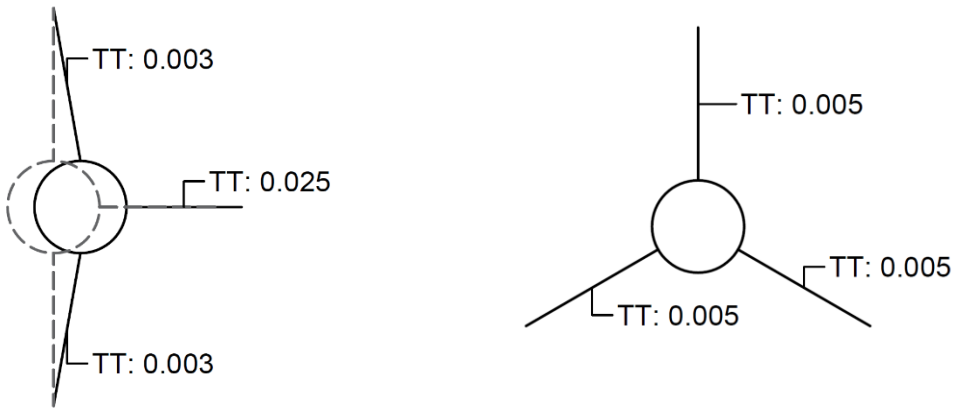

Figure 4-3 – Target Tension Example of a) cords distributed in 180° and b) cords evenly distributed in 360° space (Tice, 2017)

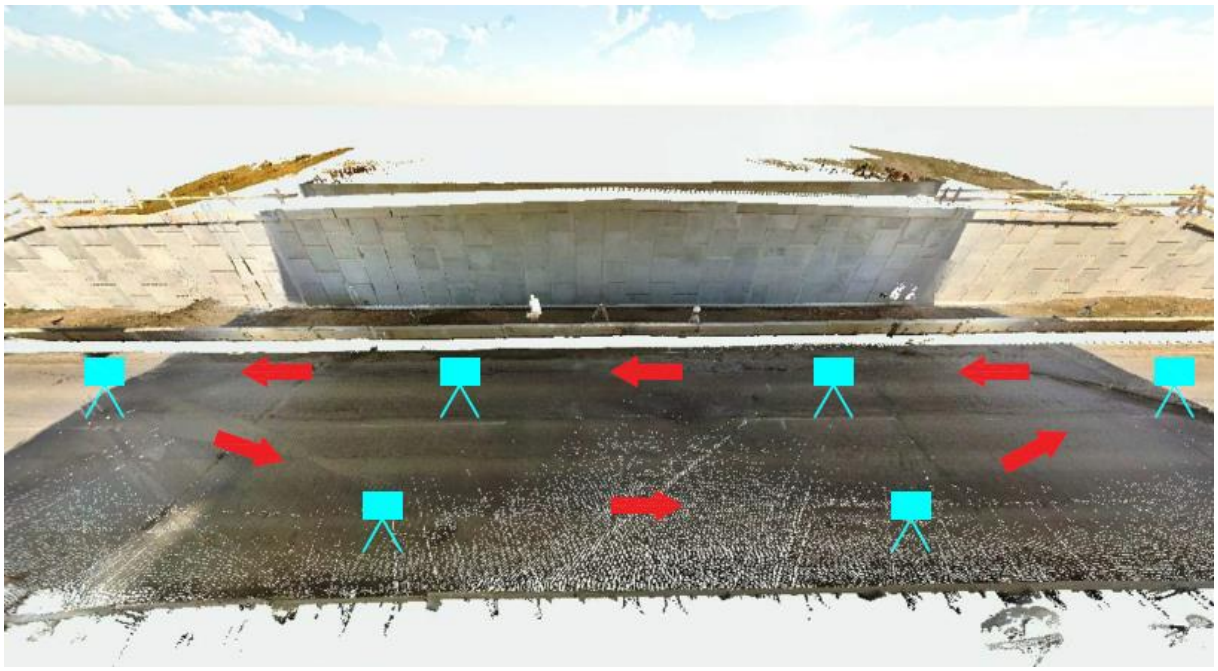

Figure 4-4 – Example Survey Layout for Loop Misclosure

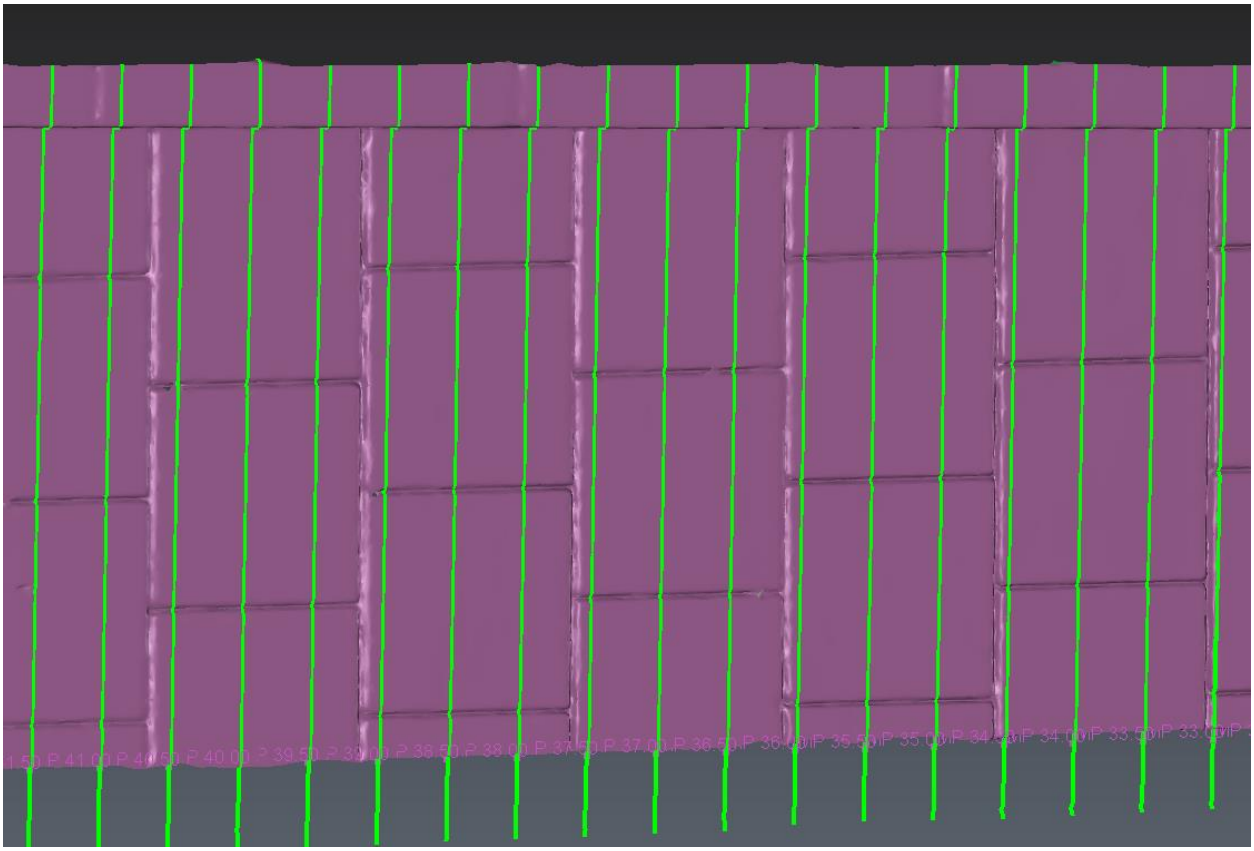

Figure 4-5 – Cross-Sections Taken along the Point Clouds for Deformation Analysis

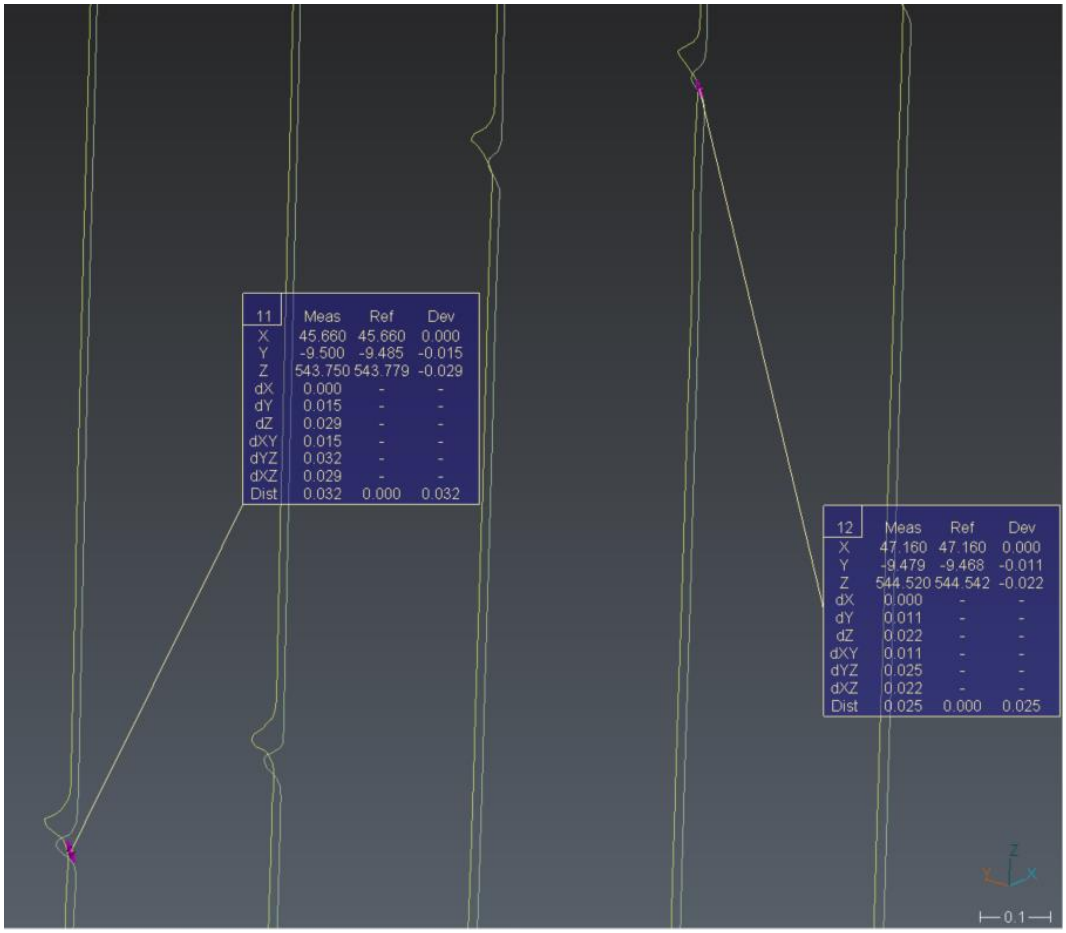

Figure 4-6 – Deformation Measurements in 3D Reshaper

5 Finite Element Method Deformation Analysis

5.1 Introduction

This chapter will discuss the application of Finite Element Method (FEM) for calculating the wall deformations under the loading conditions based on in-situ field instrumentation and borehole log data obtained in Chapter 3. The numerical modelling was carried out using the Geostudio 2019 software program, using the SIGMA/W component to determine the deformations of each bridge abutment. Wall deformations were calculated using both Load/Deformation analyses and Coupled Stress/Pore Water Pressure (PWP) to predict final settlements incurred from each backfill lift of staged construction and the settlement rate influenced by the dissipation of excess pore water pressures.

5.2 Model Characteristics

5.2.1 FEM Software Analysis

The SIGMA/W software component within GeoStudio allows the user to analyze deformations in foundation design, either with or without the influence of excess pore water pressure and can determine the interactions between the soil and structural elements (Geo-Slope International Ltd., 2013). SIGMA/W can also be coupled with SEEP/W analysis to compute the consolidation in saturated soils. This is done using an incremental load formulation that computes relative change in parameters during each stage of analysis, according to the user specified conditions. If in-situ parameters are provided, final conditions on the system performance can be computed. This type of analysis is limited to observing the performance or behaviour of the system as stress and hydraulic parameters are introduced, but it will not compute the stability of the system.

In the case of this research, SIGMA/W was used to compute the deformations and excess pore water pressure responses in the foundation. GeoStudio does not analyze in 3D but can analyze in profile and cross-sectional models, converting axisymmetric parameters in plane strain

conditions. There are many methods to achieve this conversion outlined in Chapter 2.3and a less complex 2D analysis is still effective for computing settlement and pore water pressure behaviour. Load/Deformation analyses apply or remove loads at the beginning of the time step and compute the resulting stresses and displacements (Geo-Slope International Ltd., 2013). They are used in applications such as embankments and excavations. The Coupled Stress/PWP analysis replaces the need for SEEP/W and analyzes the model within the SIGMA/W component. This works by adding a flow equation analysis at each node in the model mesh, along with the displacement equations.

5.2.2 Material Parameters

Table 5-1 provides a summary of the effective-stress parameters used in each deformation analysis and Table 5-4 provides the hydraulic parameters used for the Coupled Stress/PWP analyses based on axisymmetric (two-dimensional) conditions. Material properties were determined as effective-stress parameters from various lab testing results and consulting experience from TREK Geotechnical Inc. (TREK Geotechnical Inc., 2017). The 400kPa preconsolidation pressure (P'c) of the silty clay was determined not to be surpassed by the calculated 360kPa overburden pressure from the embankment backfill. The addition of the rockfill columns reinforcing the foundation beneath the abutment allowed load to be distributed directly into the stronger clay till, rather than the weaker silty clay. The silty clay parameters were given E' = 15,000kPa, v = 0.3, and γ' = 18kN/m3. The clay fill was assumed to behave similarly but have a slightly higher stiffness with E' = 20,000kPa, v = 0.3, and γ' = 18kN/m3. Granular material was assumed to be taken from the same source and therefore the granular fill, rockfill columns, and load transfer pad were all assumed to be linear elastic with E' = 60,000kPa, v = 0.3, and γ' = 21kN/m3. The clay till strength properties were determined from Standard Penetration Test (SPT), and was documented along the entire length of each borehole log. Parameters were set at E' = 60,000kPa, v = 0.3, and γ' = 21kN/m3. The soft silty clay layer however was modelled as a

Modified Cam Clay (MCC) model as this better represents slightly over-consolidated clay than a linear-elastic model in Geostudio (Geo-Slope International Ltd., 2013). MCC parameters were not collected but using the compression and recompression index coefficients, Cc and Cr, the gradient of swelling line and compression line, κ and λ, were found respectively (Skempton & Jones, 1944):

$$\kappa = \frac{C_r}{\ln 10} \text{ and } \lambda = \frac{C_c}{\ln 10} \qquad \text{Eq. 5-1 and 5-2}$$

The effective friction angle, ϕ', can also be converted to the MCC parameter critical state failure, M, found by the equation:

$$M = \frac{6 \sin \phi'}{3 - \sin \phi'} \qquad \text{Eq. 5-3}$$

This equation is used for normally consolidated clay but because the soft silty clay is slightly over-consolidated and a lack of other data for conversion, it was assumed to follow this relationship. The soft silty clay parameters were determined as M = 0.772, γ' = 18kN/m^3, ν = 0.3, λ = 0.17, κ = 0.036, e = 1, and OCR = 1.2 from the TREK Design Report (2017) and from one-dimensional settlement analysis.

The segmented wall panels and high strength geogrid were modelled as structural beam elements, as provided in Table 5-2, as they both exhibited compressive, tensile, and moment resistances, but weight were considered negligible. The concrete wall panels were void of tensile forces and were given parameters E' = 27,900MPa, A = 0.45m^2, and I = 0.0035m^4, where E' was estimated using the modulus of elasticity equation (CSA International, 2000) with a concrete compressive strength of 45MPa. The geogrid was exempt of compressive forces and the parameters were provided by TREK Geotechnical Inc. with an E-modulus of 492MPa, A = 0.004m^2, and I = 0m^4 (height to width ratio considers this to be zero).

Since 3D parameters cannot be analyzed in the Geostudio software, as explained in Chapter 5.2.1, axisymmetric conditions were converted to plane strain conditions. Rockfill column

parameters were converted as 2D models assume continuity through the third dimension. The different cases will be categorized as Case A, B, and C to observe the influence of different conversion methods (Ariyarathne, et al., 2013). The model parameters used by TREK was also be compared, all outlined in Table 5-3. Case A and the TREK model maintained the same column properties, but Case B and C converted the column properties using the plane strain conversion equation Eq. 2-5, computing the stiffness of rectangular and triangular spaced columns for both model orientations.

Hydraulic conductivity, k, parameters for soil materials were determined from back calculating pore water pressure responses in piezometric elevation readings in the south abutment, as explained in Chapter 5.3.1, and summarized in Table 5-4. Silty clay and clay fill were the least permeable with a k of 4.32×10^{-4}m/d, soft silty clay was more permeable with k = 4.32×10^{-3}m/d (higher silt content) and clay till was the most permeable out of the foundation soils with k = 2.16×10^{-2}m/d. Granular material was given a high value of k = 10m/d to signify a free-flowing material. These hydraulic conductivity values were then used for the north abutment model.

Once the axisymmetric hydraulic properties were determined for each abutment, conversion into plane strain conditions were required for the Drainage Influenced Soil Zone (DISZ) of each abutment. Eq. 2-12 and 2-13 were considered to determine the hydraulic conductivities in the silty clay and soft silty clay as shown in Table 5-5 for both north and south abutments. These values differ between columns as each had different spacings in the third-dimension direction, resulting in different magnitudes of drainage influence. Tan et al. (2008) cites that if the model will use Eqs. 2-8, 2-10, and 2-11 for the conversion of strength properties, it cannot be combined with Eq. 2-12 and 2-13 as these equations assume equal flow path between axisymmetric and plane strain drainage zones. The flow path R was considered equal to the drainage zone diameter B to ensure equation applicability (in Figure 2-6).

5.2.3 Geometry and Boundary Conditions

Two section models were created for deformation analysis: a profile view running perpendicular to the wall along the centreline of the embankment and a cross-section view running parallel along the base of the wall facing panels. The profile model was not a true plane strain model as the embankments were not at the same height infinitely long in the third dimension but the top width was long enough to explore the stress/strain response of the foundation to the embankment and how the pore water pressure dissipated. The cross-sectional model was not a true plane strain model as well as it was taken just behind the wall, within the reinforced zone. The embankment height could be considered infinitely long away from the bridge but past the wall there was no stress acting on the foundation. Because of these limitations, the results from this analysis were observed for behaviour and predicted magnitude of settlement will be expected to have discrepancies from the surveying results.

The belled piles as part of the foundation design were not included in this analysis as their inclusion was too complex to model in plane strain conditions. The location of the belled piles within the spacing of the rectangular spaced columns could create skin friction to reduce the settlement of the foundation beneath the wall.

Profile Model

The in-situ stage was modelled with the rockfill columns installed, the granular transfer pad overlying the foundation, and the first row of wall panels placed without the backfill. Figure 5-1 shows the model geometry for the south abutment. A geogrid sheet modelled as a structural beam element was placed on top of the granular pad and sat underneath granular backfill as indicated in the design report (TREK Geotechnical Inc., 2017). Soil layer elevations for the north and south abutments were determined by review of borehole log information collected near each abutment, initial fill elevations recorded in Figure 3-3 and Figure 3-4, and assumed linear interpolated layer boundaries for each soil material. The soil stratigraphy for the north abutment began with the

ground surface or silty clay began at 508m elevation (11.5m thickness), soft silty clay began at 496.5m (0.5m thickness), and clay till began at 496m until 490m (6m thickness) to reduce boundary influence. Underneath the wall panels, the top elevation of the granular pad was at 507.0m and ended at 506.5m. The south abutment had silty clay begin at 508m elevation (9.5m thickness), soft silty clay began at 498.5m (1.5m thickness), and clay till began at 497m until 490m (7m thickness). The granular pad top elevation underneath the wall panels was 506.5m and ended at 506.0m. An example of the completed stage for the south abutment is given in Figure 5-2 while Figure 5-3 includes the DISZ in the silty clay and soft silty clay layers. Stated in the previous chapter, different cases were developed to observe the influence of plane strain conversion for stone columns. This altered the geometry of the columns, depending on the spacing using Eq 2-2 as there were four different groups of columns altered. Case B did not alter the column thicknesses but Case A, C, and TREK split up column group thicknesses into 1.8mØ, 2.1mØ, 1.8mØ @4.1m, and 1.8mØ @5.1m, as referenced in Table 5-3 – Rockfill Column Plane Strain Parameters. The respective thicknesses for each thickness group were 0.97m, 1.04m, 0.62m, and 0.50m. Embankment backfill, as explained Chapter 5.3, was decided to be modelled in 1m lifts to simplify the construction schedule (lack of accurate knowledge of placement timing for each lift) but still limit the influence of large immediate loads on the foundation.

The staged analysis established the initial stress conditions for each soil material layer and defined the pore water pressure conditions by user-defined water table elevation (TREK Geotechnical Inc., 2017), determined from initial piezometric elevation from field instrumentation referenced in Chapter 3.6. The initial water table elevations were specified in Figure 3-3 and Figure 3-4 at 506m and 505.5m for the north and south abutment respectively.

The profile model was restrained horizontally and vertically along the bottom border of clay till and only horizontal restraints along the ends of the model, into the approach embankment and existing roadway; the left and right borders were extended far enough that the foundation stresses were

not affected by these boundary conditions. Horizontal restraints were added to each clay fill lift as they were constructed.

The pore water pressure analysis used the same geometry as the Effective Stress Analysis (ESA) except that it included the DISZ. These zones were determined by using Eq. 2-9, developed by Barron (1948), with the plane strain flow path diameter assumed equal to its axisymmetric diameter, stated in Chapter 5.2.2. DISZ diameters are given in the last column of Table 5-5, relative to its specific column spacing section.

Additional boundary conditions for the Coupled Stress/PWP analysis were applied to soil geometry lines to indicate water pressure parameters, as shown in Figure 5-3. Constant pressure head boundary lines of 8.5m and 10m were applied to the right of the MSE wall along the soft silty clay/clay till interface for the south and north abutments respectively. This was to simulate the long-term clay till pressure head that had been maintained prior to construction (Van Helden, et al., 2008). Along the granular pad perimeter, constant pressure head boundaries were applied to simulate the flow of pore water pressure into this material.

Cross-Section Model

The boundary conditions applied on the model were horizontal restraints along the extents of the model while the bottom of the clay till was restrained vertically and horizontally. Included for pore water pressure analysis, a constant water pressure head along the clay till/soft silty clay interface, and the constant pressure head conditions along granular material boundaries were applied, same as the profile models.

The cross-section models shared the same time steps and general parameters as their respective profile models; The main difference being the geometry of the embankment fill shape and the rockfill column thicknesses. The embankment fill shape was constructed following the MSE wall facing panels design elevations as granular material was backfilled up until the height

of the wall. Since the model was taken just behind the wall (<1m), conversion for clay fill material existing beyond the reinforced zone was not considered and the granular material parameters equaled their axisymmetric values. The rectangular spaced rockfill column thicknesses were determined using the same equations as the profile model, each having a thickness of 0.88m as shown in Table 5-3. The triangular spaced columns were converted using a length of 5.74m, resulting in a thickness of 0.6m as demonstrated in Figure 5-4. The alignment of the first and third row of columns with the second row increased the number of columns outside the bridge deck by almost double, but reduced the thickness by 1/3.

The cross-sectional models are presented in Figure 5-5 and Figure 5-6, during the initial and final stages of analysis. The TREK case converted the columns underneath the wall rather than an equivalent soil wall through the embankment into the next row of columns. The width of the plane strain columns were developed from the ratio of granular fill to silty clay within a square around the column. The ratio was calculated as 0.785, resulting in column thicknesses of 1.4m and 1.7m for the 1.8mØ rectangular and the 2.1mØ triangular spaced columns respectively. The storm water and sewer pipes underneath the east section of each wall were sketched underneath to acknowledge their presence as the interaction between the pipes and soil was not known. Therefore, the silty clay and soft silty clay were modelled in the area without parameter alteration. This may result in increased settlement as reference in Chapter 3.4 but installation of the pipes may have removed the soft silty clay and replaced it with a more granular material, resulting in less settlement. Confirmation with surveying results will provide understanding of this area's conditions.

An additional cross-section was taken at the piezometer outside of the columns (TH17-01) as the soil and embankment conditions were long enough in the third dimension to better exemplify the pore water pressure dissipation behaviour. The cross-sectional model had no foundation reinforcement and embankment material was clay fill, as be seen in Figure 5-8.

5.3 Methodology

5.3.1 Model Calibration

To begin the modelling analysis, the first objective was to replicate the results TREK Geotechnical Inc. computed in their design report addendum. This was to understand how results were obtained and provided a baseline of where to begin the model, adding more complexity where required. Relevant information was provided by TREK (2017) including the material parameters, geometries and boundary conditions, and result outputs in the form of vertical effective stress and settlement profiles.

Once the baseline model was developed, review of the borehole logs, lab testing results, and foundation design geometry was done to determine if there were any assumptions or simplifications of the model that may limit the prediction potential to site conditions. It was found that a soft silty clay layer that transitions between the silty clay and clay till layers was not included. The pressure induced from the overlying material layers on this soft layer created the potential for more settlement to develop. This effect will be assessed from the modeling results.

To determine the thickness of the soft silty clay layers, three boreholes were selected in the vicinity of the north abutment and two for the south abutment; MC-16-001, TKMC-16-01, and TKMC-16-03 for the north abutment, and TKMC-16-02 and TKMC-16-06 for the south abutment; layout provided in Figure 5-9. The south abutment had soft silt or clay layers that were generally observed to be found from 498.5m to 497.0m in both holes and thus, it was assumed to be a linear interpolation of the layer thickness due to the lack of other borehole information. The north abutment however was more complicated as the boreholes were more spread out and none were exactly taken within the reinforced zone. Elevation layers were selected based on judgement and assumptions were made to simplify the model geometry. The boreholes in this area were less conclusive on the amount of soft soil in the area: one found the soft material, the other did not, and thus it was assumed to be 0.5m thick. Observing the elevations of till in each borehole log,

they were logged at 496.18m and 496.2m on the Westside, and 498.1m on the Eastside. Clay till elevations were made constant at 496m to keep column lengths equal along the wall. This simplification overestimated the amount of weaker clay on the Eastside and increased the potential for more settlement to occur.

The embankment construction on site was staged in backfill lifts of 0.15m increments until completion. However, it was unknown when each lift was placed to the exact date. Consequently, the modelled construction schedule was determined from reviewing the fill elevations from the pore water pressure responses in the monitoring report and observing pictures taken from site visits. Lifts were modelled in 1m increments as each concrete panel was generally 1-1.5m tall, ensuring an accurate representation of the amount of fill that was placed for each row of panels. This also simplified the amount of analysis stages and time between each stage.

Once geometry dimensions were completed, pore pressure calibration was performed using the south abutment's monitoring report data and different sources containing site testing and soil classification. Ranges of hydraulic conductivities were developed for silty clay [$8.64x10^{-2}$ – $8.64x10^{-7}$]m/d, silt (soft silty clay) [$4.32x10^{-1}$ – $8.64x10^{-3}$]m/d, and clay till [$2.59x10^{-1}$ – $8.64x10^{-6}$]m/d from previous soil testing results (MDH Engineered Solutions, 2011). User-selected values within these ranges were used to create the plane strain hydraulic conductivities for the DISZ, depending on the column spacing. Using a trial and error approach, the selected values were inputted into the profile model to calibrate the piezometer reading output results outside and within the reinforced soil zone. The cross-section model developed for the piezometer located in TH17-01 was compared against the profile model to observe the influence of plane strain geometry assumptions. Once the pore water pressure response comparison was acceptable, final axisymmetric parameters were tabulated and referenced in Table 5-4. Hydraulic conductivities of silty clay and soft silty clay in plane strain are provided in Table 5-5.

5.3.2 Effective Stress Analysis

The ESA was first used to determine the final consolidation for each stage of embankment loading as less parameters were required to compute settlements. Since pore water pressure parameters were not used in this analysis, the schedule or duration of each time step was not considered, and each lift was given a time step of 1 unit (days in this case). Once wall height was reached with granular fill (513.6m for both north and south abutment), a final lift was added to reach bridge deck height or final approach embankment height (516.2m). This lift was not applied directly on top of the wall as the bridge deck girder is present, however this fill height was within the reinforced zone and load transfer from the top of fill to the top of wall. This can be better viewed in the profile model in Figure 5-2 or pictures from site located in Appendix A – Site Photos. The four different cases of converting column parameters into an equivalent soil wall were computed and compared against each other to determine the most applicable representation. Settlement was observed at the base of the granular pad, the boundary above the silty clay.

5.3.3 Coupled Stress/PWP Analysis

Coupled Stress/PWP analysis was performed after results from ESA were completed. This analysis shared the same model geometries as the accepted case of modelling the equivalent soil wall from ESA except it added DISZs within the foundation, included hydraulic parameters such as hydraulic conductivities, and included additional pore water pressure boundary conditions, as outlined in Chapter 5.2.3.

The DISZs for the cross-sectional models were assumed to influence the soil's flow path in the horizontal direction and the soil underneath the shortened columns was not considered influenced and remained using axisymmetric silty clay parameters, as seen in Figure 5-7. DISZ was not applied in this area as the change in soil material was unknown, whether granular material was used or the silty clay was backfilled, therefore parameters were not altered. Time steps were then created from analyzing the added fill lifts using site photos, and elevations from the monitoring

report. Pore water pressure analysis was best tailored to the construction schedule and was used for both the pore water pressure response in piezometers (explained in Chapter 5.3.1) and settlement over time. Time steps are recorded in Table 5-6, outlining lift durations for both the north and south abutments. Settlement again was observed at the bottom of the granular pad.

5.4 Summary of Finite Element Modelling

FEM to determine foundation settlement and excess pore water pressure response calibration were carried out using Geostudio's SIGMA/W 2D modelling software package. This modelling package had the capabilities to both analyze the load/deformation response as each lift of backfill was applied during construction, as well computing the changes in pore water pressure within the different permeable foundation materials.

From the acquired borehole log data obtained from previous site investigations and the settlement prediction models provided by TREK Geotechnical Inc. in their design report (2017), a more updated model was developed to include a soft silty clay layer in the transition between clay and till. All materials were characterized with effective stress parameters and strengths followed a linear-elastic behaviour, however the soft silty clay was modelled as MCC. Because of the 3D site being modelled in 2D, the rows of rockfill columns within the foundation were combined with the silty clay to create equivalent soil walls to represent the stiffness difference between materials. The hydraulic conductivity parameters for each material was not provided in the previous models, nor were specific permeability tests undergone. Therefore, local lab testing results on hydraulic conductivity were found and calibrated with the south abutment piezometer monitoring report results.

Because 3D modelling is not available in GeoStudio computer program, 2D modelling was used. In this case, analyses were carried out in two different models; a profile section that runs perpendicular to the wall and into the centreline of the embankment, and a cross-section that runs parallel along the wall from end to end. The profile model was primarily used to calibrate hydraulic

permeability parameters from the piezometer data and observe the settlement change from within the reinforced foundation zone and into the unreinforced zone underneath the embankment. The cross-section model was primarily used to determine the settlement underneath the MSE wall from varying underneath the side slopes and max height of embankment, as well compare the theoretical settlements to what was observed in the field from surveying.

For pore water pressure calibration modelling, the Coupled Stress/PWP analysis was chosen and nodes were placed at the coordinates of each piezometer installed on site. Then through an iterative process of selecting k values from a range provided in previous literature was performed until the pore water pressure response was representative of what was obtained from the piezometers.

For settlement analysis, ESA was first performed to determine settlements without the need for additional information on hydraulic properties. Then after pore water pressure calibration was accepted and preliminary settlement results were considered adequate for what site parameters were selected, time stamps were designated for each lift of backfill and settlement recordings corresponded with the dates of TLS surveying for direct comparisons.

Table 5-1– Axisymmetric Effective-Stress Parameters (TREK Geotechnical Inc., 2017)

Material	Model	E'(kPa)	M(°)	γ(kN/m3)	ν	λ	κ	e	OCR
Clay Fill	Linear-Elastic	20000		18	0.3				
Granular Fill	Linear-Elastic	60000		21	0.3				
Reinforced Granular Fill	Linear-Elastic	60000		21	0.3				
Stone Columns	Linear-Elastic	60000		21	0.3				
Silty Clay	Linear-Elastic	15000		18	0.3				
Soft Silty Clay	Modified Cam Clay		0.772	18	0.3	0.17	0.036	1	1.2
Clay Till	Linear-Elastic	60000		21	0.3				

Table 5-2 – Structural Member Parameters

Material	E' (MPa)	Cross-Sectional Area (m^2)	Moment of Inertia (m^4)
MSE Wall Panel (concrete)	27,900	0.45	0.0035
Geosynthetic (Tensar BX1500)	492	0.004	0

Table 5-3 – Rockfill Column Plane Strain Parameters

CASE A	Material	t (m)	E (kPa)	γ (kN/m³)
Profile Model	1.8mØ Stone Columns	0.97	60000	21
	2.1mØ Stone Columns	1.04	60000	21
	1.8mØ Stone Columns @4.1m	0.62	60000	21
	1.8mØ Stone Columns @5.1m	0.50	60000	21
Cross-Section Model	1.8mØ Stone Columns	0.88	60000	21
	2.1mØ Stone Columns	0.60	60000	21

CASE B	Material	t (m)	E (kPa)	γ (kN/m³)
Profile Model	1.8mØ Stone Columns	1.8	39236	19.62
	2.1mØ Stone Columns	2.1	37287	19.49
	1.8mØ Stone Columns @4.1m	1.8	30475	19.03
	1.8mØ Stone Columns @5.1m	1.8	27452	18.83
Cross-Section Model	1.8mØ Stone Columns	1.8	36885	19.46
	2.1mØ Stone Columns	2.1	33367	19.22

CASE C	Material	t (m)	E (kPa)	γ (kN/m³)
Profile Model	1.8mØ Stone Columns	0.97	39236	19.62
	2.1mØ Stone Columns	1.04	37287	19.49
	1.8mØ Stone Columns @4.1m	0.62	30475	19.03
	1.8mØ Stone Columns @5.1m	0.50	27452	18.83
Cross-Section Model	1.8mØ Stone Columns	0.88	36885	19.46
	2.1mØ Stone Columns	0.60	25281	18.69

TREK	Material	t (m)	E (kPa)	γ (kN/m³)
Profile Model	1.8mØ Stone Columns	0.97	60000	21
	2.1mØ Stone Columns	1.04	60000	21
	1.8mØ Stone Columns @4.1m	0.62	60000	21
	1.8mØ Stone Columns @5.1m	0.50	60000	21
Cross-Section Model	1.8mØ Stone Columns	1.4	60000	21
	2.1mØ Stone Columns	1.7	60000	21

Table 5-4 – Two-dimensional Hydraulic Properties of Soil Materials

Material	Saturated W.C.	Hydraulic Conductivity (m/d)	k_y'/k_x'
Clay Fill	0.4	4.32×10^{-4}	1
Granular Fill	0.2	1.00×10^{1}	1
Reinforced Granular Fill	0.2	1.00×10^{1}	1
Stone Columns	0.2	1.00×10^{1}	1
Silty Clay	0.4	4.32×10^{-4}	1
Soft Silty Clay	0.4	4.32×10^{-3}	1
Clay Till	0.4	2.16×10^{-2}	1

Table 5-5 – Silty Clay Hydraulic Conductivity Plane Strain Parameters

	Material	k_{pl} (m/d)	Drain Influence Soil Zone Diameter (m)
Profile Model	Silty Clay – 1.8mØ Stone Columns	1.55×10^{-3}	2.97
	Silty Clay – 2.1mØ Stone Columns	1.54×10^{-3}	3.50
	Silty Clay – 1.8mØ Stone Columns @4.1m	0.71×10^{-3}	4.65
	Silty Clay – 1.8mØ Stone Columns @5.1m	0.51×10^{-3}	5.77
	Soft Silty Clay – 1.8mØ Stone Columns	1.55×10^{-2}	2.97
	Soft Silty Clay – 2.1mØ Stone Columns	1.54×10^{-2}	3.50
	Soft Silty Clay – 1.8mØ Stone Columns @4.1m	0.71×10^{-2}	4.65
	Soft Silty Clay – 1.8mØ Stone Columns @5.1m	0.51×10^{-2}	5.77
Cross-Section Model	Silty Clay – 1.8mØ Stone Columns	1.33×10^{-3}	3.28
	Silty Clay – 2.1mØ Stone Columns	1.61×10^{-3}	3.35
	Soft Silty Clay – 1.8mØ Stone Columns	1.33×10^{-2}	3.28
	Soft Silty Clay – 2.1mØ Stone Columns	1.61×10^{-2}	3.35

Table 5-6 – Time Step Durations in Coupled Stress/PWP Analysis for North and South Abutments

North Abutment	Time Step	Time (Days)
Profile Model	First Lift	5
	Second Lift	7
	Third Lift Part 1	12
	Third Lift Part 2	15
	Third Lift Part 3	16
	Fourth Lift Part 1	8
	Completion Part 1	8
	Completion Part 2	8
	Completion Part 3	8
	Completion Part 4	12
	Completion Part 5	369
Cross-Section Model	First Lift	5
	Second Lift	7
	Third Lift Part 1	12
	Third Lift Part 2	31
	Fourth Lift	8
	Completion Part 1	8
	Completion Part 2	20
	Completion Part 3	381

South Abutment	Time Step	Time (Days)
Profile Model	First Lift	10
	Second Lift	8
	Third Lift Part 1	20
	Third Lift Part 2	10
	Third Lift Part 3	10
	Fourth Lift Part 1	10
	Fourth Lift Part 2	10
	Fourth Lift Part 3	10
	Fourth Lift Part 4	10
	Completion Part 1	14
	Completion Part 2	360
Cross-Section Model	First Lift	10
	Second Lift	8
	Third Lift Part 1	30
	Third Lift Part 2	10
	Fourth Lift Part 1	20
	Fourth Lift Part 2	20
	Completion Part 1	14
	Completion Part 2	360

Color	Name
	Clay Fill
	Clay Till
	Granular Fill
	Reinforced Granular Fill
	Silty Clay
	Soft Silty Clay
	Stone Columns 1.8m
	Stone Columns 1.8m 4.1m spacing
	Stone Columns 1.8m 5.1m spacing
	Stone Columns 2.1m

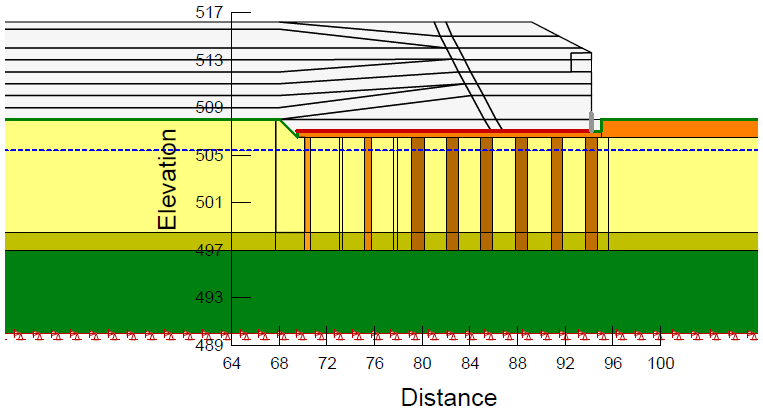

Figure 5-1 – FEM South Abutment Profile Model In-situ Stage

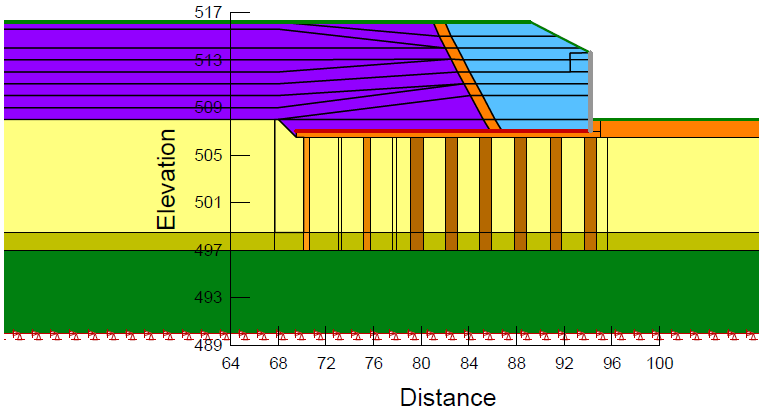

Figure 5-2 – FEM South Abutment Profile Model Completed Stage

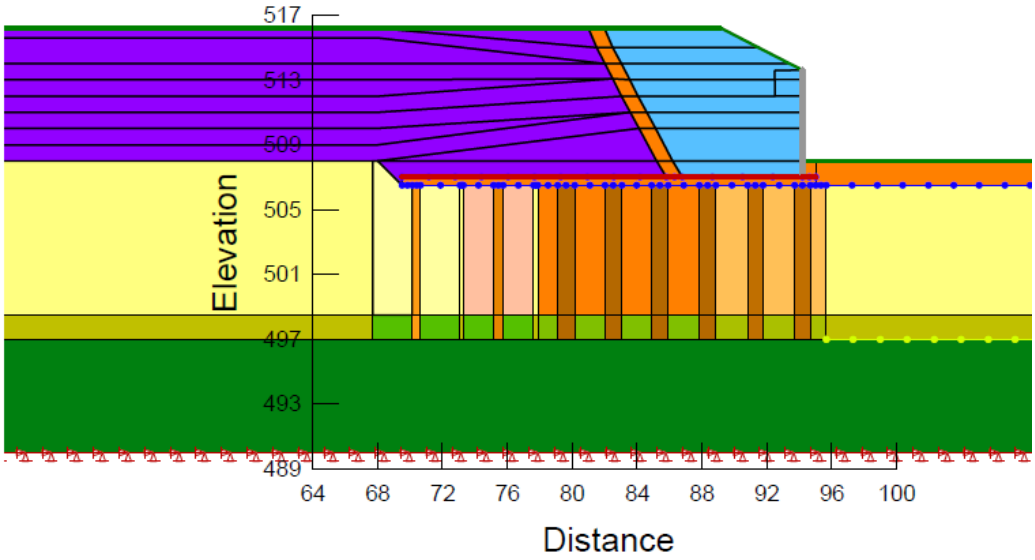

Figure 5-3 – FEM South Abutment Profile Model Completed Stage with Drainage Influenced Soil Zones

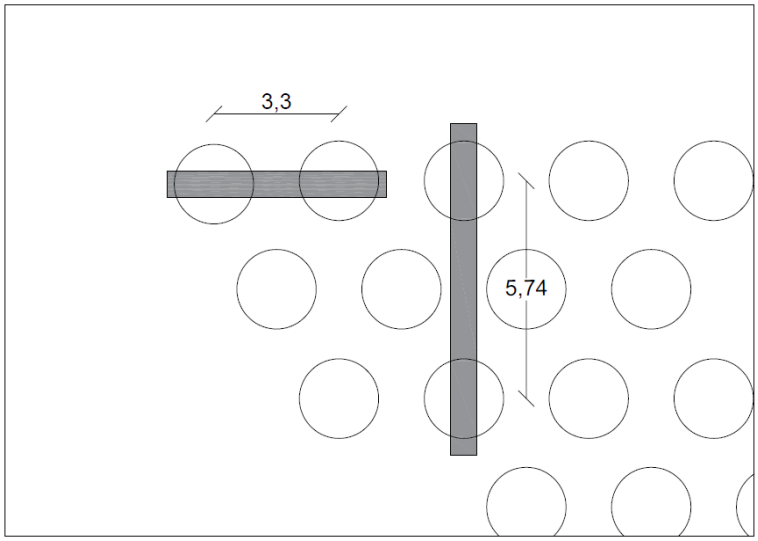

Figure 5-4 – Equivalent Wall Spacing for Profile and Cross-Section Models

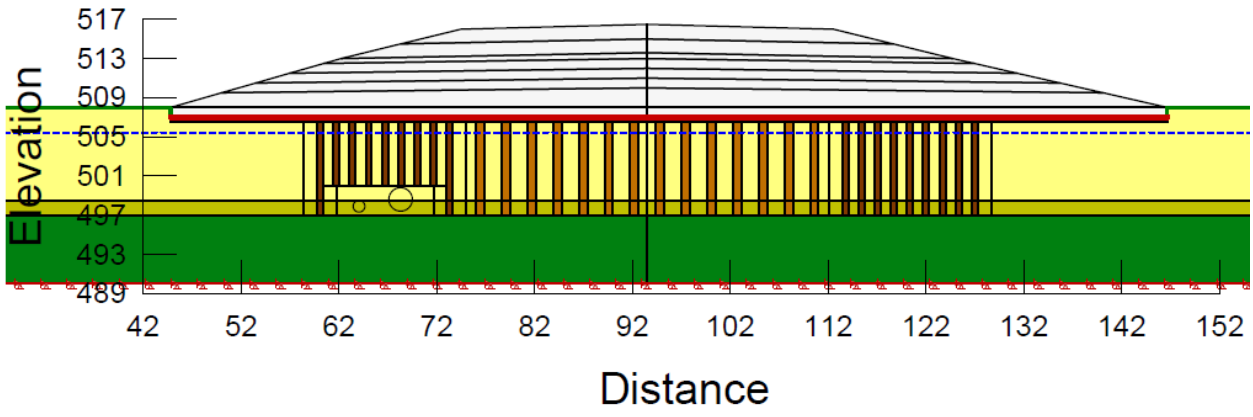

Figure 5-5 – FEM South Abutment Cross-Section Model In-situ Stage

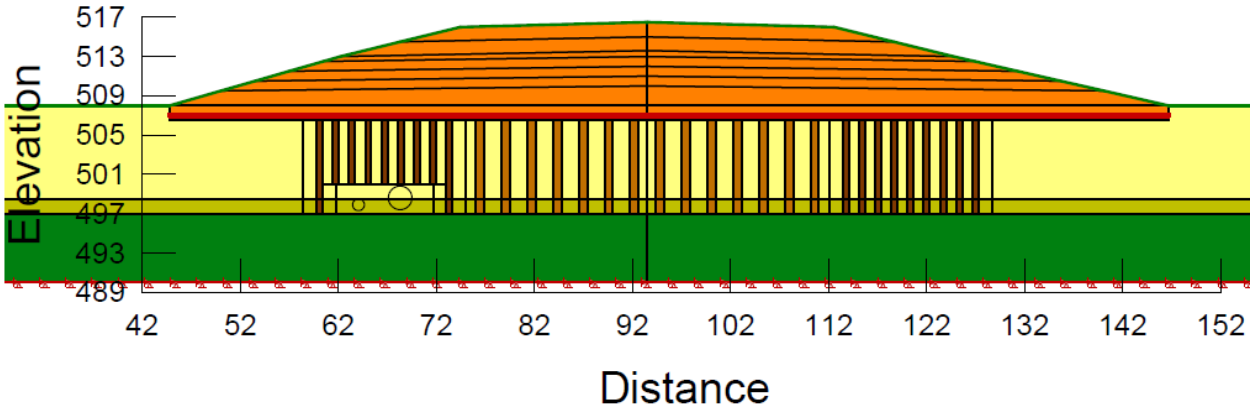

Figure 5-6 – FEM South Abutment Cross-Section Model Completed Stage

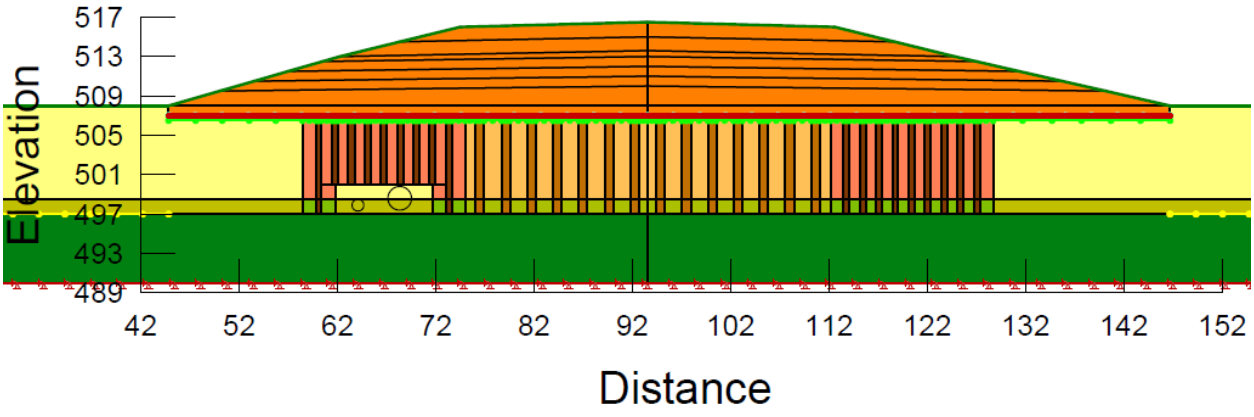

Figure 5-7 – FEM South Abutment Cross-Section Model Completed Stage with Drainage Influenced Soil Zones

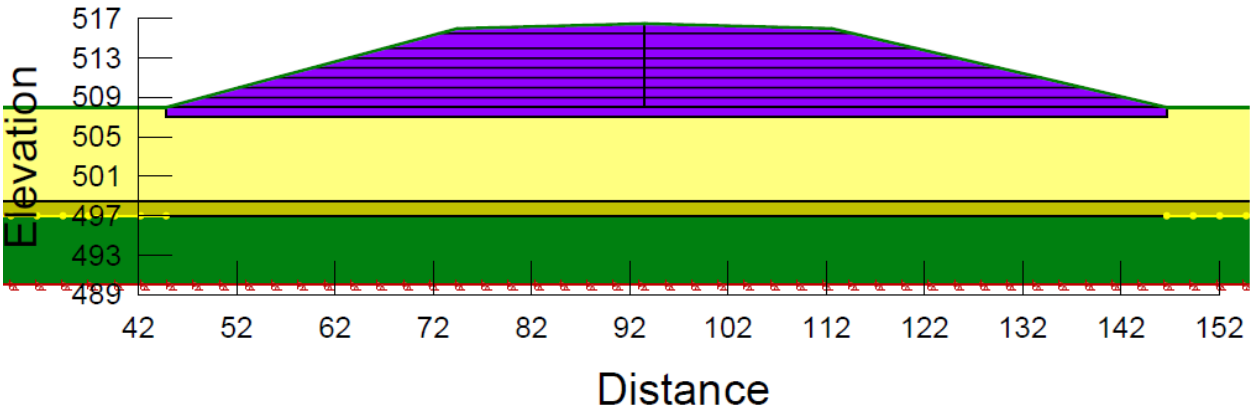

Figure 5-8 – FEM South Abutment Cross-Section Model TH17-01 Piezometer Water Pressure Model

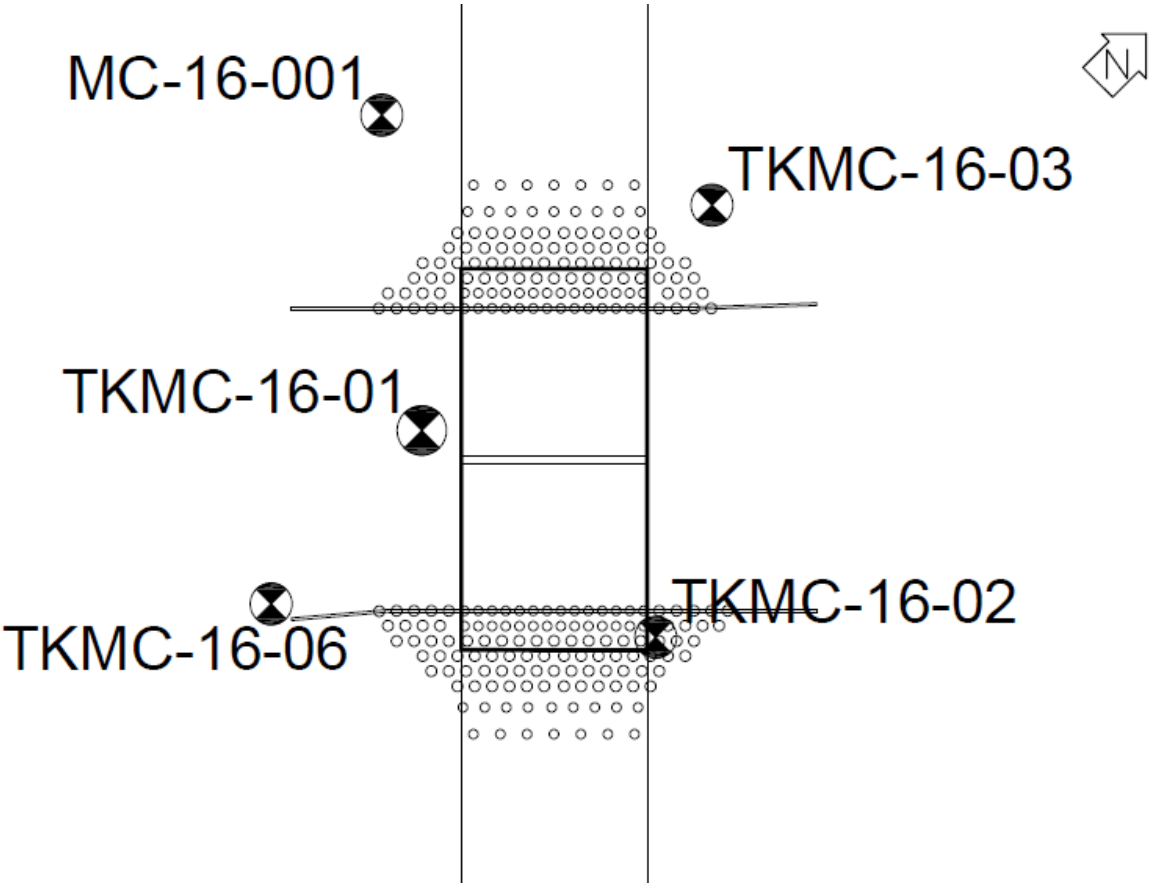

Figure 5-9 – Boreholes used for each Abutment (TREK Geotechnical Inc., 2017)

6 1D Consolidation Analysis

6.1 1D Consolidation Software Background

Settle3 is a modelling program developed by RocScience that analyzes vertical settlement within foundation soils from embankment and fill loading cases in a 3D model space (RocScience Inc., 2020). Settlement is computed in three stages: 1) Immediate settlement, determined based on the soil material's stiffness; 2) Primary consolidation, influenced by the material's consolidation and pore water pressure properties; and 3) Secondary consolidation, the creep settlement of the material computed from the secondary compression indexes (RocScience Inc., 2009). User-specified stress behaviour of the analysis can select either Boussinesq, the 2:1 method, Multi-layer, and Westergaard to name a few, allowing for different loading cases and assumptions for design. Soil layers are developed by inputting borehole data with specific XY coordinates and given Z elevations or depth below ground surface for layer boundaries. Figure 6-1 provides an example of the model foundation created from the borehole data. Then when layers are generated, the lab tested strength and hydraulic properties can specify settlement behaviour.

The main limitation of this software is that it uses 1D consolidation analysis to compute vertical settlements and therefore, the model geometry does not influence the behaviour of stresses in the XY direction. The advantages of using the 1D consolidation analysis within a 3D model space is that it will cut down on computation time compared to FEM modelling and avoids the assumption of converting soil properties into plane strain conditions when using a 2D model analysis. The purpose of this analysis was to compare the 2D FEM modelling against the 1D consolidation analysis in 3D space and determine if each model results agree with the other method.

6.2 Material Parameters

Table 6-1 provides a summary of all the soil material parameters used for the settlement analysis. The soil materials repeated the stiffness values used for FEM to calculate the immediate settlement; $E_{Granular}$ = 60MPa, $E_{Silty\ Clay}$ = 15MPa, $E_{Soft\ Silty\ Clay}$ = 15MPa, and $E_{Clay\ Till}$ = 60MPa. Each

material was also given a poisson's ratio v = 0.3. Behaviours were either classified as linear or non-linear for primary consolidation. Granular material and clay till layers were considered only to experience immediate settlements and therefore, will only settle based on elastic stiffness values. Silty clay and soft silty clay layers were modelled to settle non-linearly and thus parameters were determined from 1D consolidation lab testing. Oedometer testing results provided in the TREK Design Report (2017) provided silty clay consolidation parameters were Cc = 0.246, Cr = 0.115, e_0 = 1, P'c = 550kPa; and soft silty clay were Cc = 0.365, Cr = 0.083, e_0 = 1 , and P'c = 400kPa. The hydraulic conductivities for these two soil layers were copied from the FEM analysis, with $k_{Silty\ Clay}$ = $4.32x10^{-4}$m/day and $k_{Soft\ Silty\ Clay}$ = $4.32x10^{-3}$m/day.

Table 6-2 provides each of the ratio and factor values and the computed equivalent stiffnesses for the stone column reinforced zones. The stone columns were given a stiffness of 60MPa as outlined in the methodology chapter. Discussed in Chapter 6.4, wick drains were selected to have single drainage as pore water would only flow up through the columns to the granular pad at the ground surface.

The embankment loading on the foundation was modelled by a flexible pressure applied at the ground surface, only requiring the unit weight. Taken to be the same from the FEM modelling, granular fill was 21kN/m^3 and clay fill was 18kN/m^3.

The absence of the high strength geogrid located on the top of the granular pad was due to the software not having the capability to include structural beams within the model. This exclusion would promote larger differential settlements and increase the magnitude of settlements in weaker soil areas.

6.3 Model Geometry

Boundary conditions used in FEM were not applied in this analysis because settlement was analyzed in 1D strings and each string was independent of each other. For pore water pressure

conditions, a drainage boundary was designated along the bottom layer of the granular material to signify pore pressure flow towards this surface. Pore water pressure conditions were based on the piezometric line, located at a depth of 1.5m below ground surface in both abutment models.

The geometry of the analysis was created in three dimensions, containing the reinforced zone and extending 20m through the approach embankment. In Figure 6-2, a model of the in-situ stage of just the foundation soil and the column reinforcement is presented. The ground surface elevation was 507.5m and 506.5m for the north and south abutments respectively; the surface elevation behind the MSE wall. Soil layer thicknesses selected within the reinforced zone for the south abutment were 0.5m for granular material, 9.5m for silty clay, 1.5m for soft silty clay, and 6m for clay till. The north abutment shared similar thicknesses except the silty clay was 10.5m and soft silty clay was 0.5m. Outside of the reinforced zone, the granular material layer was reduced to 0m and the silty clay layer was increased by 0.5m (north abutment layer was 11m and the south abutment layer is 10m).

Each of the reinforced soil regions were traced around the areas of each column grouping as shown in Figure 3-1. The specified spacings and diameters of each column group were also designated a depth of 11m, drilled 1m into the clay till layer. The wick drain regions were added to the same column region boundaries. The belled piles were not included within the model as there was no option to include their geometry within the rockfill columns. This exclusion will also increase the amount of settlement computed within the centre section, like the situation from FEM modelling as stated in Chapter 5.2.3.

Modelled after the profile models from FEM, the embankment loads were split into four sections: 1) granular fill placed directly behind the wall, 2) granular fill sloping back towards the bridge deck elevation, 3) granular fill at design elevation within the reinforced zone, and 4) clay fill that completes the rest of the embankment. This can all be seen in Figure 6-3 where final embankment heights are placed on the foundation. Embankment side slopes were modelled after the MSE wall

shape and the height of each fill layer mirrored that of the finite element models. There were two side slope angles for the embankments: 1V:3H following the slope of the MSE wall and 1V:4H once past the MSE wall elevation, sloping towards the design elevation.

6.4 Methodology

The model layouts for each abutment were determined from placing boreholes in an XY coordinate space, designating soil layer elevations at a depth of Z, and interpolating soil profiles between boreholes using Delaunay triangulation method. This limitation reduced the amount of settlement analyzed farther away from the MSE wall (embankment sections 3 and 4) as the levelling pad was placed within an excavated area and the embankment load fills cannot be altered to compensate for the missing soil thickness. However, the main objective was to observe settlement along the wall and provide comparison, therefore the limitation will not impact these results.

Once soil profiles were created, the material properties were selected for each appropriate settlement analysis. Primary consolidation was selected for silty clay and soft silty clay as: 1) these are the weakest layers and would undergo larger settlements, 2) these layers have smaller hydraulic conductivities, influencing the rate of settlement, and 3) lack of 1D consolidation testing results for clay till and the granular material. Although the silty clay was assumed to be linear in FEM, it was considered non-linear here as settlement was determined by compression indexes and included a user-specified preconsolidation pressure. Secondary settlement analysis was not selected for any of the soil layers as lack of creep behaviour information and the duration of embankment loading observed from the surveying was not long enough to encounter large creep settlements.

With Settle3, ground improvement like stone columns were not considered individual material regions but a large equivalent improvement region. Settle3 determines stone column influence through three different methods: Area Replacement Ratio (ARR), Stress Concentration Ratio

(SCR) and Stress Reduction Factor (SRF) (RocScience Inc., n.d.). The ARR uses Eq. 2-1 for rectangular spaced columns and the following equation for triangular spaced columns.

$$\alpha_S = 0.907\left(\frac{d_c}{s}\right)^2 \quad \text{Eq. 6-1}$$

Where: d_c = diameter of the column; s = centre-to-centre spacing between columns in an equilateral triangular pattern; and 0.907 = constant for triangular spaced columns.

The SCR is computed, based on empirical data formulated from Barksdale and Bachus (1983), to approximate the ratio:

$$n = 1 + 0.217\left(\frac{E_c}{E_s} - 1\right) \quad \text{Eq. 6-2}$$

Where: n = Stress Concentration Ratio; E_c = stiffness of column; and E_s = stiffness of soil.

The SRF assumes rigid loading and includes the ARR to formulate the decrease in stress applied to the soil.

$$\mu = \frac{\Delta\sigma_s}{\Delta\sigma_z} = \frac{1}{1+(n-1)\alpha_s} \quad \text{Eq. 6-3}$$

Where: μ = Stress Reduction Factor; $\Delta\sigma_z$ = average vertical stress on foundation; and $\Delta\sigma_s$ = vertical stress on soil.

From this equation, the stress induced on the soil decreases as the ARR and SCR increase. This equation is also applied to determine an equivalent stiffness of the reinforced soil region. The equivalent stiffness is given as:

$$E_{eq} = \frac{E_s}{\mu} \quad \text{Eq. 6-4}$$

Different equivalent stiffnesses are developed for each of the four reinforcement regions; 1.8mØ @2.6m spacing, 2.1mØ @3.3m spacing, 1.8mØ @4.1m spacing, and 1.8mØ @5.1m spacing. This equivalent stiffness is required as 1D consolidation analysis within the soil would compute

large settlements and not represent the influence of columns in the area. Therefore, this was not a true axisymmetric analysis of the foundation. Wick drains were required to contribute the hydraulic conductivity properties within the column reinforcement regions.

The embankment lifts for both abutments were modelled after the stages provided in the FEM analysis. The stresses developed underneath the embankment followed the Westergaard solution as soil underneath the embankment was not homogenous and isotropic, and it better computed settlements for soft soils interbedded within strong layers. This solution better defined site conditions as opposed to Boussineq's theory and multiple layer theory and therefore, would not see overconservative settlement results.

Settlement analysis was performed in three different cases: 1) along the length of the MSE wall (cross-section), 2) along the centreline of the embankment (profile), and 3) the XY plane of the site. The first two analysis cases were selected to compare against what was observed from FEM, where the third case was selected for its 3D capabilities to determine how the rest of the site responded to the embankment loading.

6.5 Summary of 1D Consolidation Analysis

To compare the predicted settlement from FEM, 1D consolidation analysis was carried out using RocScience's Settle3 software. Settlement is determined in three stages: immediate settlement (based on soil stiffness), primary consolidation (based on consolidation parameters), and secondary consolidation (based on creep values). The main limitation with this method is that because it is using 1-D consolidation theory, the model geometry does not influence the behaviour of stresses in the XY direction.

The material parameters used in the analysis modelled all soils to experience immediate settlement with only silty clay and soft silty clay to experience non-linear primary consolidation.

Immediate settlement parameters were used from the FEM analysis and primary consolidation parameters were taken from the oedometer tests performed by TREK.

Soil layer elevations were determined by inputting boreholes of known layer thicknesses in designated locations, interpolating the layers between each borehole. Because the surrounding model geometry does not influence each ‘string’ of consolidation analysis, the modelling of individual rockfill columns was not possible and the program creates an equivalent composite material as the foundation soil. Wick drain parameters were included in the same area to apply drainage behaviour.

Embankment loading followed the same step sequence from FEM, however it was modelled as a dead load rather than a material body load. The stresses developed in the foundation from the loading followed the Westergaard solution for it is not homogenous, isotropic soil and has high strength soil layers

Table 6-1 – 1D Consolidation Analysis Soil Material Properties

Parameter	Granular Material	Silty Clay	Soft Silty Clay	Clay Till
γ (kN/m^3)	21	18	18	21
E (kPa)	60000	15000	15000	60000
C_c	-	0.246	0.365	-
C_r	-	0.115	0.083	-
e_0	-	1	1	-
P'c (kPa)	-	550	400	-
k (m/day)	-	0.000432	0.00432	-

Table 6-2 – Stone Column Reinforcement Parameters

Parameter	1.8mØ @2.6m	2.1mØ @3.3m	1.8mØ @4.1m	1.8mØ @5.1m
E (kPa)	60000	60000	60000	60000
A (m^2)	2.5	3.5	2.5	2.5
a_s	0.38	0.37	0.17	0.11
n	1.65	1.65	1.65	1.65
μ	0.8	0.81	0.9	0.93
E_{eq} (kPa)	18665	18587	16707	16103

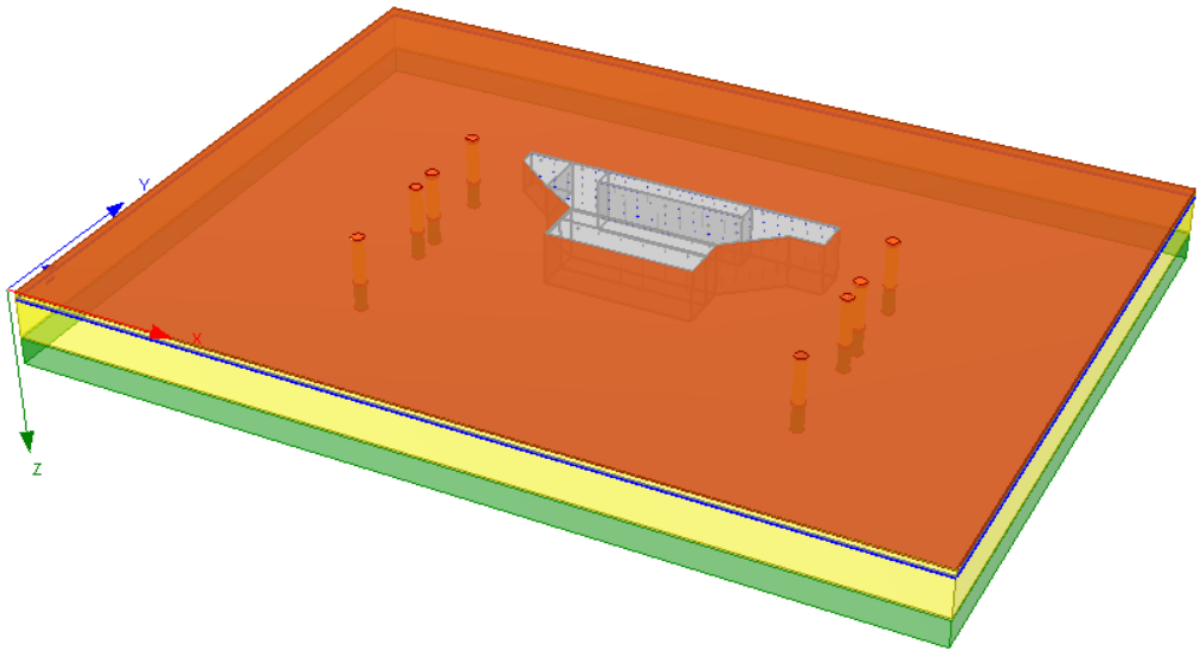

Figure 6-1 – 1D Consolidation 3D Model Space

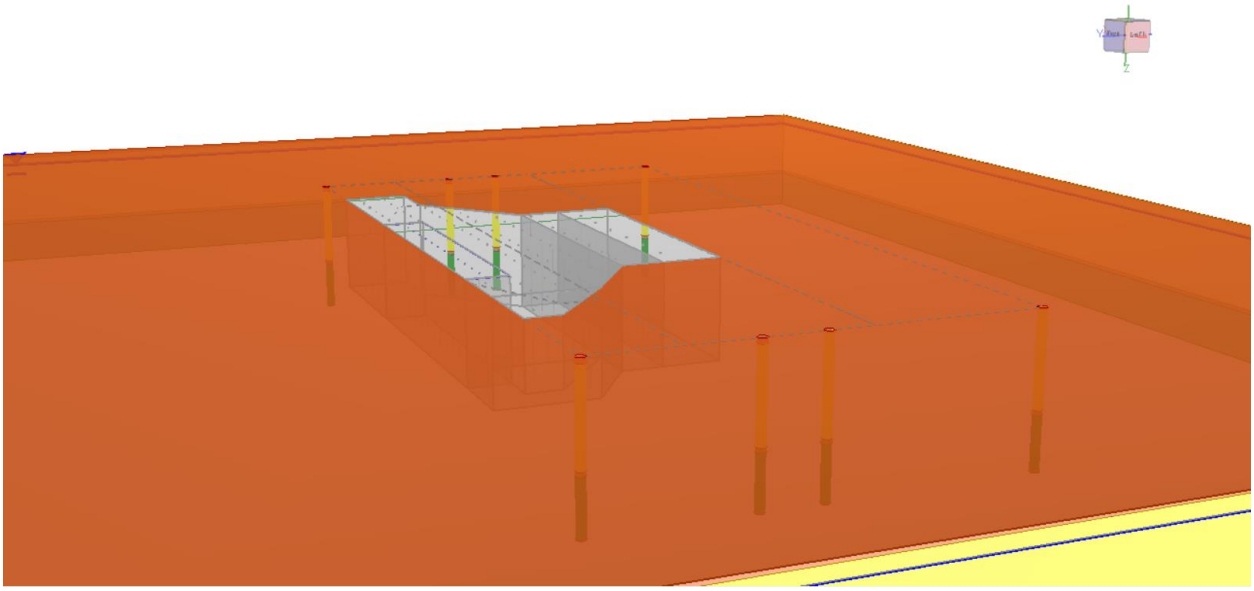

Figure 6-2 – 1D Consolidation North Abutment In-situ Stage

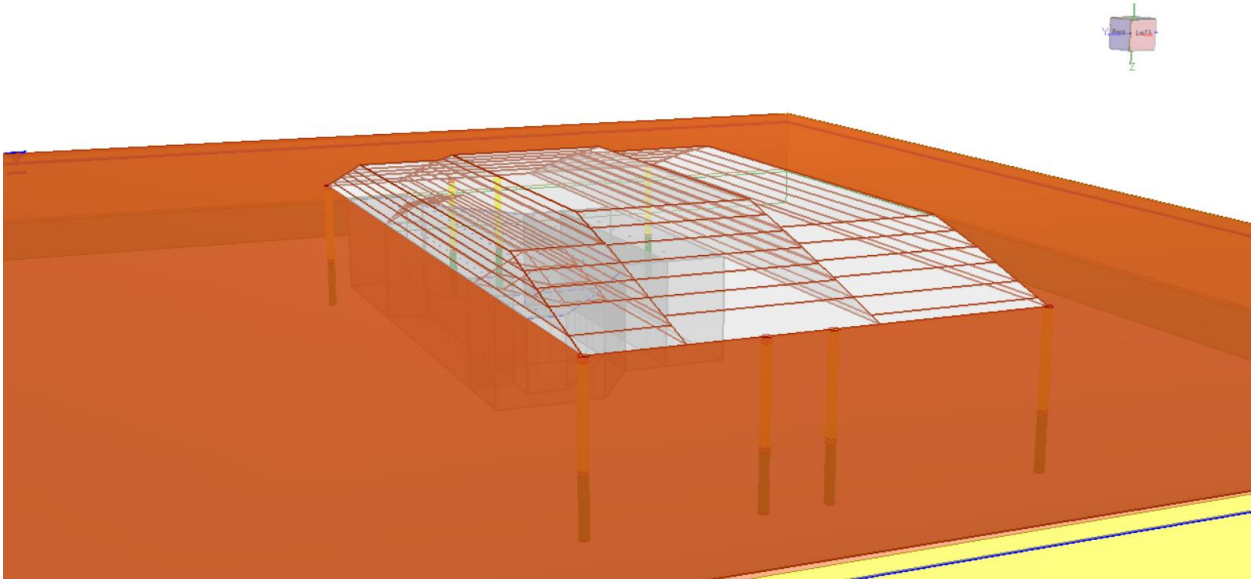

Figure 6-3 – 1D Consolidation North Abutment Completed Stage

7 Results and Discussion

7.1 Background

Results for both surveying methods and modelling methods are presented in this section. The results and discussion are split into their respective sections for each method. Surveyed points, both RL and TLS, are represented by dots or single points at surveyed locations while the numerical modelling results are represented by a continuous single line. This was to differentiate measured or surveyed settlements, compared to a computed or interpolated output.

The cross-sectional plots were developed to observe the settlement along the length of the wall and identify if differential settlement had occurred in any section. The plots for rate of settlement were made to show the progressive settlement over time and observe when the settlements reached final consolidation.

7.2 Rod and Level Surveying

Figure 7-1 and Figure 7-2 provide the cross-sectional plots, and Figure 7-3 and Figure 7-4 provide the plots for rate of settlement for the north and south abutments respectively (TREK Geotechnical Inc., 2019). Lines connecting points on the rate plot were used to show the slope of the settlement over time and interpolated lines for the cross-sectional plot to show the slope of differential settlement along the wall.

7.2.1 North Abutment

Regarding the north abutment settlement, the magnitude of settlement was quite symmetrical as it exhibited a ‘W’ formation with the maximum observed settlements on both the east and west side (NA5 and NA2 respectively) being 47mm and 56mm respectively. This was interesting as the initial thought of the Eastside settling more due to shortened columns seemed to not be influenced by more load bearing in the clay, as mentioned in Chapter 3.4. This could have been from the installation of the sewer and storm water pipes laid on the clay till. During installation of

the pipes on the clay till, the layer of soft silty clay could have been replaced with a stronger, more granular material to reduce soil pressures on the pipe. The replacement of the weaker clay for the stronger granular material would reduce the settlements within the area. However, lack of confirmed pipe installation considers this theory to be plausible until actual pipe installation records are presented. The centre of the wall exhibited the least amount of movement as it reached a maximum of 20mm. This was acceptable to see as the amount of reinforcement in that area was greater inside the area of the bridge deck compared to the extents of the wall, as referenced in Figure 3-1. The maximum differential settlement observed between NA5 and NA6 was 0.31%, below the design tolerance of 1% (TREK Geotechnical Inc., 2017). The limited amount of points surveyed along the wall made it difficult to know the true magnitude, but it was much lower than the design tolerance and therefore was considered safe. The addition of the caissons within the first two rows of columns behind the MSE wall provided more load bearing into the strong clay till section, resulting in less settlement in this section. The rockfill columns in this section were also installed in a tighter spacing (2.62m compared to 3.30m), further fortifying that section of soil.

The rate at which the north abutment settled was consistent proceeding the completion of wall construction. From initial survey to completion of the wall, the magnitudes of settlement were nearly at final consolidation, as each section of wall (west, east, centre) only settled up to an additional 2cm. The centre of the wall however experienced greater settlement after wall completion as embankment height required 3m more of backfill to reach bridge deck elevation. This extra loading of the embankment fill consolidated the soil more but due to the rockfill columns acting as drains, the settlement occurred rapidly and equalized later in the year (October - January).

The surveying error when compared to the other surveyed dates was kept minimal as the observed upward movement was only a couple millimetres, except for Points NA1 and NA2 where

it was an increase in 8mm. These couple of millimetres can be contributed to the 1.5mm sighting error in the level, indicating little to no movement during this time, whereas Points NA1 and NA2 may include errors from the backsight of the benchmark to orient the survey level or frost heave from the seasonal change. Overall, the measurement rates were consistent with each survey and therefore, were considered an accurate assessment of structure performance.

7.2.2 South Abutment

The south abutment settlement was comparable in shape to the north abutment but had greater magnitudes of settlement observed across the length of the wall. The increased amount of fill required to reach design elevation contributed to this extra settlement beneath the structure, as expected. However, it settled a lot more on the west side (SA2) with 119mm compared to 79mm on the east side (SA5) and 68mm within the centre section (SA4). Like the north abutment, this goes against the initial theory of more settlement underneath the shortened columns; albeit the difference between sections had a greater difference of settlement. Further review of the borehole in the West section (TKMC-16-06) does not provide any more justification of why this section settled more than the east side but comparison with the laser scanner results would provide more detail into analysis. The maximum differential settlement observed from SA1 and SA2 was calculated to be 0.64%, which was also lower than the design tolerance. Like the north abutment, surveyed locations were six points along a 100m long wall and may not tell the true value.

The settlement rate varied with each loading case. During construction of the wall, settlement was fairly rapid between baseline survey and July 5th but slowed down once backfill lifts were completed. There was an increase in settlement again between August 2nd and September 13th as the approach embankment was built to design elevation. This second surge of movement was reason for the underlying lightly consolidated, soft soil layer enduring increased loading from the embankment fill. After the load was applied, settlements were quickly equalized signifying final consolidation was near or completed.

Surveying errors on this wall were slightly larger than observed on the north wall as the magnitude of upward movement and inconsistent deviations between survey locations was more frequent. Point SA1 and SA6 (end sections of the wall) appeared to lift upwards after reinforced backfill lifts were completed and minimal deviations were observed after September 13th across all the points, Point SA3 shifted upwards by 8mm between September 13th and October 18th. The small deviations could be considered little to no movement in the structure and larger movements could be attributed to survey orientation. Overall, the surveyed measurements were considered accurate with minimal errors.

7.3 Terrestrial Laser Scanner Surveying

Results are provided in the same format as the RL to provide direct comparisons between measurement methods. Figure 7-5 and Figure 7-6 provide the cross-sectional plots and Figure 7-7 and Figure 7-8 provide the rate plots for both the north abutment and south abutment respectively. To note, the rate plots used the same surveyed locations on the MSE walls as the RL to compare measured settlement, except for SA6 as it was outside the collected points of the TLS so the next closest point at 88.5mm was used. At first glance, the addition of extra points included on the panel facings for deformation analysis allowed a much better depiction of structure settlement. This was evident in observing how far from the centre of the wall (around the 50m mark) the abutment began to exhibit greater settlements. Determining where along the wall began to settle more would better determine the differential settlement and identify possible signs of serviceability problems before they develop into safety risks (Vankavelarr & Leshchinsky, 2002) (Harpstead, et al., 2010).

7.3.1 North Abutment

From Figure 7-5, the settlement measured from TLS confirmed the ‘W’ shape as measured from RL. TLS results of the east and west sides of the north wall settled 75mm and 66mm respectively, and the centre of the wall averaged 40mm. The variation in the settlement profile line did not fit a

smooth spline curve as the soil conditions underneath the structure were not homogenous. There were also small errors in surveying the non-reflective concrete facing panels, the PS readings delayed when the lasers penetrated the air voids within the surface (Garcia-Ferandez, 2016). Looking at Figure 7-7, the abutment appeared to heave upwards from the June to July scans before gradually settling out. This obscure movement was determined as error during surveying and was considered little to no settlement. The maximum differential settlement was calculated from distances 62m to 73m along the wall, resulting in 0.41%. This was under the design tolerance of 1% and was considered safe.

The general trend for the north abutment was large initial settlements and slower descending settlement over time. Discrepancies like upward movement were observed not to be large (±10mm) and given the general trend of each location's settlement, it was acceptable to characterize this behaviour similar to what was observed from the survey RL.

Comparing both cross-sectional settlement plots in Figure 7-9, the difference between the two surveying methods averaged out to the laser scanner overestimating settlement by 20mm. Garcia-Fernandez (2016) identified that the FARO Focus laser scanner can receive large amounts of data points within an incidence angle of 0°-20° to its surveyed surface, but the amount of data received back once the angle reaches 40°, it is halved. Only two scans were selected from the comparison cloud for deformation analysis as described in Chapter 4.3.3; one from the Westside and Eastside of the wall. Data collected on the centre of the wall incurred more error as the scanner was stationed closer to that 45° incidence angle, recommended by Knaak (2017). When comparing the differential settlements, the RL result was 0.1% lower than the laser scanner, but was observed on a different section of the wall. Although both numbers were much lower than the tolerance, the difference of 0.1% could be the amount required to make a structure no longer safe.

The laser scanner proved to have larger deviations in measurement accuracy compared to the RL surveys. However, because of the additional points along the wall, a better understanding of how the wall settled is formed and can provide answers for previous assumptions or hypotheses; such as the influence of the drain pipes underneath the east sections of the walls and the location of most concern for differential settlement. Overall, the scanner agreed well with what was found using the survey RL.

7.3.2 South Abutment

The data collected on the south abutment Figure 7-6 developed the same 'W' formation as the north abutment but had greater magnitudes of settlement on the extents of the wall (<30m and 65m<). This was comparative of the relationship between both abutments, observed by the survey RL. Maximum settlements measured on the east and west sections of the wall were 119mm and 88mm respectively, and the centre section averaged settlements of 30mm. The movement exhibited in the centre section was concerning as the south abutment was expected to settle more than the north abutment (the north abutment settled 10mm more) and the differential settlement magnitude was much larger with the observed 30mm within the centre section. This did not follow the expected behaviour from the increased foundation stresses and the differences in settlement were attributed to the errors discussed in the Garcia-Fernandez (2016) paper. However, the maximum settlement observed along the Eastside of the wall agreed with the prediction of more settlement would occur within the shortened columns section. The maximum differential settlement was observed from distances 24m to 32.5m along the wall, resulting in 0.85%. This number was close to the design tolerance of 1% but was still safe with no signs of extreme distress along the wall panels noted at the time of survey.

When RL and TLS cross-section plots were compared, Figure 7-2 and Figure 7-6, the settlement profiles looked mirrored. However, lines connecting the dots for RL were linearly interpolated and did not represent the settlement between surveyed locations. When the lines were removed and

then compared directly with the TLS results, presented in Figure 7-10, the surveyed points agreed with each other better. Compared survey measurements selected for TLS and RL used July 5, 2018 for both methods, and Sept 13, 2018 for RL and August 28, 2018 for TLS. Compared survey measurements only contained summer dates as seasonal changes introduced more error, and freezing of the ground altered placement of the benchmark rebar.

Concerning the centre section, the July 5 surveys both agreed very well; however, the scanner showed little to no movement two months later when RL measured an additional 26mm (56mm total). The previous observation that the TLS undermeasured the abutment settlement was confirmed between these two dates and that final settlement of the abutment was not 30mm. The east section (0m to 30m) was interesting as the interpolation of the line between the two RL measured points would indicate a constant settlement, however TLS observed a larger amount of settlement due to the shortened columns in that section. This was the benefit of the TLS, providing more information on the total structure performance and identification of critical sections. The two points the RL surveyed matched up quite well with the TLS, however SA5 had some minor discrepancy between surveying methods which were deemed acceptable. Observing the west section, this was where the idea of a reversed graph came to thought. SA1 and SA3 were accurate within ±10mm, but SA2 had differences of 40mm. High errors incurred during the centre section scanning made it possible that the laser scanning data was incorrect in this section. However, the general understanding of how the structure settled, based on the information known about the foundation soils and reinforcement, did not agree with more settlement occurring in the west section compared to the east section. The results from the FEM analysis in Chapters 7.4.2 and 7.4.3 computed the expected settlement and provided additional justification for structure movement. When each method was compared for differential settlement the RL was lower by 0.21% and like the north wall, was calculated from a different section of wall. However, both were under the tolerance and were safe.

7.3.3 Surveying Methods Comparison Summary

There were pros and cons for both methods used, some highlighted in previous literature, but they both developed proficient alternatives for monitoring structure settlements. The RL surveys accurately measured the selected target locations along the wall face, outlining the small increments of settlement over the construction process. TLS measurements were able to survey the entire wall face, allowing to observe the critical area for settlement and provide more information for QA/QC of data collection results. The shortcomings were more errors for the laser scanner compared to the RL (as evidence from the target comparisons of SA2 and SA4) but both methods have their applicable use for structure monitoring, depending on measurement tolerance and project specifications.

7.4 Finite Element Numerical Modelling

7.4.1 Pore Pressure Response

Pore water pressure response results from both the measured piezometer readings in the field and computed pore water pressure values from FEM are represented in Figure 7-11. Both responses were nearly identical in peak excess pore water pressures and the rate of dissipation after all lifts were completed. The peak pore water pressure responses computed outside the columns at elevations of 500m and 503m were 80.3kPa and 67.8kPa for the profile model (line colours red and orange), and 77.8kPa and 62.4kPa for the cross-sectional model (line colours dark and light green). The decrease in peak pore water pressure between models was fair as the profile model assumed embankment elevation to be constant at 516m whereas the cross-sectional model portrayed the trapezoidal geometry, allowing for pressure to dissipate toward the toe of the slopes. The difference in less pore water pressure buildup (-2.5kPa @500m and -5.4kPa @503m) can be attributed to the flow path length from piezometer elevation towards the more permeable soft silty clay and clay till layers. Underneath the centre of the embankment in Figure 7-13, the soil closer to the surface dissipated first (single drainage) and the pressure

contour gradually lowered over time. The same occurred in the profile models of the north and south abutments in Figure 7-14 and Figure 7-15 respectively, the silty clay outside the reinforced zone had greater pressure near the till. Comparing these results to the monitoring report, the accumulation of pore water pressure and dissipation are a reasonable estimation as the piezometer reading outside the reinforced zone was 61.8kPa (black line labelled OutsideColumns-Report). The sudden spike and drop as each lift were applied were a result from the immediate load application of each 1m lifts, as discussed previously this lift size was chosen to simplify loading conditions. Over time, both the models and the piezometer readings observed decreasing pressure at a parabolic rate until equilibrium.

Looking at the results for within the reinforced zone, the piezometer readings peaked at a pressure of 10.7 kPa (black line labelled WithinColumns-Report) while the models computed maximum pressures of 2.3kPa and 2.7kPa (line colours dark and light blue). The piezometer readings inside the reinforced zone were greater than the modelled results due to the assumption of plane strain parameters, influencing the flow length of pore water pressures, as can be shown in Figure 2-8. The piezometer was installed within a “dead zone” or non-influenced soil area and would take longer to dissipate, resulting in a greater peak of excess pore water pressure than the modelling results. The material properties selected for the hydraulic conditions were accepted for further analysis.

7.4.2 Effective Drained Parameters

Settlements were observed at the top of the granular pad in both the cross-sectional and profile models, along the wall and down the centreline of the embankment. Final settlements from each conversion case were presented in Figure 7-16 and Figure 7-17 for cross-sectional models of the north and south abutment. These looked to compare different transformation methods, from axisymmetric parameters to plane strain parameters; Case A altered column thicknesses, Case

B altered strength parameters, Case C altered both, and Case TREK were the parameters used in the design report. The following observations were made:

- All cases demonstrated similar settlement trends to what was observed from surveying results, with most settlement occurring along the Eastside of each abutment creating that 'W' profile.
- Case C computed the largest settlements for each abutment, with maximum displacements observed as 136mm and 98mm for the south and north abutments respectively.
- By maintaining strength parameters while reducing the thickness of the equivalent soil wall (Case A), the wall generally settled 25% less than Case C. The maximum settlements were 108mm and 82mm for the south abutment and north abutment respectively.
- Case B showed slightly lower settlements in the centre of the wall compared to Case A (generally 6-8mm less) but settled more in the triangular spaced column area in the north abutment; the south abutment only settled more for Case B on the Westside triangular columns. The maximum settlements were 96mm and 85mm for the south and north abutments respectively.
- The TREK model resulted in the least settlement within the rectangular spaced columns but settled more on the extents of the reinforced zone than Cases A and B (except the Westside of the north abutment). Maximum settlements were 122mm and 98mm for the south and north abutment respectively.
- The parameter that was observed to affect settlement behaviour the most was the thickness or arrangement of columns rather than the stiffness. This was evident from Case A and C settling more than Case B and TREK within the rectangular spaced columns. Case B settled more than both TREK and Case A within the triangular spaced column regions (except for the Eastside of the south abutment).

From these observations, along with the assumed model limitations and simplifications, it was determined that Case C best simulated conditions on site and the settlement induced from each lift is provided in Figure 7-18 and Figure 7-19 for the north and south abutments respectively.

Looking at the north abutment, the increments of settlement were proportional across the length of wall, however the final lift to complete the embankment, labelled “Complete”, dropped the middle of the abutment settlement from 60mm to 90mm and the settlement on the West end of the reinforced area ceased to move. The other local maximums observed were computed as 67mm on the east side and 98mm on the west side. The settlement profile lost the ‘W’ behaviour made evident from the surveying data as a result of this final lift but from the incurred assumption of the reinforced granular fill not actually built to embankment elevation overtop the MSE wall and the lost skin friction forces from the exclusion of the belled piles, as shown in Figure 5-2, the computed settlement from this lift was considered an overestimation. The load transfer of fill material between the top of the wall and top of embankment is unknown so the difference between the last two lifts were considered upper bound and lower bound cases to compare against the scanning results, labelled “Lift 4” and “Complete” in their respective cross-section figures. Comparing the final survey in August 13, 2019 from TLS, Figure 7-20 confirms the final settlement computed from FEM was overestimated. The centre and Eastside of the abutment were under the lower bound of settlement, however the settlement under the Westside of the abutment was within the range.

Like the north abutment, the south abutment too had proportional settlements with each lift, no additional settlement on the West end of the reinforced zone, and a large increase in settlement within the bridge deck area, dropping from 63mm to 90mm. The east end of the abutment reached a final settlement of 136mm, and 90mm for the west end. Unlike the north abutment, there was a slight local settlement maximum on the Westside of the abutment. However, the ‘W’ profile was not discernable from the exclusion of the additional frictional forces provided by the belled piles

and the impact of the additional fill to embankment elevation within the 2D plane overestimated the final consolidation, resulting in the development of upper and lower bounds for final estimated settlement (Lift 4 and Complete). The comparison of the last TLS survey performed on the south abutment and the computed final settlement is provided in Figure 7-21. The errors incurred from surveying the centre of the south abutment has been discussed in Chapter 7.3 and thus the RL survey of the wall's centre and the rest of the TLS measurements will be used for comparison. The first impressions are that the TLS and RL surveys agreed well with the limits placed by FEM as all but a 5mm difference on the Westside were within the upper and lower bounds. The RL measurement in the centre placed at 68mm bodes well for the FEM range as it closer to the lower bound (8mm to lower, 21mm to upper).

Figure 7-22 and Figure 7-23 show the profile settlement from FEM for both the north and south abutments. The profile of the settlement generally follows a slope from underneath the wall (right most of the graph) and trends downwards towards the end of the reinforced zone. Settlement occurred in equal increments from the wall location to the end of the 2.1m diameter columns spaced at 3.0m, before an increase in magnitude, signifying the silty clay took on more load from the embankment. The magnitude of settlement underneath the wall and end of reinforced zone for the north abutment was 44mm and 89mm, and the south abutment was 59mm and 136mm. The computed results for both the profile and cross-sectional model have mixed results for the abutments as the centre settlement did not match. The cross-sectional model of the north abutment computed more than double the results from the profile model (90mm compared to 44mm). This was a big difference, resulting from an assumed equal embankment geometry and not accounting for the absence of overburden soil past the MSE wall. When compared with the surveying, TLS agreed with the profile model results (40mm) and RL survey was lower at 20mm. The exclusion of the belled piles in the numerical modelling resulted in increased settlement within the centre of the wall, as discussed in Chapter 5.2.3. Looking at the south abutment, the results

compared similarly to what the north abutment computed (90mm for cross-section vs 59mm for profile). Again, the assumption of constant embankment geometry was the main contributor to this difference. However, the surveying done by the RL had the settlement at 68mm (the centre of the TLS scanning incurred too much bounce back error to be considered for this comparison), which boded well for the modelling results as the cross-sectional model's assumption of constant embankment height applied more load than in reality.

7.4.3 Effective Drained with Coupled Stress/PWP

Figure 7-24 and Figure 7-25 show the settlement influenced by pore water pressure parameters for the north and south profile model, and Figure 7-26 and Figure 7-27 are for the cross-sectional models respectively. The immediate settlement underneath the walls for both abutments were steep with very little incremental movements in between loading cases whereas the settling over time at the end of the reinforced zone in the profile models took longer to settle. This was in part due to the rate of pore water pressure dissipation, explained in Chapter 7.4.1, and the decreased stiffness of soil allowing larger final settlements. The cross-sectional models had almost all immediate settlements, excess pore water pressures did not exceed 5kPa as shown in Figure 7-11 and Figure 7-12.

When comparing FEM against the TLS data, results were quite comparable. Reviewing the north abutment comparison in Figure 7-28, it was discussed in Chapter 5.2.3 and observed in the previous section that the modelling performed on the north abutment overestimated the final settlements, however it was shown that settlements between August 28, 2018 to August 13, 2019, were little to none. This behaviour coincided with the RL survey data, as well as the TLS data; although TLS had a larger range of measurement values, the precision of the data agrees with the modelling pattern. The comparison for the south abutment is shown in Figure 7-29, with similar results. The TLS measurements made along the centre of the wall may not agree (as discussed in the previous Chapter), but the RL survey agreed with the incremental settlement magnitudes,

particularly between July 5, 2018 to August 28, 2018. Along the East and West sides of each wall, the profile shapes of the TLS and FEM matched very well. Unlike the north abutment, there was still movement after Aug 28, 2018 but this was attributed to the north abutment completing construction a couple weeks before the south abutment.

7.5 1D Consolidation Numerical Modelling

The results from the settlement analysis are presented in separate sections for cross-section, profile, and XY planar analyses. The settlement profile for each section would not be a continuous line because of the variation of column reinforcement spacing and dimensions. The creation of the reinforced region within the foundation will assume homogenous parameters within the selected area and because of 1D consolidation analysis, the transfer from one region to another, such as going from a non-reinforced area into a reinforced area, will cause an immediate change in settlement that is not representative of the actual settlement in the area. In reality, the change in settlement would behave more like a continuous spline and loading stress would be distributed to the stronger material.

7.5.1 Cross-Section Results

Settlements for the north abutment is presented in Figure 7-30. Looking at the north abutment, the shape of the settlement underneath the embankment takes on more of the big U-shape rather than the W-shape like what was observed with surveying and FEM. This is attributed to the absence of both geosynthetics the belled piles, and the analysis in 1D as load could not be distributed along the entire reinforced region. Settle3 does not incorporate geosynthetics for analysis as the behaviour of a structural beam member (the geosynthetics) can not be accurately portrayed in the model analysis. The maximum observed settlement was underneath the centre at 55mm and the east and west sections settling 51mm and 37mm respectively. This was less settlement observed than the FEM results, shown in Figure 7-18, but the greater settlements located near the shortened columns agreed with both FEM and TLS results. However, the large

centre section settlements only agree with the FEM results, signifying that there may have been some discrepancies with material properties and/or assumptions and limitations with computer modelling that has affected the behaviour of settlement. However, the decreased magnitude between the 1D analysis and the FEM results (90mm to 55mm within the centre section in Figure 7-34) was contributed to modelling the embankment in 3D space, avoiding the assumption of constant embankment elevation needed for the 2D analysis.

Comparing the south to the north abutment, the shape of settlement does in fact take on the W-shape but to a greater magnitude, shown in Figure 7-31. The maximum settlements observed were along the east and west unreinforced sections with 145mm each, and 126mm within the centre section. This increase in magnitude from the north abutment was attributed to the additional embankment fill required to reach design elevations as the silty clay was modelled using non-linear settlement characteristics, rather than solely relying on stiffness properties. The change in settlement between regions is more prevalent in the south abutment due to higher magnitudes, even more so within the west section of the wall (distance 15m-30m along X-axis). Transferring from non-reinforced soil to columns, to short columns, and back to columns, the settlement magnitudes move up and down with the varying stiffnesses. When compared to the effective stress contours developed by the FEM in Figure 7-38, the stress within the shortened column area was transferred to the bordering columns drilled to till depth as the effective stress within the columns are much greater than the surrounding silty clay. Thus, the settlement profile developed by the 1D analysis was discontinuous and did not represent actual differential settlement behaviour. When the magnitudes were compared with the FEM results, shown in Figure 7-35, the 1D analysis computed 20-30mm more along the wall. This can be attributed to the load transfer, however like the north abutment, more information within the centre section would better explain the difference between modelling and surveying.

7.5.2 Profile Results

The north abutment settlements along the centreline of the embankment is presented in Figure 7-32. Like what was observed in FEM, the minimum settlement is observed under the wall (55mm at X = 49m) and slopes downwards as it travels through the reinforced zone. At 42m there is a local maximum of 111mm signifying this was where the reinforced fill reached bridge deck elevation. The magnitude of settlement is then reduced as it reaches the end of granular fill and beginning of clay fill, hovering around 100mm along the rest of the reinforced zone, and reaching a maximum magnitude of 115mm within the non-reinforced zone. However, the settlement observed between 0 and 20m (unreinforced foundation soil) was under-estimated because of the assumed constant ground surface elevation required for column reinforcement inclusion and the settlement would be more constant than as shown. The ground surface elevation within the approach embankment to the north abutment was measured at 510m before construction began, as seen in Figure 3-3, whereas the assumed elevation had to be set at 507.5m, disregarding an additional 2.5m of silty clay to consolidate and contribute to the analysis. The settlement observes to decrease as it gets towards the end of the analyzed zone, however this is due to a finite length of embankment used to apply load and in reality, the embankment is much longer and would see a constant magnitude of settlement. When comparing graph results from FEM to 1D analysis, they both exhibit fairly constant settlement underneath the levelling pad albeit the 1D estimated 20-30mm more.

For the south abutment, again the foundation exhibited greater magnitudes of settlement especially outside the reinforced zone. Like the north abutment, Figure 7-33 shows minimum settlement underneath the wall (126mm at X = 49m) and increases in magnitude the farther into the reinforced zone until reaching maximum settlements outside of the stone column area. The local maximum observed at top of backfill height is observed to not influence the south abutment as much as the north abutment, due to both clay layers enduring plastic strains from the increased

backfill stress. Then as the stone column spacings get larger, the settlements increase within the foundation, with a maximum of 380mm outside the reinforced area. The settlement tailing off is the same problem explained with the north abutment. When compared to the FEM profile analysis, they both exhibit a constant settlement magnitude within the rectangular spaced columns and 3.3m triangular spaced columns before a constant increase in settlement through the larger spaced column regions. The main difference however is the magnitude of settlement computed for each method, as 1D observed 200mm within the 3.3m triangular spaced section whereas FEM observed within 80mm. This is due to how each modelling software computed the settlement, FEM used plane strain columns and 1D analysis used an equivalent composite block; FEM used material stiffness and Modified Cam clay for soft silty clay, and 1D analysis used material stiffness and oedometer lab results for both silty clay and soft silty clay. However, the behaviour of settlement was fairly consistent for both north and south abutments and therefore, provided a different understanding and justification for how FEM computed results.

7.5.3 Grid Results

The XY plane for the north and south abutment is provided in Figure 7-36 and Figure 7-37 respectively. The grid analysis aimed to observe how the foundation settled within the whole reinforced area and identify critical sections of settlement. Most settlement occurred outside the boundaries of reinforced and non-reinforced soil sections, specifically the 5.1m spaced column region.The north abutment had a greater amount of settlement induced just behind the rectangular spaced columns (within the belled pile area), indicating larger settlements would occur when the approach embankment connects with the bridge deck. This analysis would provide useful information for the contractor to determine overfill locations along the embankment, reducing infrastructure damage long term.

7.6 Summary of Results and Discussion

The magnitudes of settlement between the surveying methods had small differences but were generally within the precision tolerance of ±20mm. The errors were larger in TLS due to more data processing, but the amount of information collected on the wall was better for OA/QC for monitoring structure performance. Overall, the author concludes that if TLS was the selected method of survey monitoring, that a control survey like the TS should supplement the scanner.

The piezometer data was able to calibrate the FEM model successfully and provided the hydraulic properties needed for the Coupled Stress/PWP analysis. The computed settlements from FEM had the same behaviour as observed from surveying, however the settlements in the centre of the wall was overestimated for both abutments. The reason for the overestimation of centre settlement was deemed to be from the 2D model, not allowing the sloping of the top of wall elevation towards the top of approach embankment elevation (513.6m vs 516.0m) and lost skin friction forces from excluding the belled piles supporting the bridge deck. Between the 4th lift and 'Complete' lift is an upper and lower bounds of where the final settlements would lie.

From the 1D consolidation, the load transfer between strings of computed consolidation was evident as the lines of settlement in both the cross-section and profile section analyses were not smooth. The magnitudes of settlement were underestimated in the north abutment and overestimated in the south abutment, but the behaviours were similar to FEM. Overall, FEM is the preferred method of settlement prediction but 1D consolidation analysis provided an adequate comparative tool.

From the acceptable comparisons between settlement prediction tools and the surveyed settlement measurements, the ability to better determine how a structure will behave with the foundation materials and how a change in monitoring equipment can affect how "safe" the structure actually is. The RL produced relatively safe % values when determining differential settlements whereas the TLS had safe values as well, but slightly increased in different surveyed

locations. The TLS could capture the maximum settlement exhibited by the structure whereas the RL required the user to predetermine locations to survey based on simplified and interpolated foundation properties. However, the RL accompanied with the laser scanner can provide good survey control along the structure surface to compare with the TLS for analysis accuracy.

On the modelling prediction side, including FEM numerical modelling for the preliminary design stage is beneficial but the oversimplification and/or transformation of model parameters and geometry can greatly influence your results. Take for example, the selection of stone column parameters used in this analysis varied by 40mm depending on which thickness and strength properties were used, shown in Figure 7-16 and Figure 7-17. Performing 1D consolidation analysis can provide good baseline or reference foundation settlement without the complex site conditions. This was evident from computing the south abutment to settle twice as much than the north abutment, whereas the FEM numerical modelling found the difference to be closer to 30mm. When compared with the surveying completed on site, the north abutment settlement computed from 1D consolidation was a closer approximation than the more complex FEM model. Therefore, it should be reinforced that the modelling completed to predict the performance of a structure should start out simple without making too many assumptions, then gradually add more detail into the model.

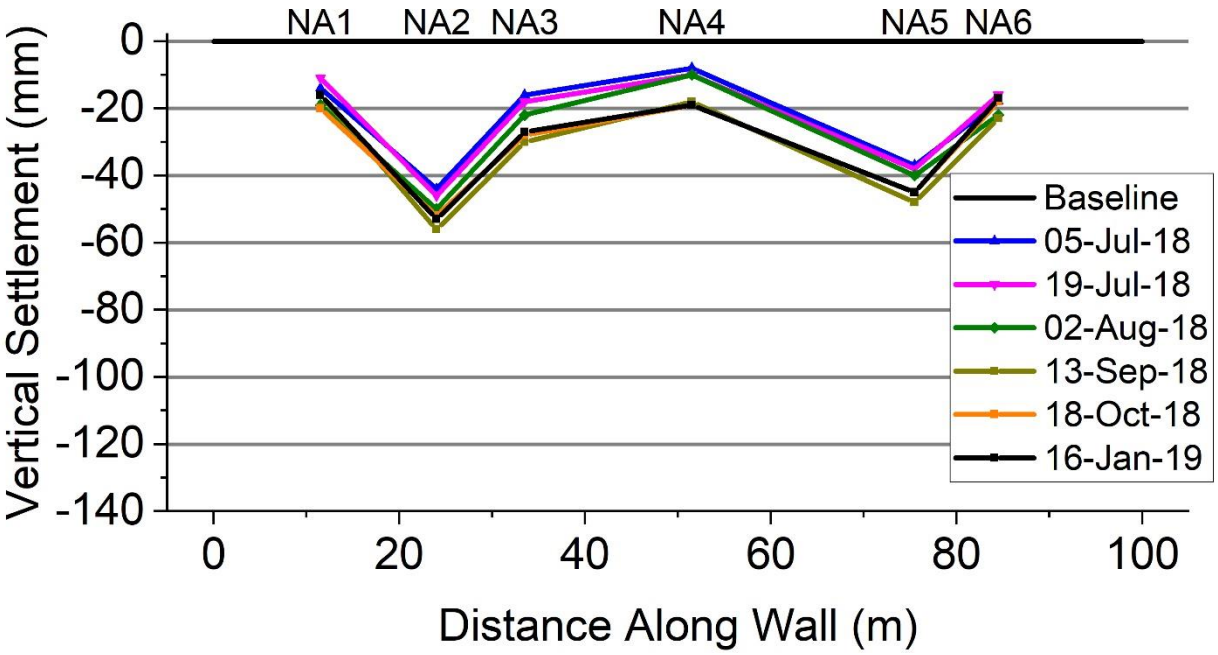

Figure 7-1 – Rod and Level Survey North Abutment Cross-Section Settlement (TREK Geotechnical Inc., 2019)

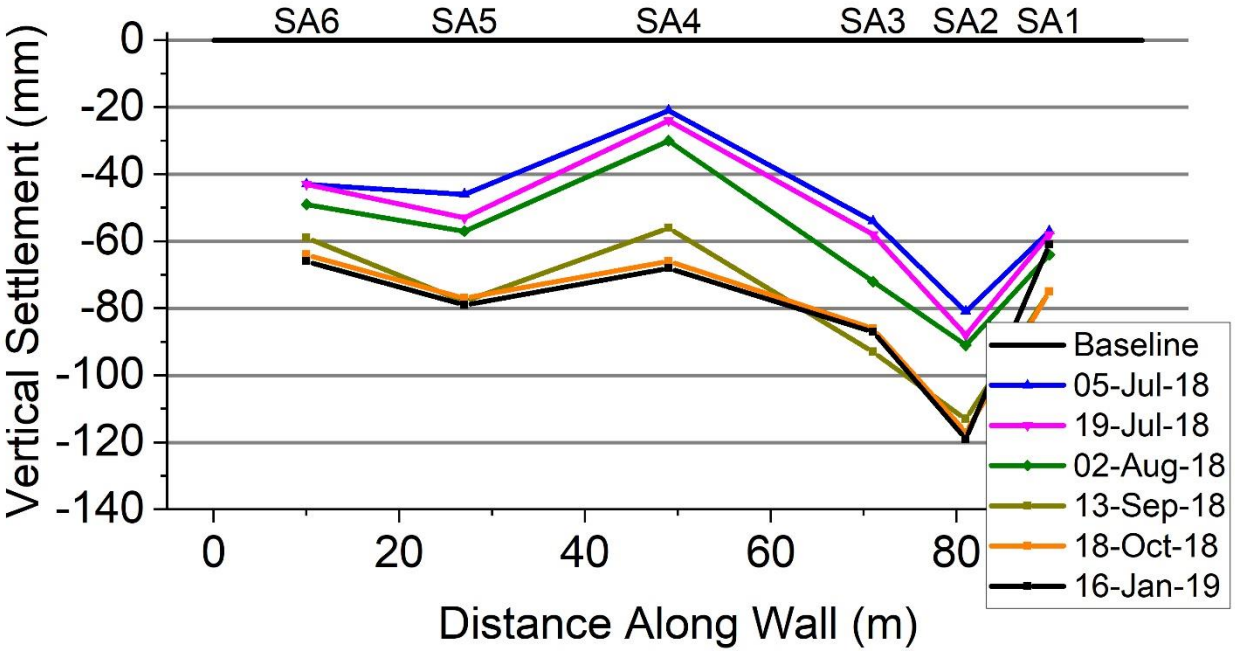

Figure 7-2 – Rod and Level Survey South Abutment Cross-Section Settlement (TREK Geotechnical Inc., 2019)

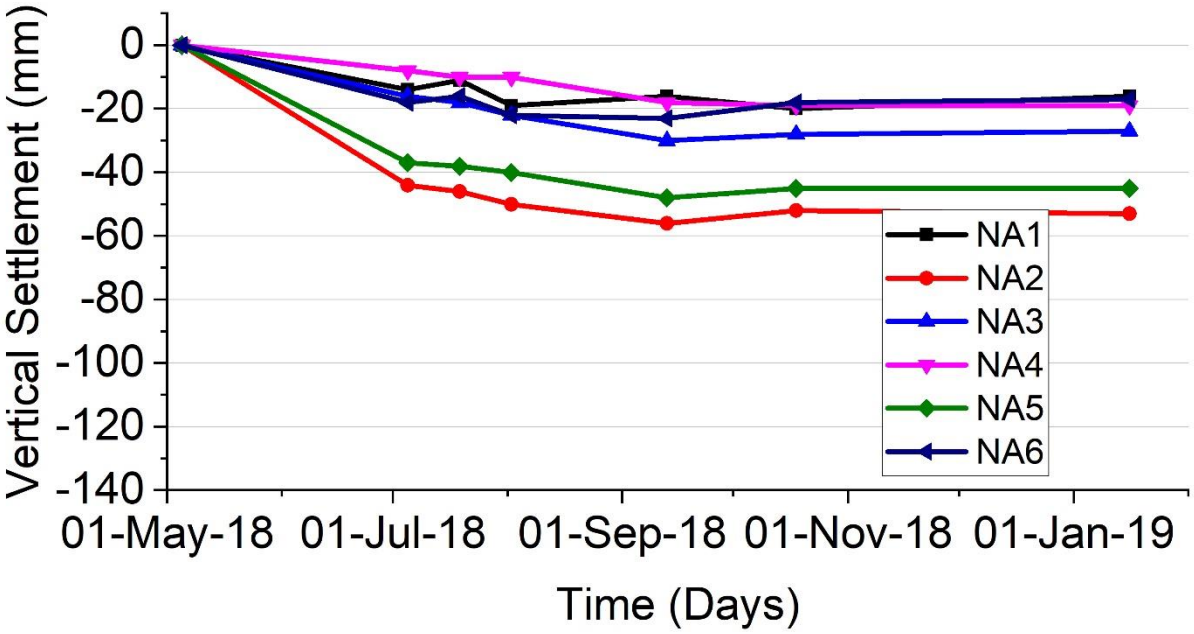

Figure 7-3 – Rod and Level Survey North Abutment Settlement Rate Plot (TREK Geotechnical Inc., 2019)

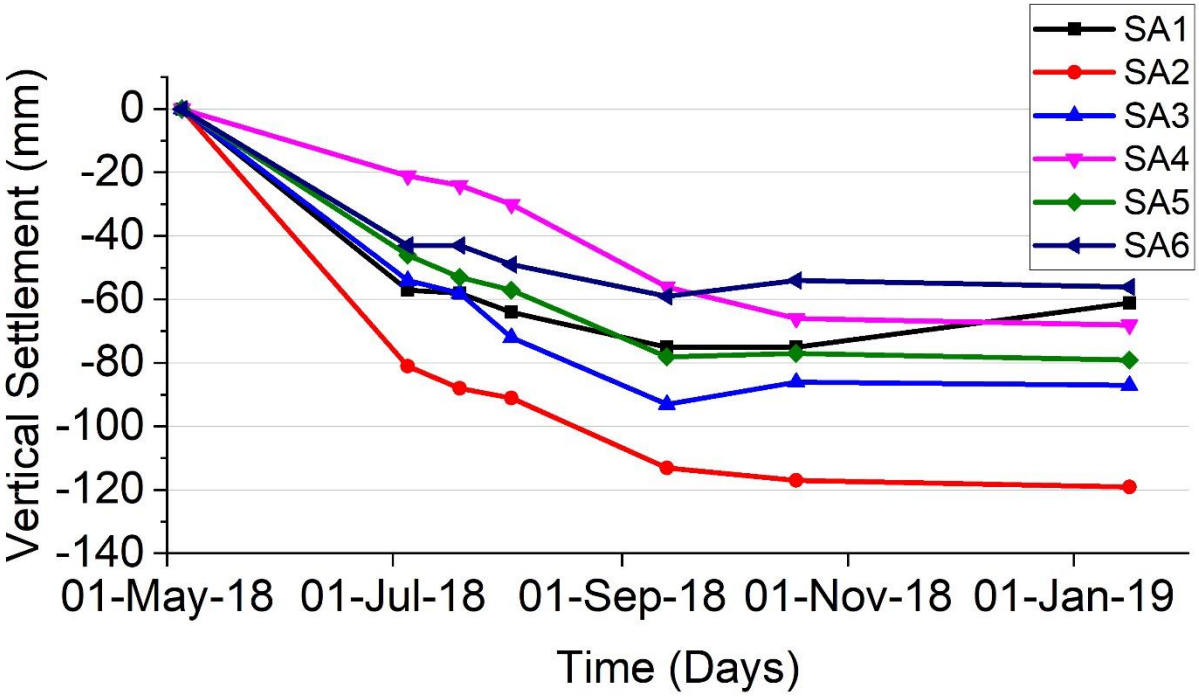

Figure 7-4 – Rod and Level Survey South Abutment Settlement Rate Plot (TREK Geotechnical Inc., 2019)

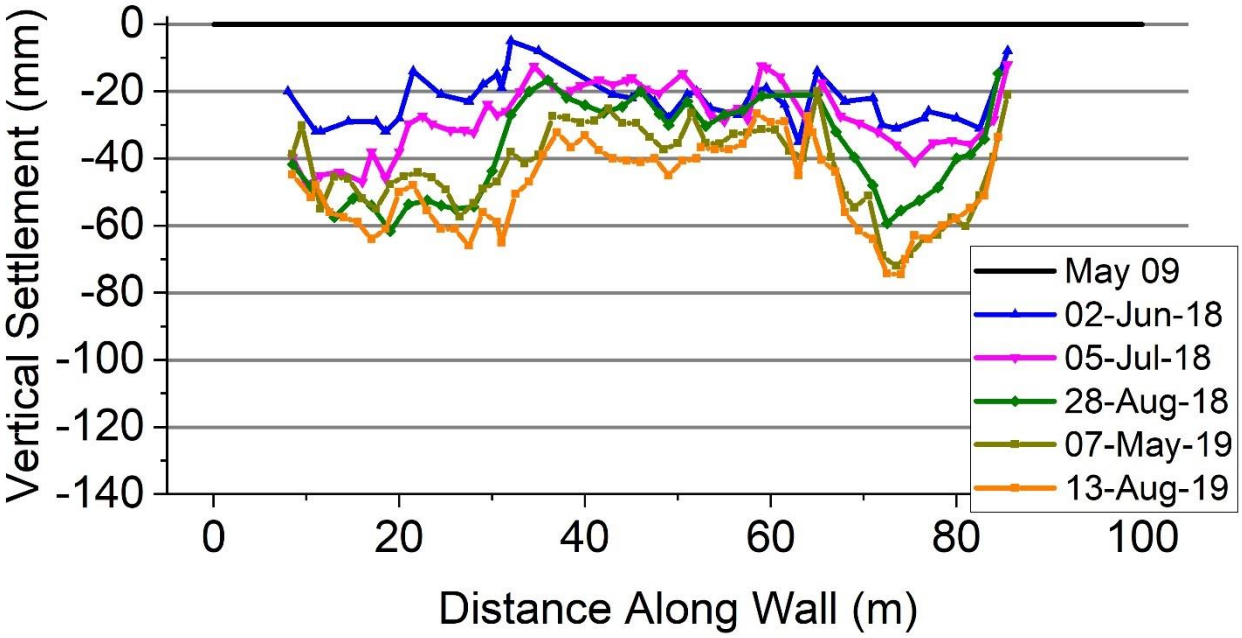

Figure 7-5 – TLS North Abutment Cross-Section Settlement

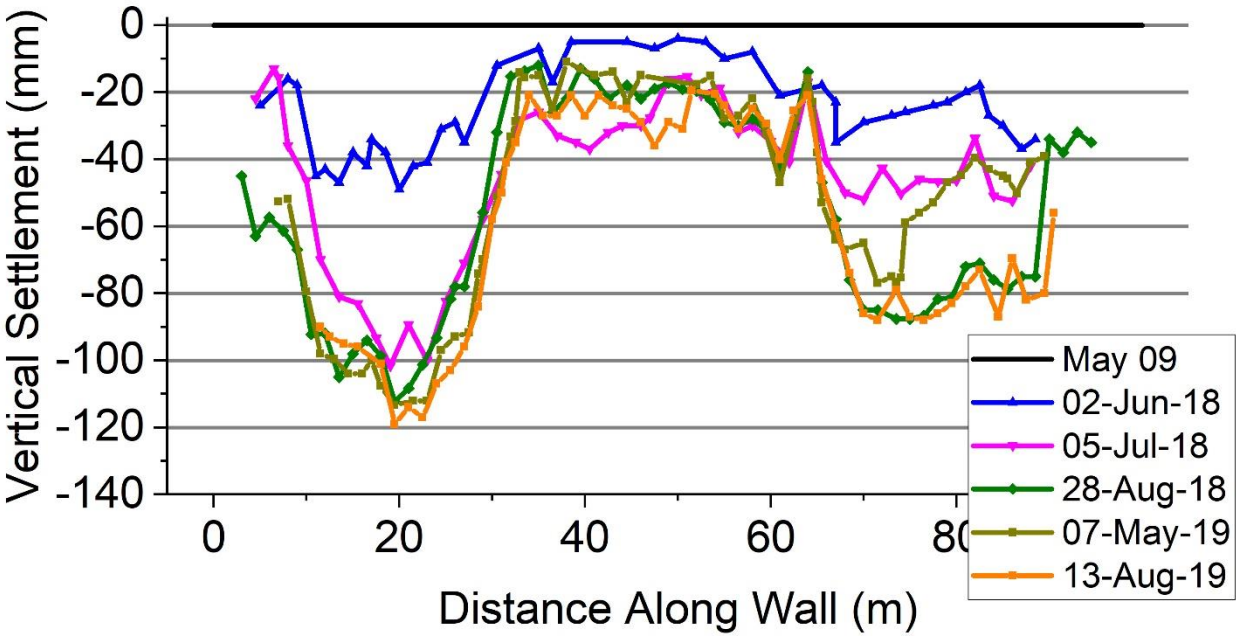

Figure 7-6 – TLS South Abutment Cross-Section Settlement

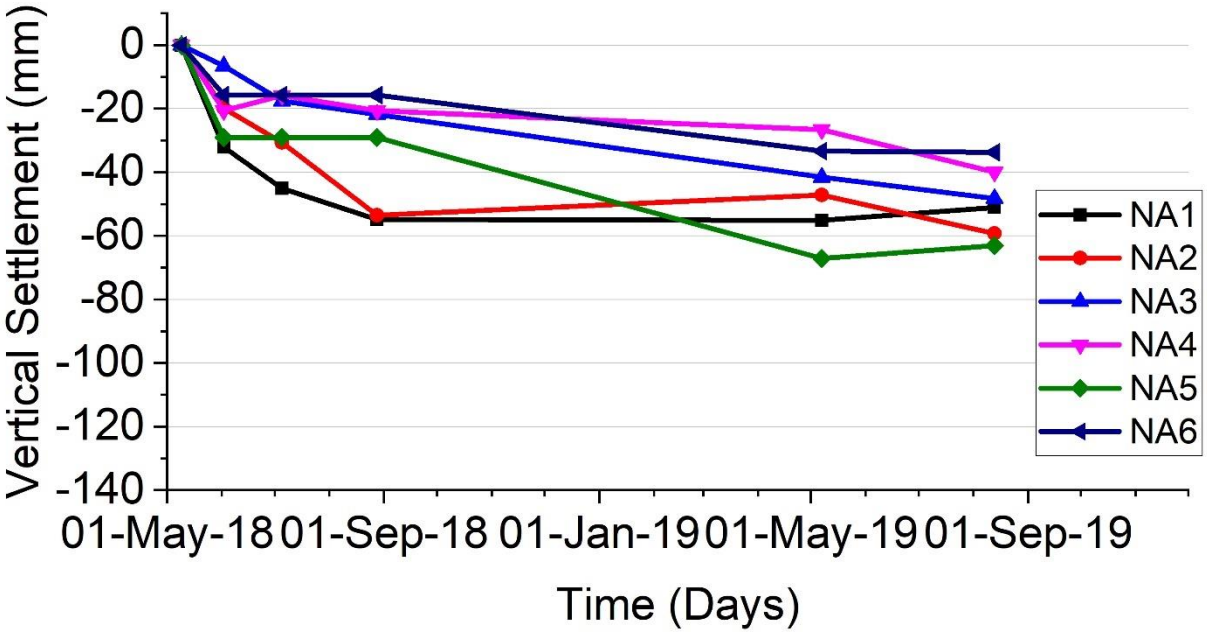

Figure 7-7 – TLS North Abutment Settlement Rate Plot

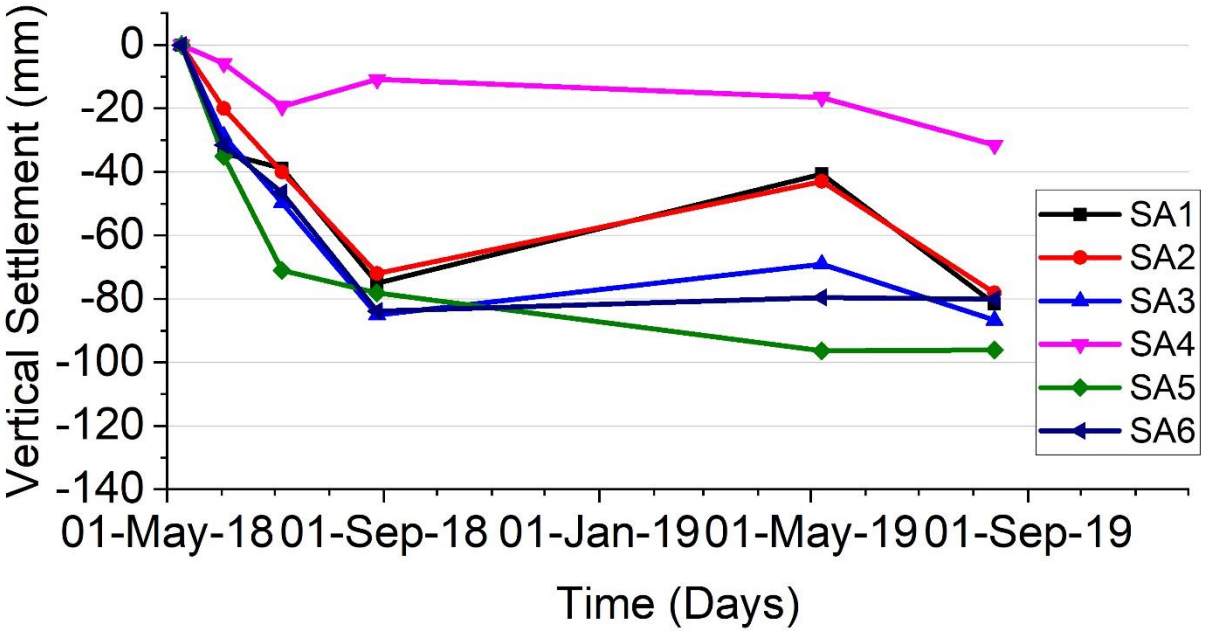

Figure 7-8 – TLS South Abutment Settlement Rate Plot

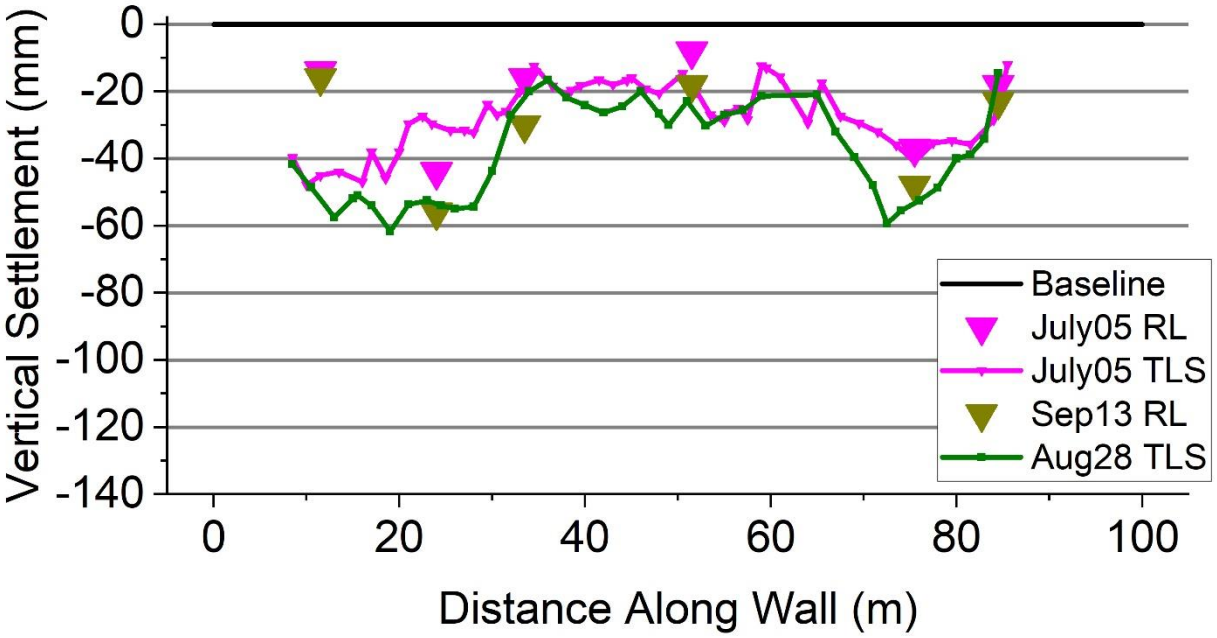

Figure 7-9 – TLS vs RL North Abutment Cross-Section Settlement Comparison

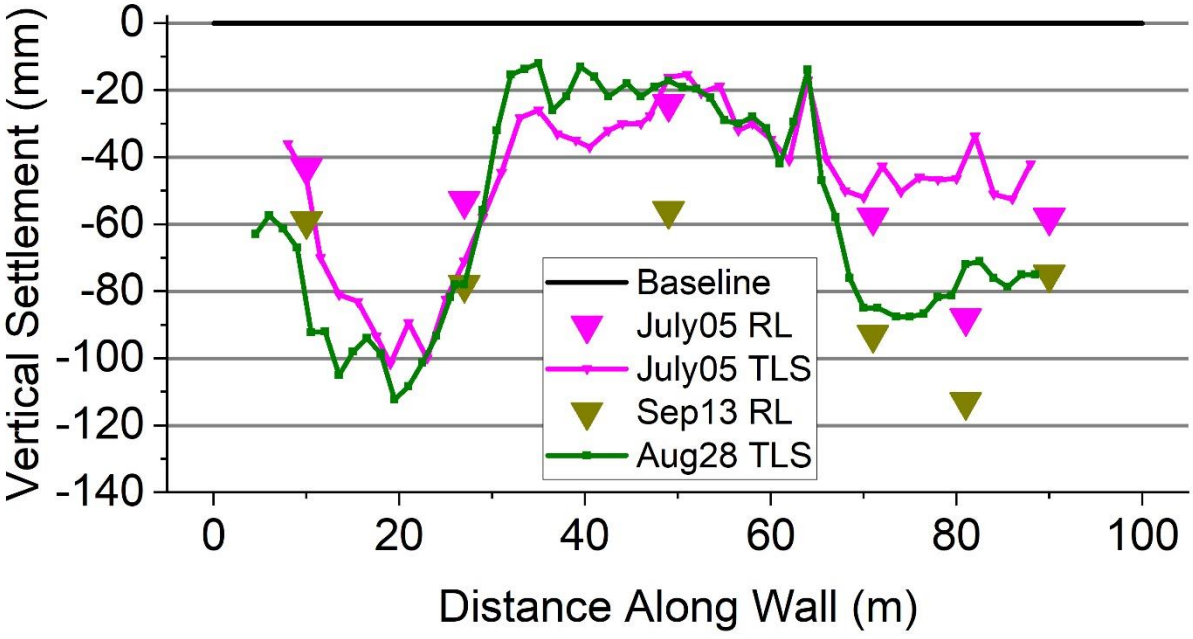

Figure 7-10 – TLS vs RL South Abutment Cross-Section Settlement Comparison

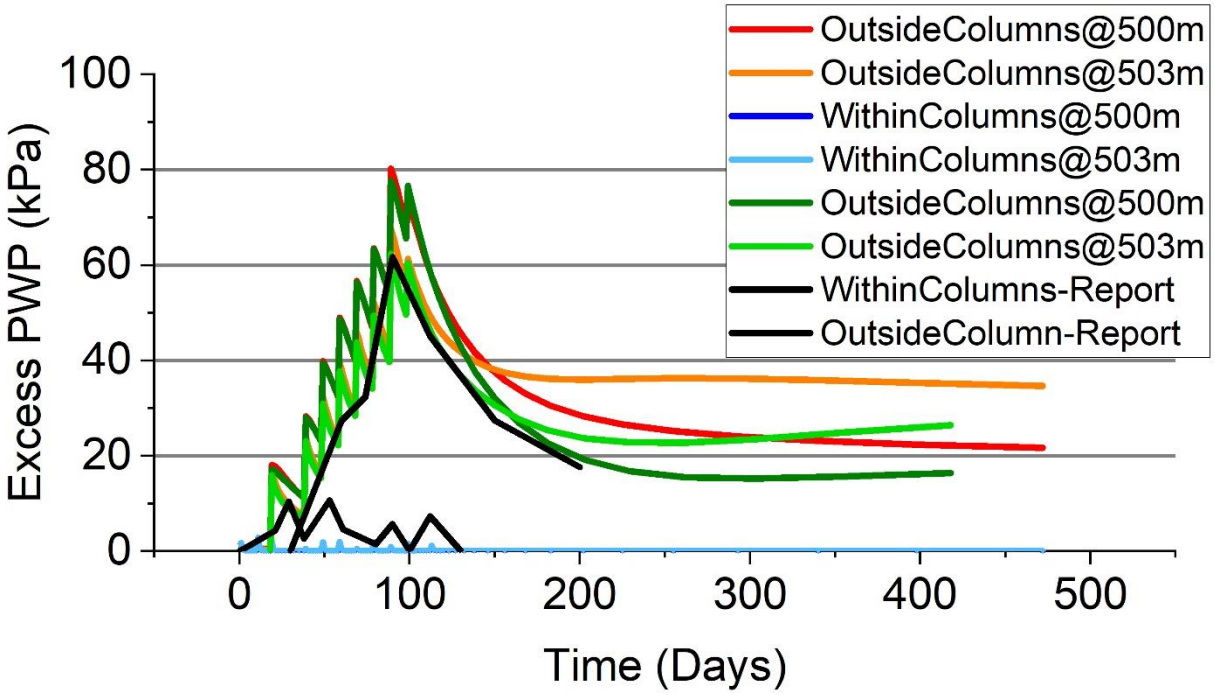

Figure 7-11 – FEM South Abutment Excess PWP Plot

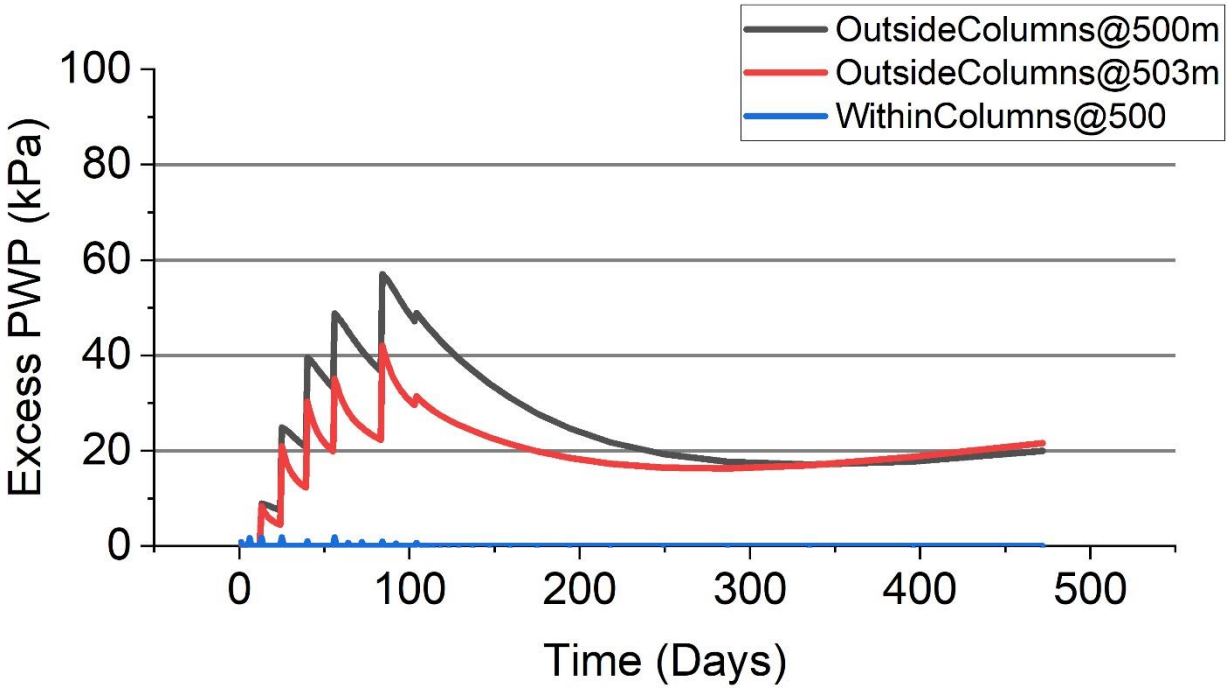

Figure 7-12 – FEM North Abutment Excess PWP Plot

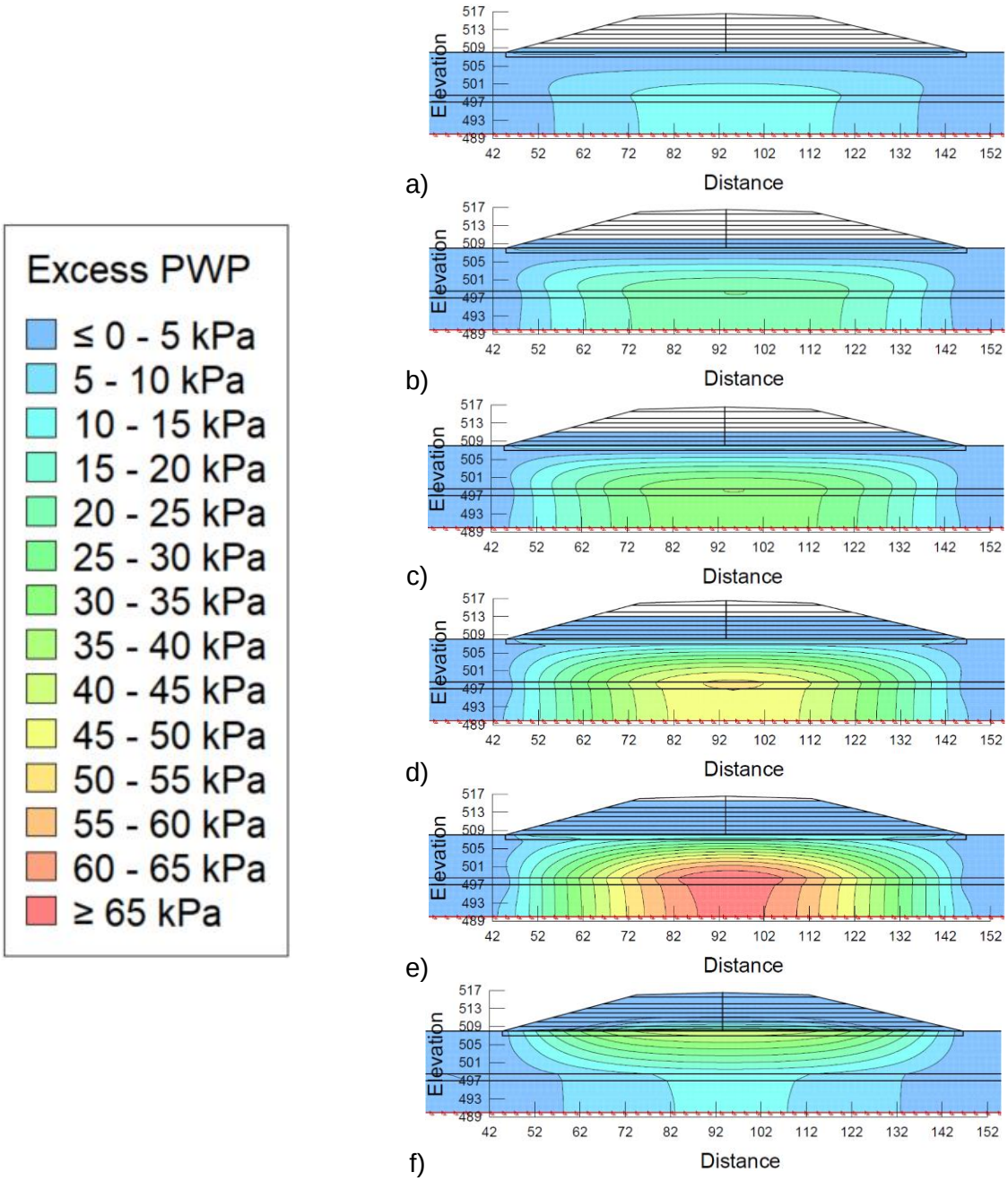

Figure 7-13 – FEM South Abutment TH17-01 Cross-Section PWP Contour for a) Lift 1, b) Lift 2, c) Lift 3, d) Lift 4, e) Embankment Complete, f) PWP Dissipated

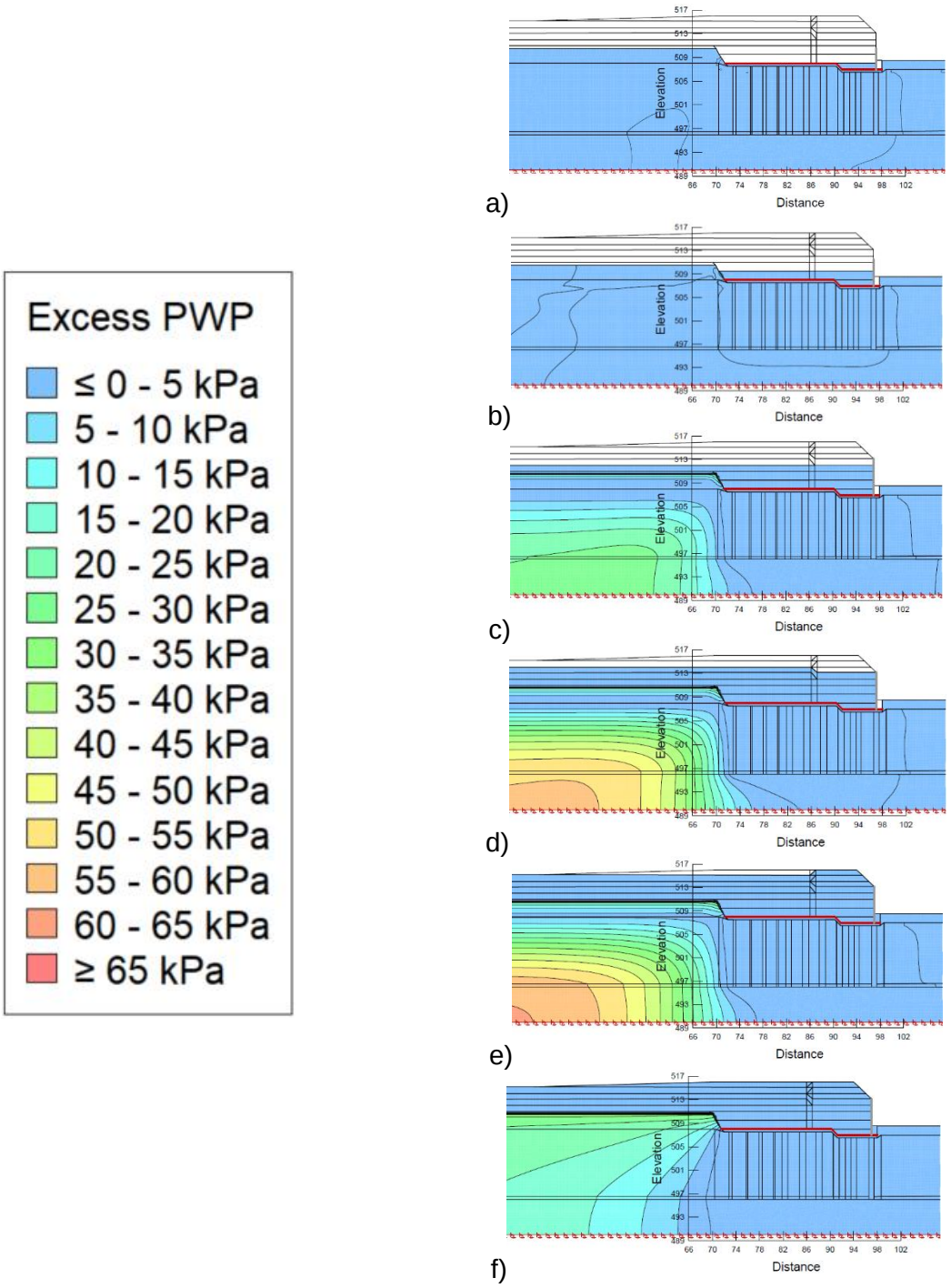

Figure 7-14 – FEM North Abutment Profile PWP Contour for a) Lift 1, b) Lift 2, c) Lift 3, d) Lift 4, e) Embankment Complete, f) PWP Dissipated

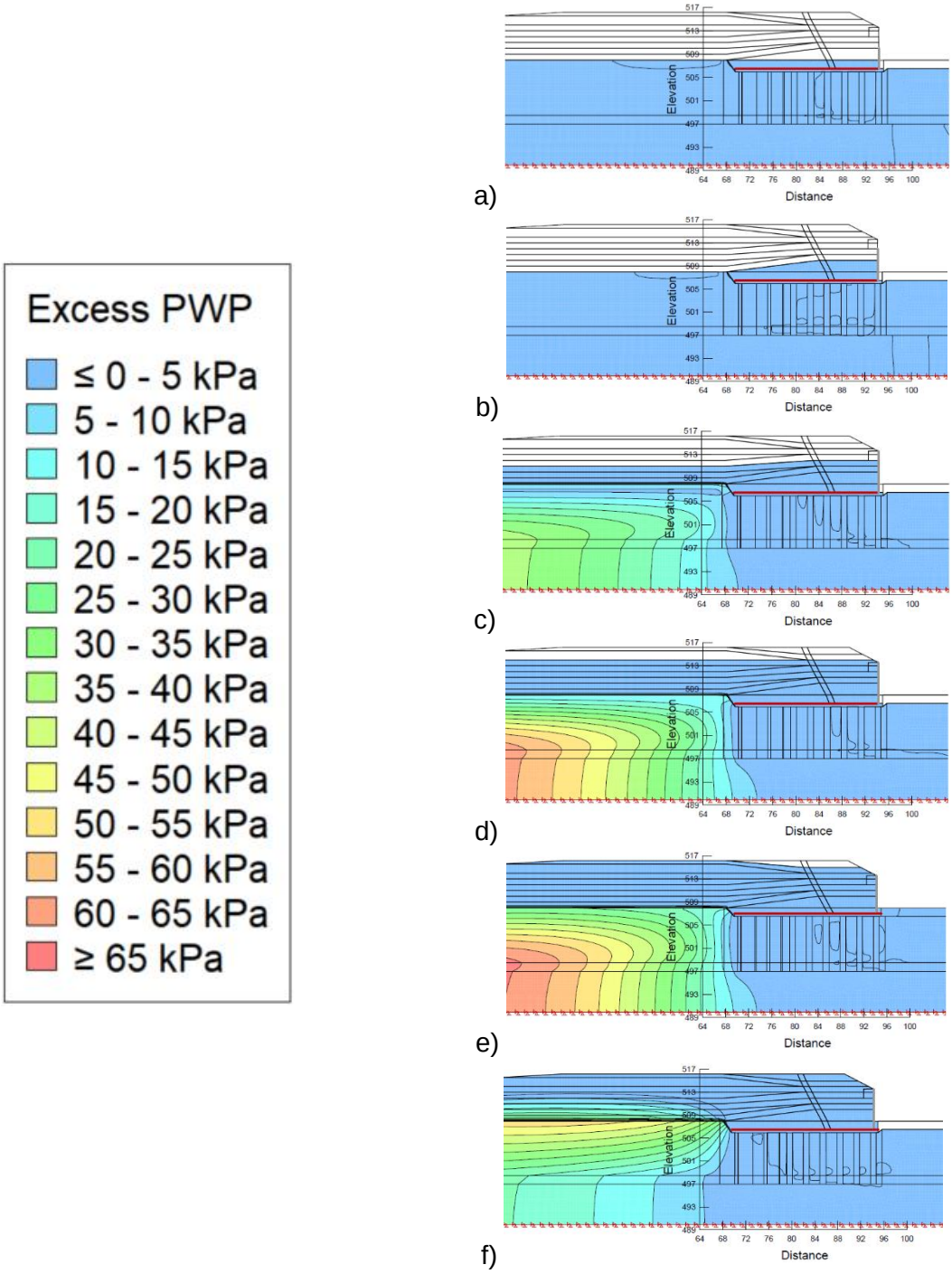

Figure 7-15 – FEM South Abutment Profile PWP Contour for a) Lift 1, b) Lift 2, c) Lift 3, d) Lift 4, e) Embankment Complete, f) PWP Dissipated

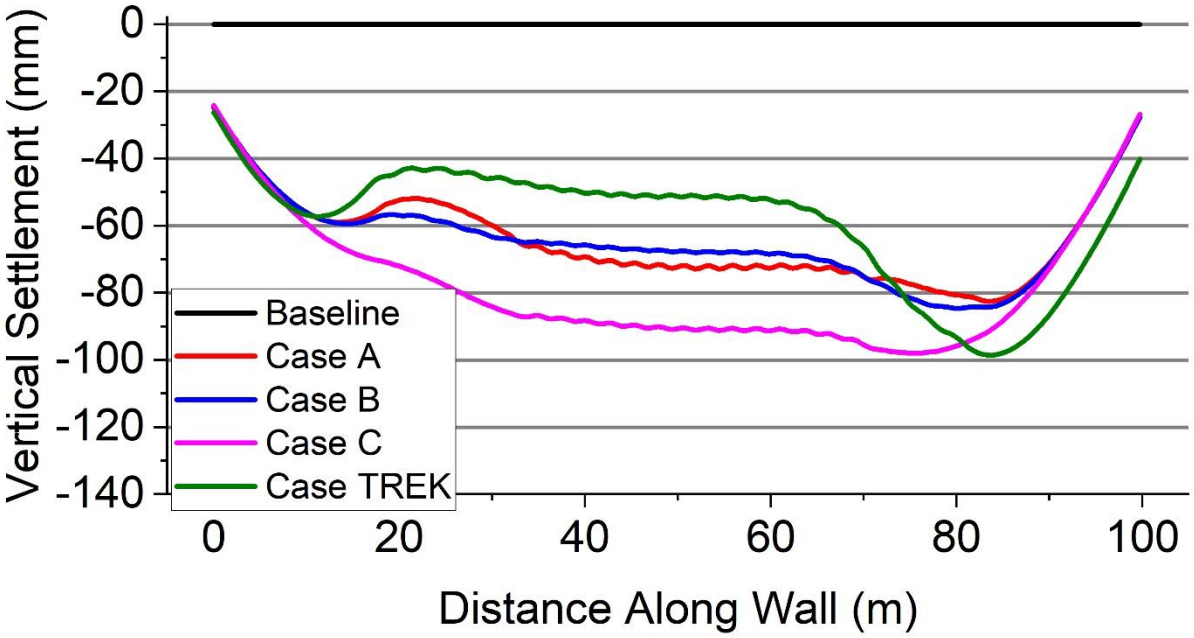

Figure 7-16 – FEM North Abutment Cross-Section Comparison of Different ESA Settlements

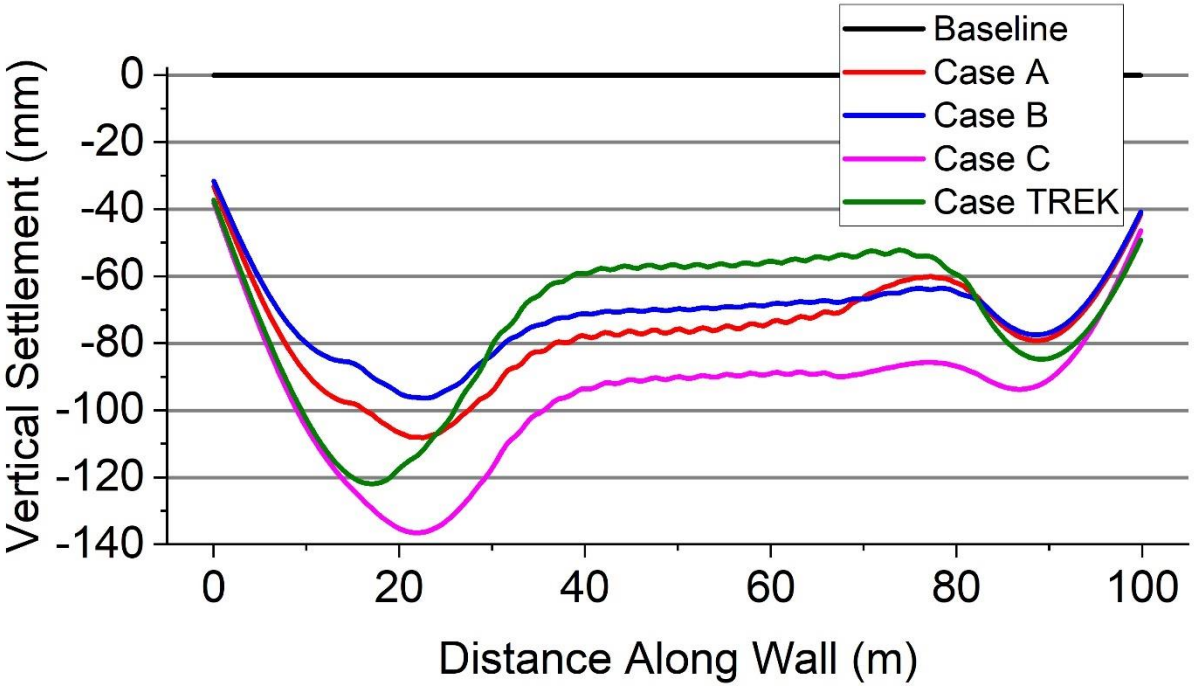

Figure 7-17 – FEM South Abutment Cross-Section Comparison of Different ESA Settlements

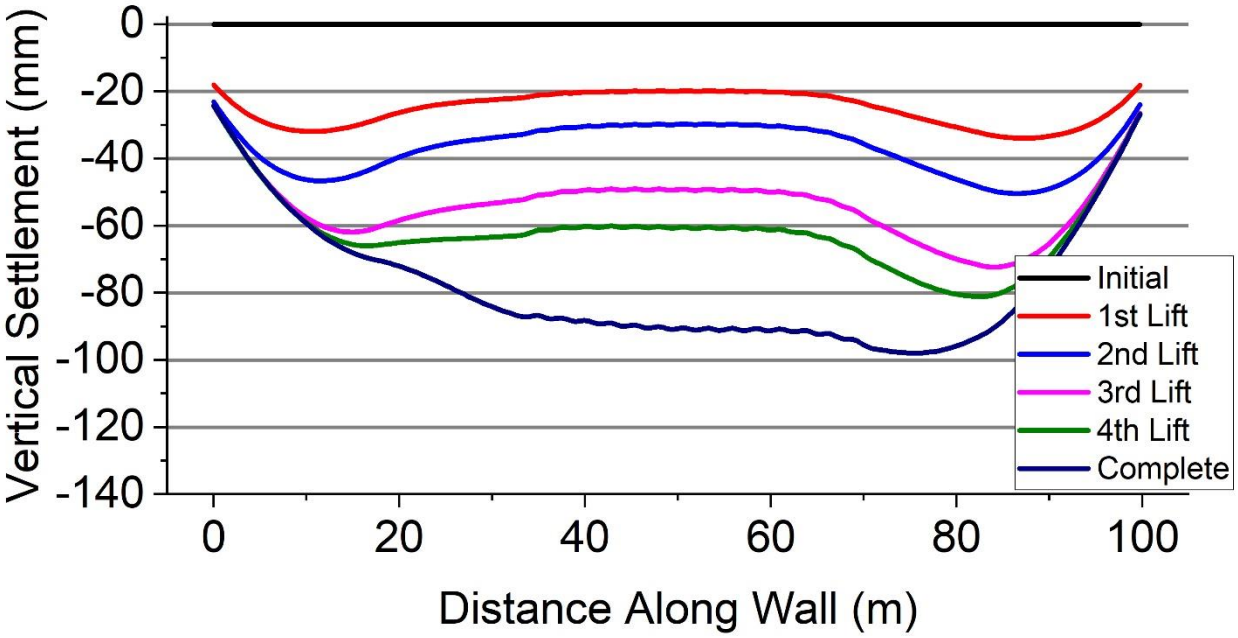

Figure 7-18 – FEM North Abutment ESA Cross-Section Settlement

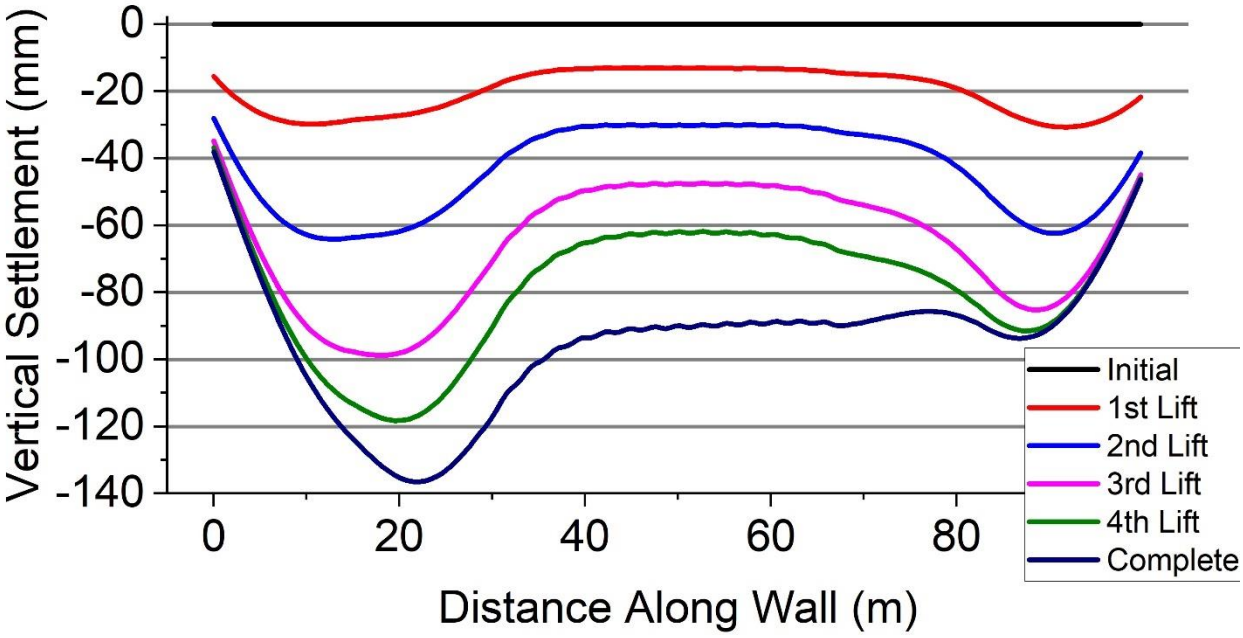

Figure 7-19 – FEM South Abutment ESA Cross-Section Settlement

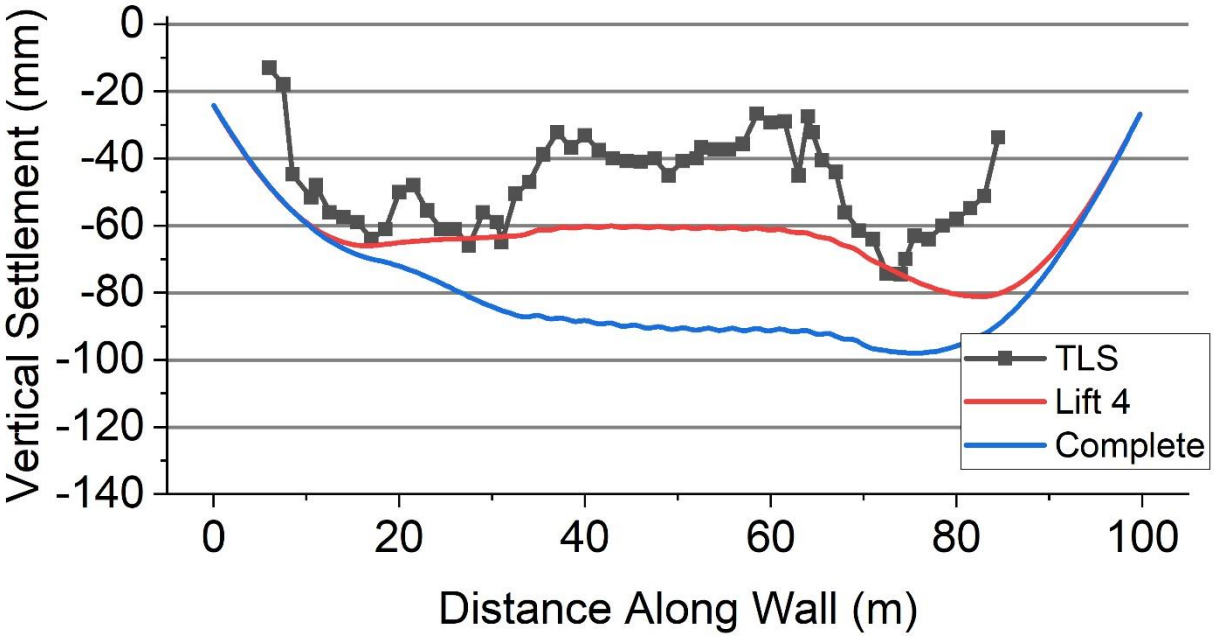

Figure 7-20 – TLS vs FEM North Abutment ESA Cross-Section Final Settlement

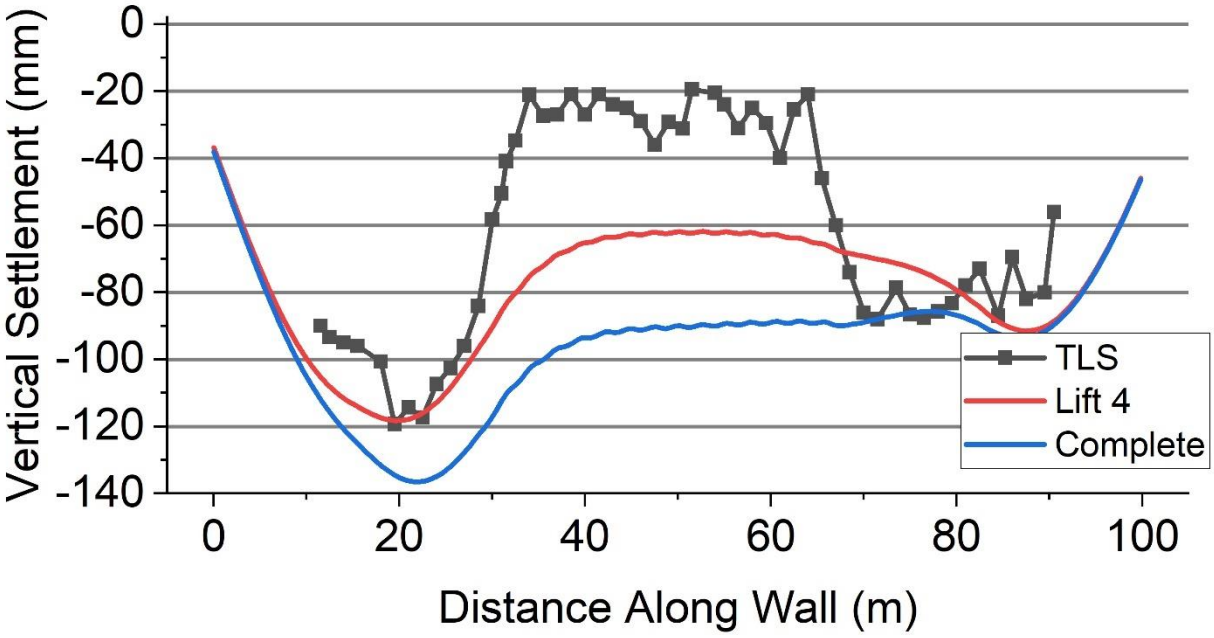

Figure 7-21 – TLS vs FEM South Abutment ESA Cross-Section Final Settlement

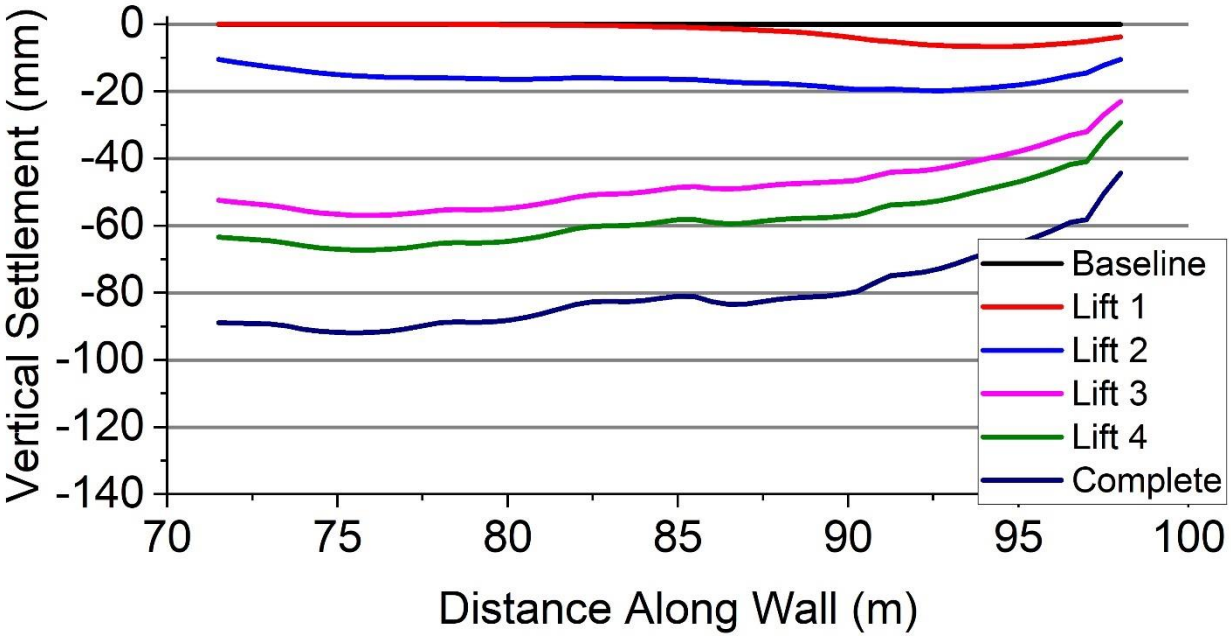

Figure 7-22 – FEM North Abutment ESA Profile Settlement

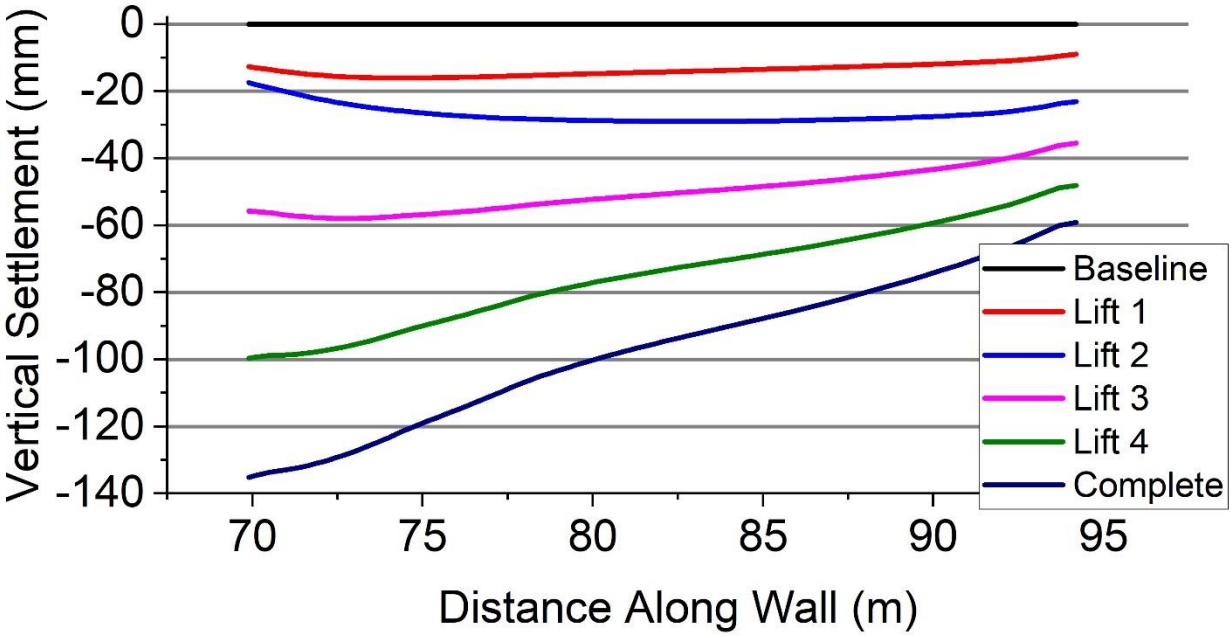

Figure 7-23 – FEM South Abutment ESA Profile Settlement

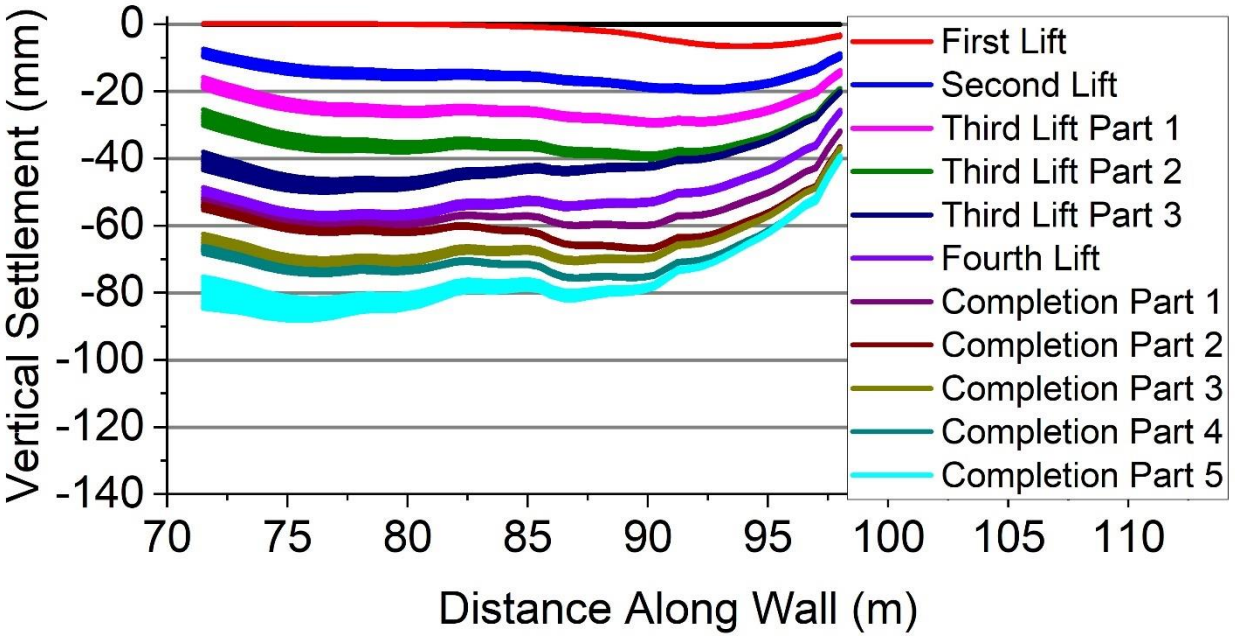

Figure 7-24 – FEM North Abutment PWP Profile Settlement

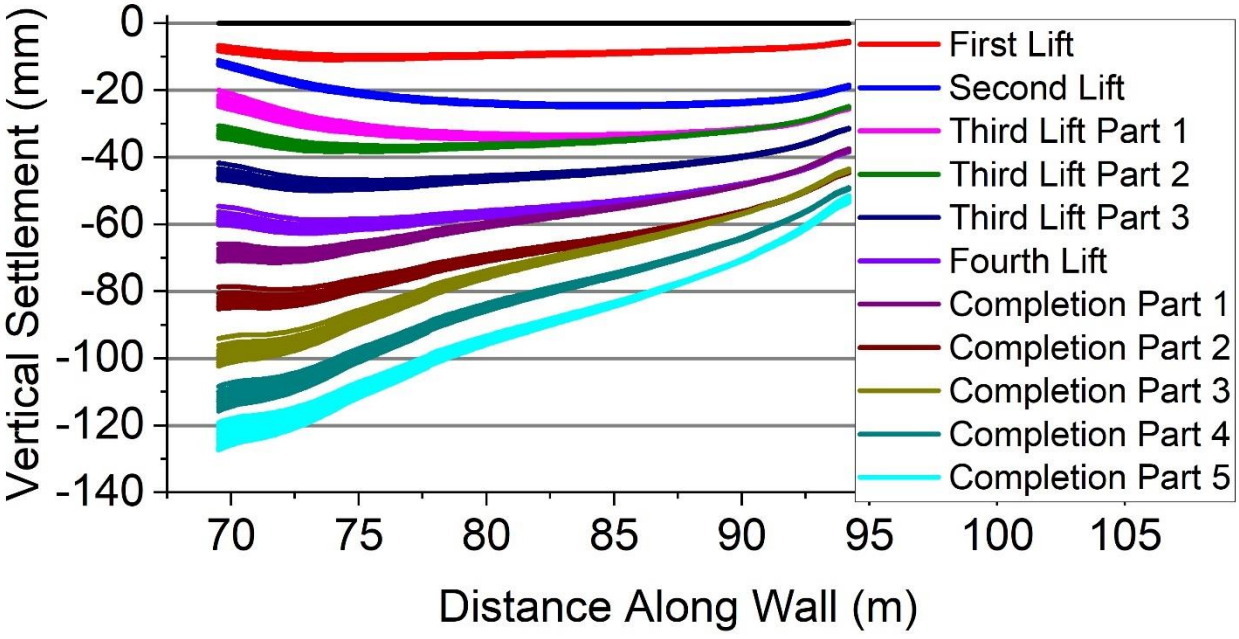

Figure 7-25 – FEM South Abutment PWP Profile Settlement

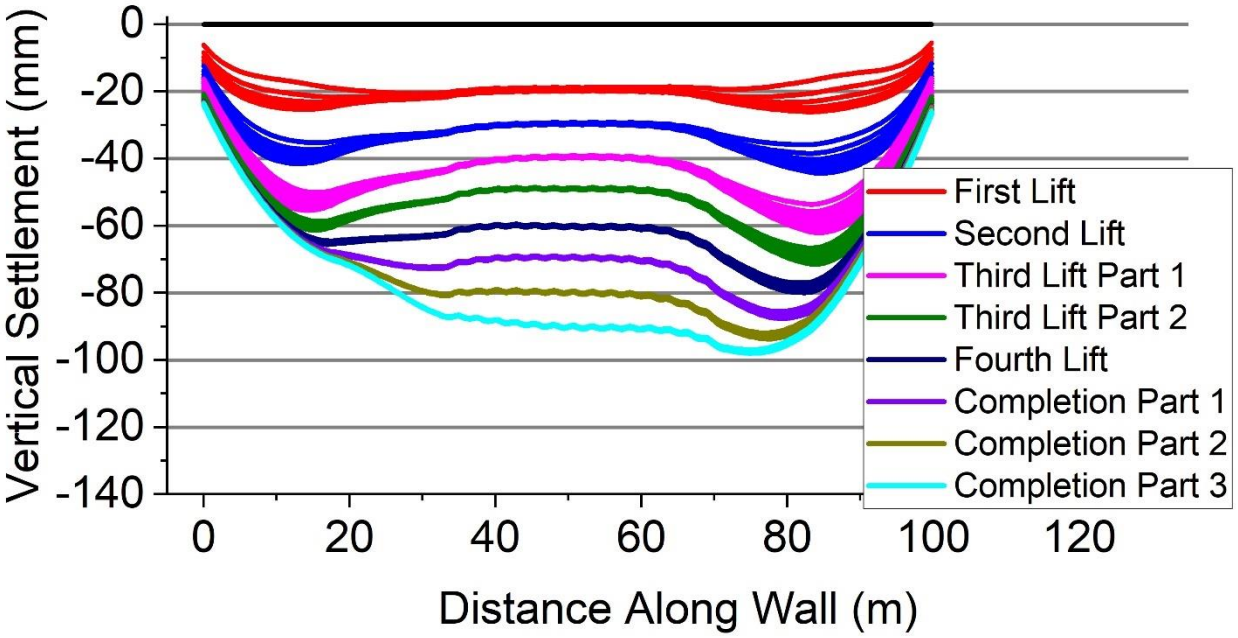

Figure 7-26 – FEM North Abutment PWP Cross-Section Settlement

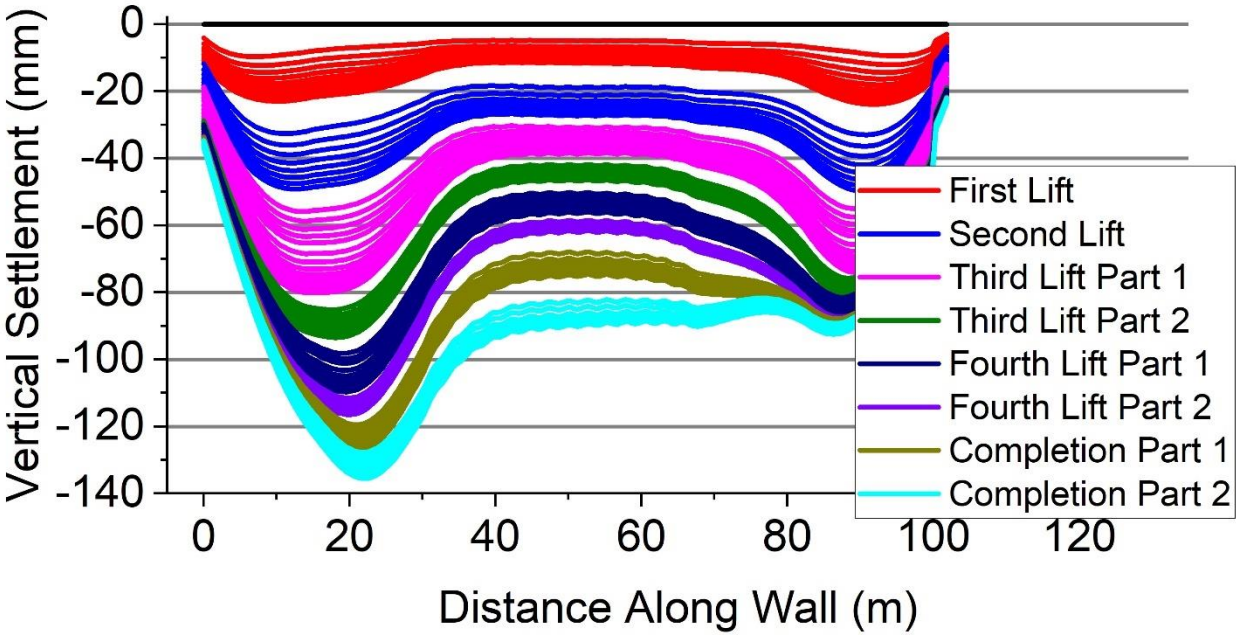

Figure 7-27 – FEM South Abutment PWP Cross-Section Settlement

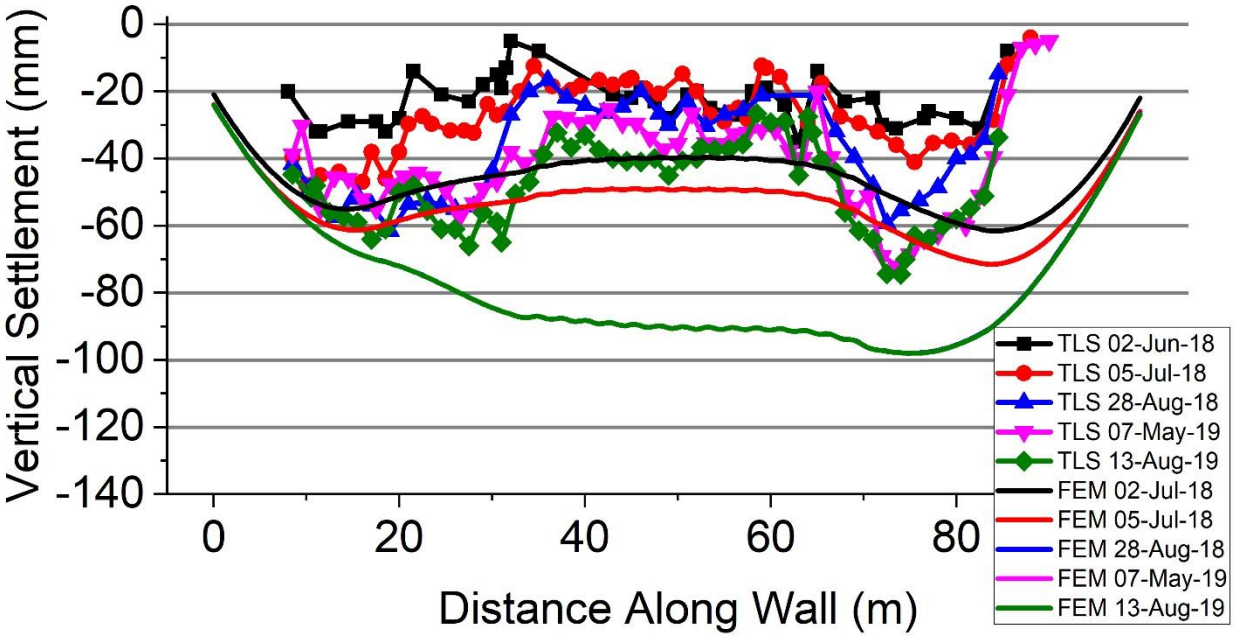

Figure 7-28 – TLS vs FEM North Abutment Cross-Section Settlement Comparison

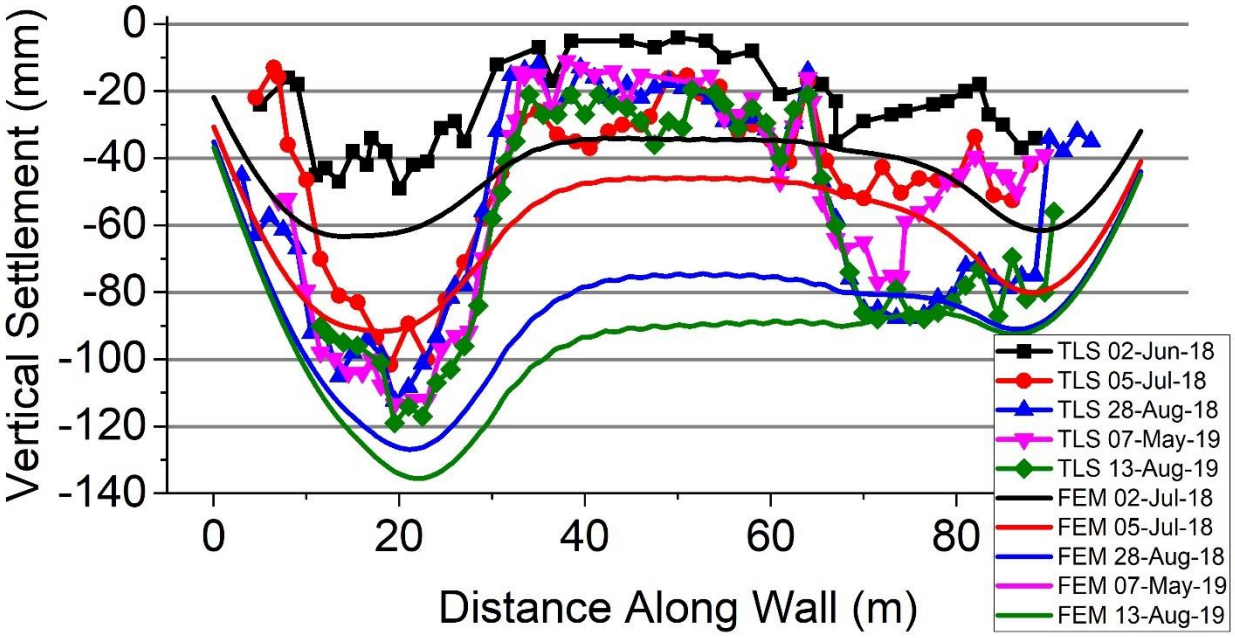

Figure 7-29 – TLS vs FEM South Abutment Cross-Section Settlement Comparison

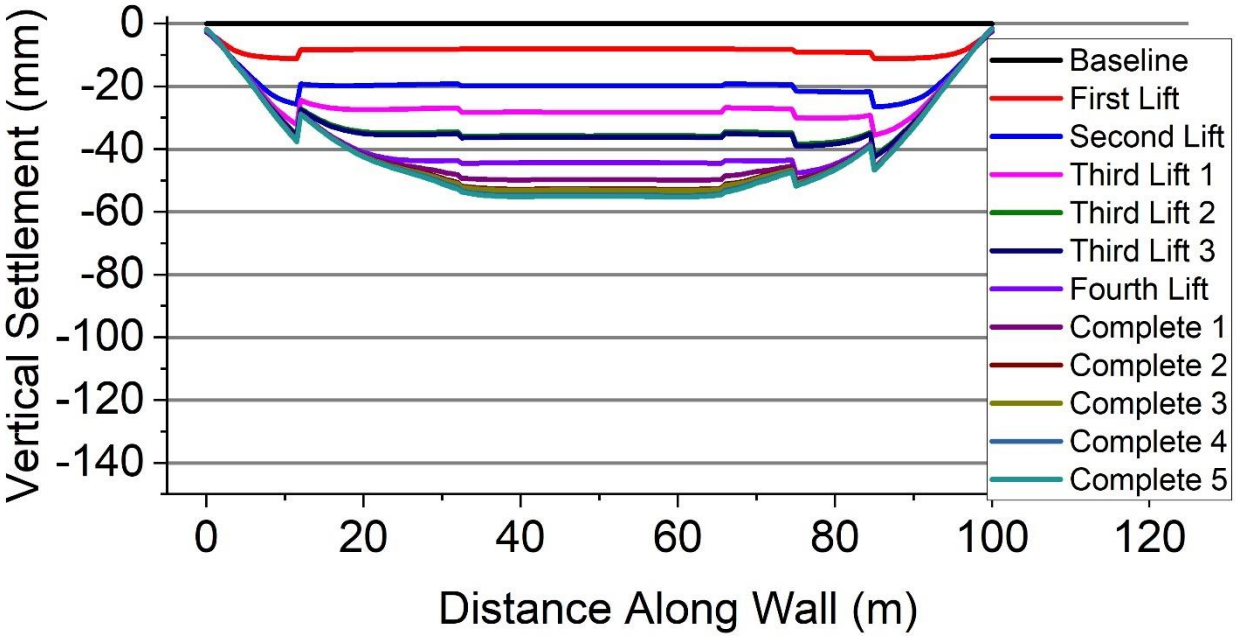

Figure 7-30 – 1D Consolidation North Abutment Cross-Section Settlement

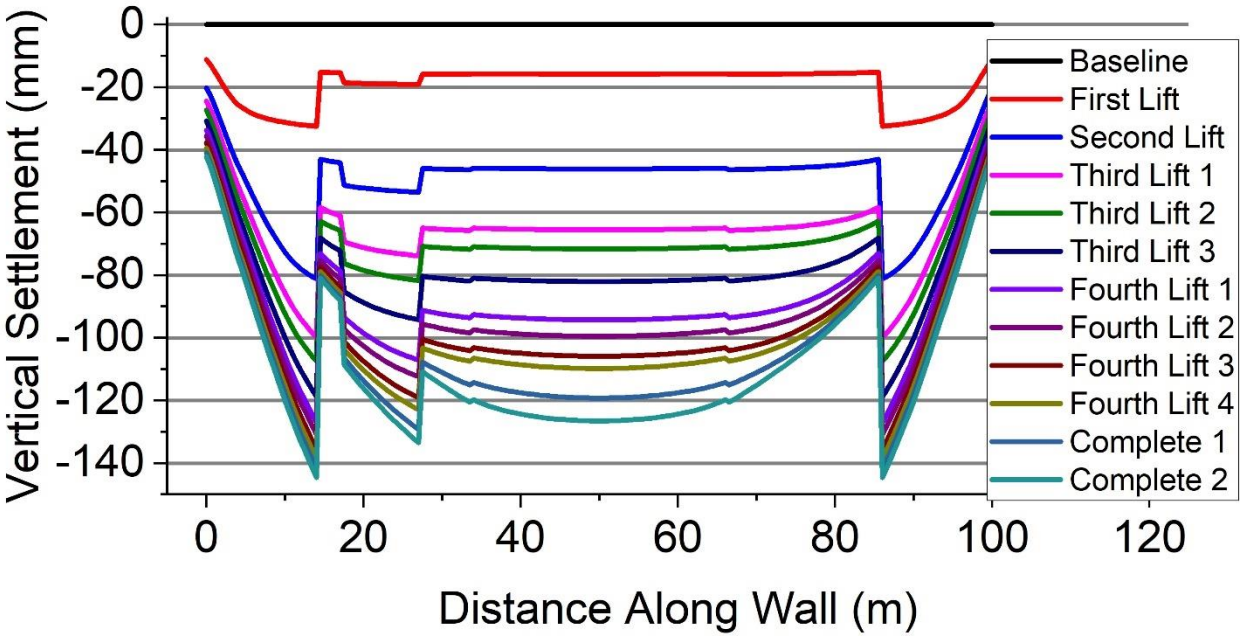

Figure 7-31 – 1D Consolidation South Abutment Cross-Section Settlement

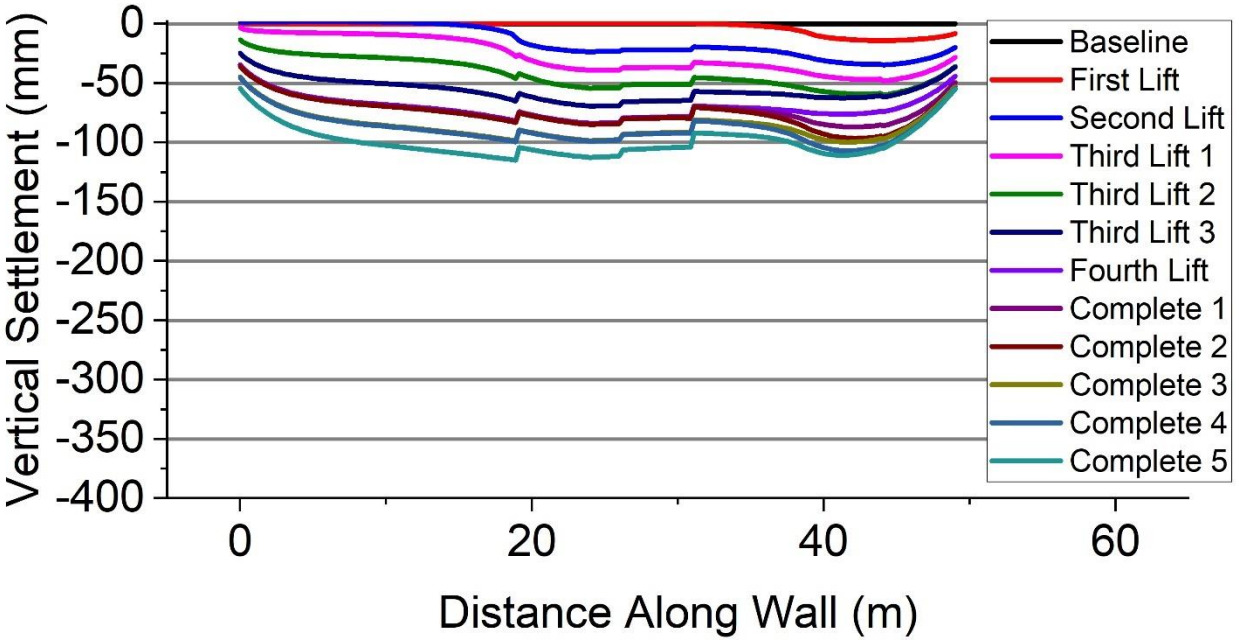

Figure 7-32 – 1D Consolidation North Abutment Profile Settlement

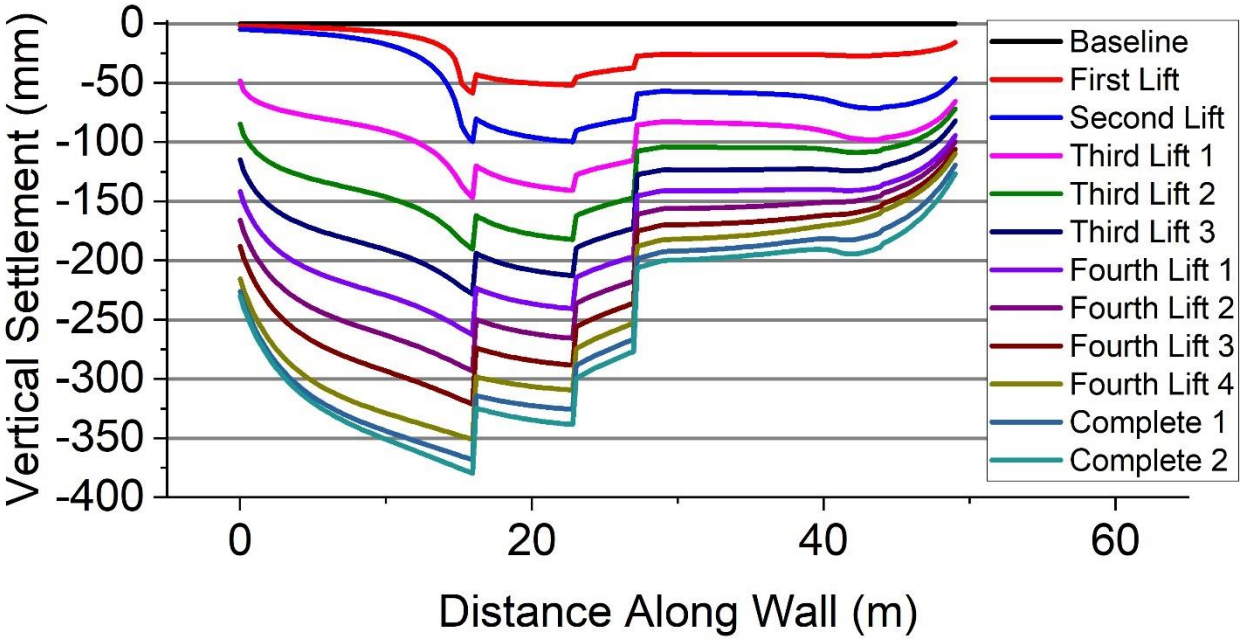

Figure 7-33 – 1D Consolidation South Abutment Profile Settlement

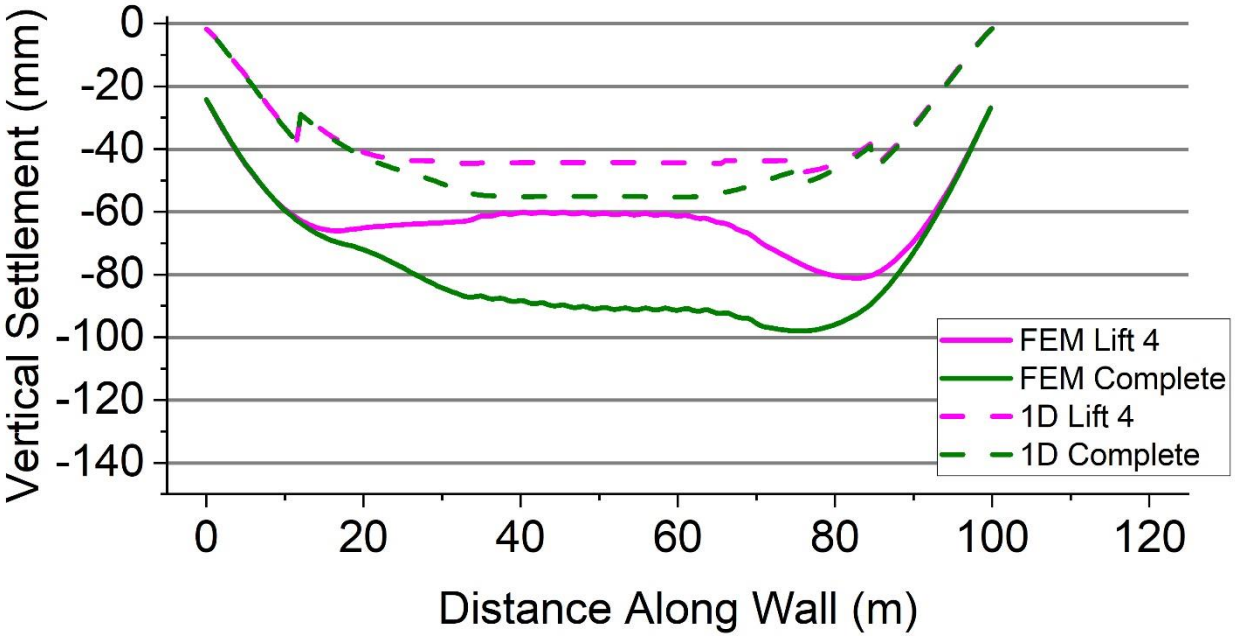

Figure 7-34 – FEM vs 1D Consolidation North Abutment Cross-Section Settlement Comparison

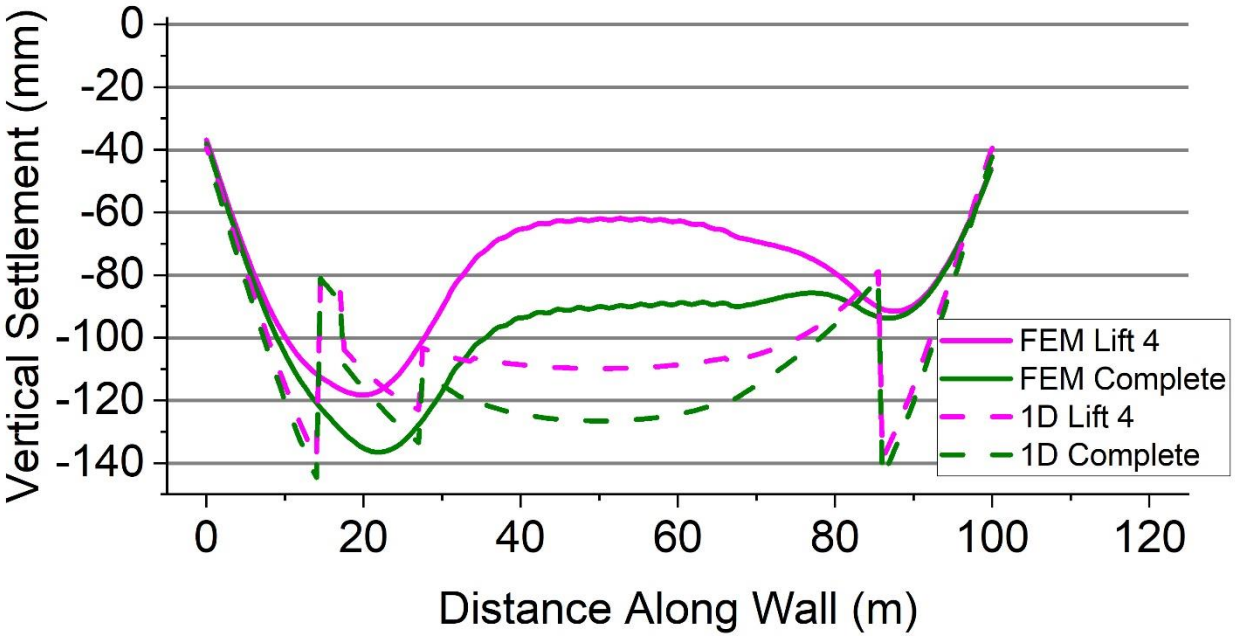

Figure 7-35 – FEM vs 1D Consolidation South Abutment Cross-Section Settlement Comparison

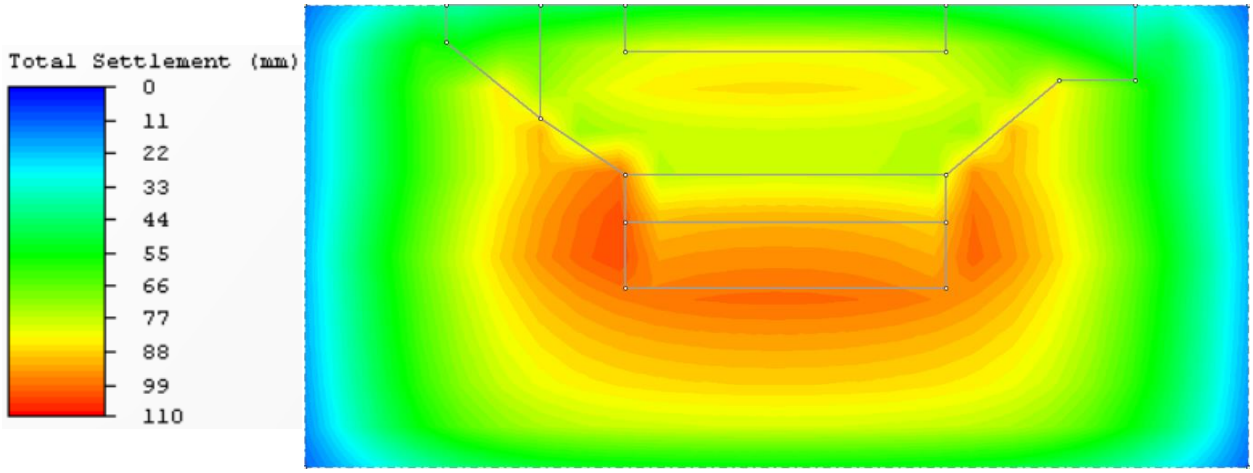

Figure 7-36 – 1D Consolidation North Abutment 3D Grid Settlement Contour

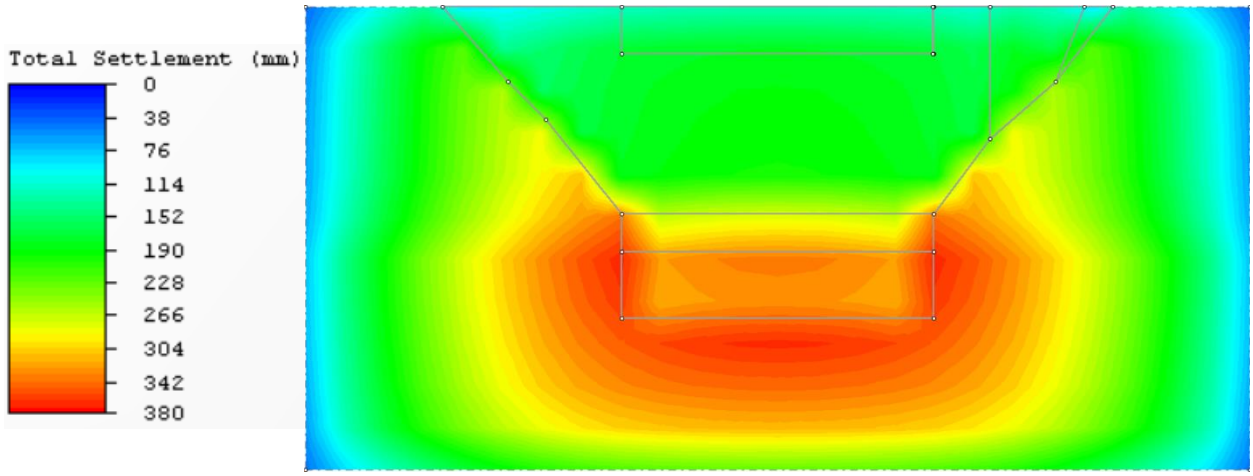

Figure 7-37 – 1D Consolidation South Abutment 3D Grid Settlement Contour

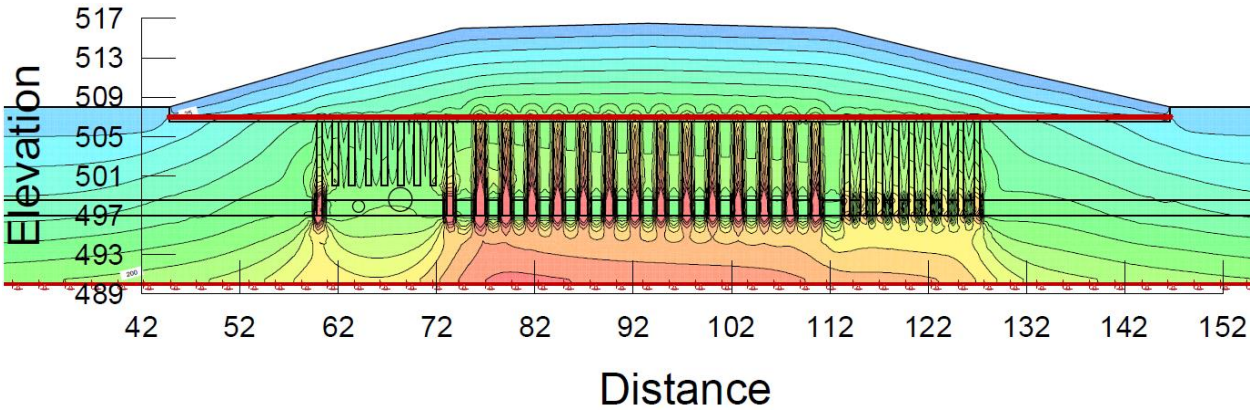

Figure 7-38 – FEM South Abutment Cross-Section Model Y-Effective Stress Contour

8 Conclusion and Recommendations

This chapter discusses the conclusions made from the previous results and discussions chapter; separated into different sub-chapters for each of the settlement surveying/prediction methods: rod and level, laser scanner, finite element method, and 1D consolidation analysis. Then from the summarized conclusions, recommendations are presented for future research practitioners who will use the equipment and/or numerical modelling software.

The purpose of this chapter is to sum up the analysis of the research results and answer the objectives and hypothesis formed at the beginning of this project.

8.1 Surveying Methods

8.1.1 Conclusions

Conclusions were developed from the experiences for data collection and processing, and data analysis and interpretation of the results:

Data Collection and Processing

Although the RL measurements had less settlement fluctuations in each survey, the ability for the laser scanner to measure the entire settlement along both 100m long walls provided more information for higher quality of monitoring. TLS may have taken longer to scan the structure on site than surveying with the RL, but one user could setup and perform the TLS survey whereas it was required for one person to hold the rod and another person to operate the level.

The TLS was more complex with requiring additional targets on site to help orient the scanner and additional geocaching. However, with trying to geocache all the targets on site, the scanner was subjected to more processing errors and manual adjustments of the clouds were required. In the end, the combination of registering clouds with target selection and manual manipulation of the clouds translation and rotation proved to have the best results for deformation analysis.

Data Analysis and Interpretation of Results

The results from RL and TLS were generally in good agreement, falling within the ±20mm tolerance range as they both measured more settlement exhibited by the south abutment than the north abutment. Discrepancies between the results were evident as the laser scanner measured less settlement within the centre section of the south wall (30mm compared to 68mm), or the RL measuring maximum settlement within the west section as opposed to TLS measuring maximum settlements within the east section (RL measured 79mm and 119mm for east and west sections respectively; TLS measured 119mm and 88mm for east and west sections respectively). However, these discrepancies were interpreted to be errors incurred from the registration process of point clouds and the lack of RL surveying locations along the wall.

8.1.2 Recommendations

For future research on monitoring MSE walls with segmented precast concrete panels using TLS, measuring the horizontal deflection would be interesting. In the case of this MSE wall, settlement was to be monitored closely for the low design tolerance while horizontal movement was not expected to be large enough to warrant monitoring. The inclusion of instrumentation of surveying at the end of the reinforced zone could provide insight on the down drag effects from differential settlement.

Another useful tip to obtain accurate measurements is by limiting the amount of scans for monitoring. The more scans that are introduced into the survey, more registration error will be incurred from alignment and if the point cloud software used does not calculate loop misclosure error (in this case FARO Scene), compounded errors cannot be quantified and accounted for. In the case of the baseline measurement, the supports used to keep the panels in place for backfill obstructed the line of sight, allowing less data points to be collected on the wall panel surfaces. Placing the scanner farther from the wall and increasing the resolution would solve this issue.

For future design and monitoring of structures like the MSE wall, it is recommended to use TLS as it can collect large amounts of datasets on the entire structure with high accuracy. If the error tolerance is very strict or the structure is not expected to deform much, an additional survey like the RL or the Total Station should be used as well to provide control at specific locations along the structure.

8.2 Numerical Modelling

8.2.1 Conclusions

Conclusions were developed from the model setup and analysis, and interpretation of the results:

Model Setup and Analysis

Model parameters and geometry for both software programs were relatively easy to find as some modelling was carried out by TREK and online publications helped to fill any gaps of unknown material properties that were not in the design report. Piezometer data was only available for the south abutment and with little to hydraulic conductivity results obtained from lab testing, back analysis using local lab testing publications was performed for the south abutment and then assumed equal for the north abutment.

Although RocScience's Settle3 can model in three dimensions, both programs do not analyze settlement in 3D and there were large assumptions made to accommodate this limitation. Using Geostudio's SIGMA/W component, models were developed for profile and cross-sectional analyses to measure both the settlement along the length of the wall and the settlement underneath the approach embankment, converting the individually spaced rockfill columns into an equivalent soil wall (2D parameters). Settle3 was able to model ground conditions using borehole log information but modelled the approach embankments as live loads and the rockfill columns and foundation soil were converted into one large equivalent soil mass block.

Interpretation of the Results

The finite element model results agreed with the surveying completed by the laser scanner for the east and west sections of both north and south abutments with some margin of error (±20mm). However, the settlements computed for the centre sections were overestimated by magnitudes of 50-60mm. This was believed to be attributed to the conversion of rockfill column properties from axisymmetric to plane strain conditions and the lack of detailed borehole information within the reinforced region of both abutments.

How the rockfill columns' parameters were converted from axisymmetric to plane strain played a large role in computing the settlements. The difference in settlement could vary by ±40mm when comparing the different conversion techniques. Depending on the structure, this magnitude of settlement could cause concerns over performance and therefore, careful consideration for site conditions was required.

The results obtained from 1D Consolidation analysis was not a smooth spline curve as compared to the finite element results. This was from the different sized rockfill column regions within the foundation. Along the wall, there were varying sections of unreinforced soil, 1.8m diameter columns, and 2.1m diameter columns. The load transfer between column groups adjacent to each other could not be modelled and created the instant change in settlement.

1D Consolidation analysis computed a more 'U' shaped settlement profile as opposed to the 'W' shape depicted from the surveying. This was from the above conclusion that the load transfer between columns could not performed and that the geogrid placed under the embankment could not be modelled. These components would have resulted in more stress distributed to the outer columns and flatten the settlement profile.

Comparing the results from 1D Consolidation to the surveying agreed well with the magnitude of settlement exhibited by each abutment. The measured values from TLS and 1D Consolidation for the maximum settlements of each abutment were 75mm and 55mm for the north, 119mm and

145mm for the south respectively. Location and magnitudes of these computed settlements would change but the overall settlement profile would be in good agreement with what was surveyed on site.

8.2.2 Recommendations

Concerning the numerical modelling of abutment settlement, more information about site conditions in the form of boreholes inside the abutment area will be more beneficial. Assumptions and simplifications of geometry and material properties are expected but identification of characteristics that will affect structure performance (silt layers, soil layer elevations, etc.) will help to enhance calibration and understanding of model results.

Another recommendation would be including some lab testing on the hydraulic conductivity of the different soil layers. For this project, the installation of rockfill columns underneath the abutment reduced the influence of clay permeability on the settlement performance but for abutments that have a higher tolerance and would not require additional reinforcement in the foundation, it will greatly alter the immediate settlement with each backfill lift.

For future construction projects, a Coupled Stress/PWP analysis would be beneficial to optimize time durations for stage construction schedules and determine the amount of settlement over time. The need for good lab testing data for accurate soil parameters will require a thorough site investigation program that an experienced engineer will need to take on. However, more resources during the preliminary phase of design can not only prevent scheduling delays and unpredicted costs, but also keep the public safe from issues arising from unknown ground conditions.

References

Abdul Shukar, S. A. et al., 2015. 3D Terrestrial Laser Scanner for Managing Existing Building. *Junal Teknologi,* pp. 133-139.

Alhasan, A., McGuire, M. P., Vennapusa, P. K. & White, D. J., 2016. *Application of Terrestrial Laser Scanning for the Displacement Monitoring of GRS-IBS Abutments.* Chicago, American Society of Civil Engineers, pp. 453-461.

Ariyarathne, P., Liyanapathirana, D. S. & Leo, C. J., 2013. Comparison of Different Two-Dimensional Idealizations for a Geosynthetic-Reinforced Pile-Supported Embankment. *International Journal of Geomechanics,* pp. 754-768.

Barazzetti, L. et al., 2012. 3D Scanning and Imaging for Quick Documentation of Crime and Accident Scenes. *Proc. SPIE. 8359, Sensors, and Command, Control, Communications, and Intelligence (C3I) Technologies for Homeland Security and Homeland Defense XI,* pp. 835910 (1-14).

Barron, R. A., 1948. Consolidation of Fine-Grained Soils by Drain Wells. *Transactions of the American Society of Civil Engineers,* Volume 113, pp. 718-742.

Bergado, D. T. & Long, P. V., 1994. *Numerical Analysis of Embankment on Subsiding Ground Improvement by Vertical Drains and Granular Piles.".* New Delhi, Oxford and IBH, pp. 1361-1366.

Borodinecs, A., Zemitis, J., Dobelis, M. & Kalinka, M., 2018. 3D Scanning Data Use for Modular Building Renovation Based on BIM Model. *MATEC Web of Conferences,* pp. 1-11.

Calders, K. et al., 2015. *Terrestrial LIDAR for forest monitoring,* London: ResearchGate.

Canadian Geotechnical Society, 2006. *Canadian Foundation Engineering Manual Fourth Edition.* Richmond: The Canadian Geotechnical Society.

Chai, J.-C., Shen, S.-L., Miura, N. & Bergado, D. T., 2001. Simple Method of Modeling PVD-Improved Subsoil. *Journal of Geotechnical and Geoenvironmental Engineering,* pp. 965-972.

Chan, K. & Poon, B., 2012. *Designing Stone Columns using 2D FEA with Equivalent Strips.* Wollongong, International Society for Soil Mechanics & Geotechnical Engineering , pp. 1-10.

Christiansen, E. A., 1968. Pliestocene Stratigraphy of the Saskatoon Area, Saskatchewan, Canada. *Canadian Journal of Earth Sciences, Vol 5,* pp. 1167-1173.

Christiansen, E. A., 1979. The Wisconsinan deglaciation of southern Saskatchewan and adjacent areas. *Canadian Journal of Earth Sciences Vol 16,* pp. 913-938.

Christiansen, E. A., 1992. Pliestocene Stratigraphy of the Saskatoon Area, Saskatchewan, Canada: an update. *Canadian Journal of Earth Sciences Vol 29,* pp. 1767-1778.

City of Saskatoon, 2017. *Saskatoon Interchange Project,* Saskatoon: City of Saskatoon.

Clifton, W., 2018. *Geotechnical Considerations in Design and construction of North Commuter Parkway, Saskatoon SK.* Saskatoon, Transportation Aassociation of Canada, pp. 1-16.

CSA International, 2000. *CSA-S6-00 Canadian Highway Bridge Design Code.* Toronto: CSA International.

DiFiore, S. J. & Strohman, B. P., 2012. *Look Out Below!!! Potential Pitfalls and Suggested Improvements in Design and Construction of Mechanically Stabilized Earth (MSE) Walls.* San Francisco, American Society for Civil Engineers, pp. 641-650.

Elias, V. & Christopher, B. R., 2001. *Mechanically Stabilized Earth Walls and Reinforced Soil Slopes Design and Construction Guidelines,* Washington: Naitonal Highway Institute.

Encardo-rite Group, 2020. *Vibrating Wire Piezometer - Types and Operating Principle.* [Online]
Available at: https://medium.com/@encardio/vibrating-wire-piezometer-types-and-operating-principle-7ab93d046cf
[Accessed 02 05 2020].

Envco Global, 2020. *Heavy Duty Vibrating Wire Piezometer.* [Online]
Available at: https://envcoglobal.com/catalog/civil-and-geotechnical/geotechnical-and-structural-instrumentation/heavy-duty-vibrating-wire
[Accessed 02 05 2020].

Fanti, R. et al., 2013. Terrestrial Laser Scanning for Rockfall Stability Analysis in the Cultural Heritage Site of Pitigliano (Italy). *Journal of the International Consortium on Landslides,* pp. 409-420.

FARO Technologies Inc., 2013. *Features, Benefits & Technical Specifications,* s.l.: FARO Technologies Inc..

FARO Technologies Inc., 2016. *FARO Laser Scanner Focus X 330 HDR User Manual,* Lake Mary: Faro Technologies Inc..

FARO Technologies Inc, 2019. *Laser Scanner Best Practices.* [Online]
Available at:
https://knowledge.faro.com/Hardware/3D_Scanners/Focus/Laser_Scanner_Best_Practices
[Accessed 02 May 2019].

FARO, 2019. *Laser Scanner Best Practices.* [Online]
Available at:
https://knowledge.faro.com/Hardware/3D_Scanners/Focus/Laser_Scanner_Best_Practices
[Accessed 02 May 2019].

Federal Highway Administration, 2009. *Design of Mechanically Stabilized Earth Walls and Reinforced Soil Slopes - Volume 1,* Washington: US Department of Transportation.

Garcia-Ferandez, J., 2016. *An Assessment of Errors and Their Reduction in Terrestrial Laser Scanner Measurements in Marmorean Surfaces,* Berlin: 3D Research Centre.

Geokon, 2011. *Models 4800, 4810, 4815, 4820 and 4830 VW Earth Pressure Cells Instruction Manual,* Lebanon: Geokon.

GEOKON, 2020. *Settlement Plate - Model 4625.* [Online]
Available at: https://www.geokon.com/4625
[Accessed 02 05 2020].

Geo-Slope International Ltd., 2013. *Stress-Deformation Modelling with SIGMA/W,* Calgary: s.n.

Golakiya, H. D. & Lad, M. D., 2015. Design and Behaviour of Mechanically Stabilized Earth Wall. *Journal of Emerging Technologies and Innovative Research,* pp. 145-153.

Guo, J., Yuan, L. & Wang, Q., 2019. Time and Cost Analysis of Geometric Quality Assessment of Structural Columns Based on 3D Terrestrial Laser Scanning. *Automation in Construction,* pp. 1-14.

Haggerty, M. B. & Contreras, I., 2020. *Case Study: Geotechnical Site Characterization for the I-35W Stormwater Storage Facility.* Minneapolis, American Society of Civil Engineers.

Harpstead, D. L., Schmidt, J. M. & Christopher, B. R., 2010. *Applying Lessons Learned in the Past 20 Years of MSE Wall Design & Construction.* Bellevue, American Society of Civil Engineers, pp. 478-485.

Hird, C. C., Pyrah, I. C. & Russell, D., 1992. Finite Element Modelling of Vertical Drains Beneath Embankments on Soft Ground. *Geotechnique,* pp. 499-511.

Hossain, M. S. et al., 2012. Effects of Backfill Soil on Excessive Movement of MSE Wall. *Journal of Performance of Constructed Facilities,* pp. 793-802.

Huang, J., Han, J. & Oztoprak, S., 2009. Coupled Mechanical and Hydraulic Modelling of a Geosynthetic-Reinforced Deep Mixed Column-Supported Embankment. *Journal of Geotechnical and Geoenvironmental Engineering,* pp. 1011-1021.

Hutchinson, D. L., 2011. *Case Study of a Foundation Improvement Beneath MSE walls for a Highway Embankment.* Dallas, American Society of Civil Engineers, pp. 3409-3418.

Indraratna, B. & Redana, I. W., 1997. Plane-Strain Modeling of smear Effects Associated with Vertical Drains. *Journal of Geotechnical and Geoenvironmental Engineering,* pp. 474-478.

ISIS Canada, 2007. *Reinforcing Concrete Structures with Fibre Reinforced Polymers Design Manual No. 3, Version 2.* Winnipeg: ISIS Canada Corporation.

Jiang, Y., Han, J., Parsons, R. L. & Brennan, J. J., 2016. Field Instrumentation and Evaluation of Modular-Block MSE Walls with Secondary Geogrid Layers. *Journal of Geotechnical and Geoenvironmental Engineering,* pp. (05016002) 1-15.

Jiang, Y., Han, J., Parsons, R. L. & Cai, H., 2015. *Field Monitoring of Mechanically Stabilized Earth Walls to Investigate Secondary Reinforcement Effects,* Topeka: Kansas Department of Transportation.

Knaak, T., 2017. *Structural Wall Monitoring (#1017) rev: C,* Orlando: Certainty 3D.

Koerner, R. M. & Koerner, G. R., 2011. *Recommended Layout of Instrumentation to Monitor Potential Movement of MSE Walls, Berms and Slopes,* Folsom: Geosynthetic Institute.

Kromer, R. A., 2017. *Identifying and Monitoring Rockfall Precursors using Terrestrial Laser Scanning for Improved Rockfall Hazard Management,* Kingston: Queen's University.

Kromer, R. A. et al., 2015. Identifying Rock Slope Failure Precursors using LiDAR for Transportation Corridor Hazard Management. *Engineering Geology,* pp. 93-103.

Kromer, R. et al., 2017. Managing Rockfall Risk Through Baseline Monitoring of Precursors using a Terrestrial Laser Scanner. *Canadian Geotechnical Journal,* pp. 1-15.

Laefer, D. F. & Lennon, D., 2008. *Viability Assessment of Terrestrial LiDAR for Retaining Wall Monitoring.* New Orleans, American Society of Civil Engineering.

Lato, M., Mitchell, A. & Porter, M., 2017. *Monitoring Landslide Velocity at Ten Mile Slide with Ground Based LiDAR.* Ottawa, Canadian Geotechnical Society, pp. 1-11.

Leica Geosystems, 2015. *Leica NA720/724/728/730/730 Plus User Manual,* Heerbrugg: Leica Geosystems AG.

Leica Geosystems, 2018. *Leica RTC360 3D Reality Capture Solution,* Heerburg: Leica Geosystems AG.

Little, D., 2018. *Using 3D Laser Scanners in Crime Scenes: Understanding Advantages and Disadvantages,* Utah: Weber State University.

Lopez, F. d. A., Ordonez, C., Roca-Pardinas, J. & Garcia-Cortes, S., 2014. Point Cloud Comparison under Uncertainty. Application to Beam Bridge Measurement with Terrestrial Laser Scanning. *Journal of the International Measurement Confederation (IMEKO),* pp. 259-264.

Machan, G. & Bennett, V. G., 2008. *Use of Inclinometers for Geotechnical Insrtumentation on Transportation Projects,* Washington: Transportation Research Board.

MacIntosh, M. & Rrokaj, T., 2018. *Challenges in the Design and Construction of MSE Walls on the Regina Bypass Project.* Edmonton, Canadian Geotechnical Society, pp. 1-6.

McGuire, M. P., Yust, M. B. S. & Shippee, B. J., 2017. *Application of Terrestrial Lidar and Photogrammetry to the As-Built Verification and Displacement Monitoring of a Segmental Retaining Wall.* Orlando, American Society of Civil Engineers, pp. 461-471.

MDH Engineered Solutions, 2011. *Hydrogeology Mapping of NTS Mapsheet Saskatoon 73B,* Saskatoon: Saskatchewan Watershed Authourity.

Mohamedzein, Y. E. -A. & Al-Shibani, I. H., 2010. Performance of an embankment supported on soft soil reinforced by stone columns. *Ground Improvement Volume 164, Issue GI4,* pp. 213-224.

Oleksuik, W. & Sankey, E., 2014. *Comparison of Laser Scanner and Total Station Survey Methods: Analysis of Time and Accuracy for Building Modeling,* Burnaby: British Columbia Institue of Technology Geomatics Department.

Reinforced Earth Company Ltd., 2020. *Reinforced Earth Technology.* [Online] Available at: http://www.recocanada.com/ta/wRECO_en.nsf/sb/techniques.reinforced-earth

RocScience Inc., 2009. *Settle3D: Settlement and Consolidation Analysis,* s.l.: RocScience Inc..

RocScience Inc., 2020. *Settle 3 Program.* [Online] Available at: https://www.rocscience.com/software/settle3

RocScience Inc., n.d. *Ground Improvement Feature: Verification of Settlement Calculations for Stone Columns,* s.l.: s.n.

RST Instruments, 2020. *Load Stress and Pressure.* [Online] Available at: https://www.rstinstruments.com/product/load-stress-and-pressure/total-earth-pressure-cells

Samtani, N. C. & Nowatzki, E. A., 2006. *Soils and Foundations Reference Manual - Volume 2,* Washington: National Highway Institue.

Sankey, J. E., Brabant, K. & Masse, F., 2011. *Stand Alone and Combined Technologies for MSE Walls: State of Practice for Compressible Soils.* Dallas, American Society for Civil Engineers, pp. 3419-3428.

Scarborough, J. A., 2005. *A Tale of Two Walls: Case Histories of Failed MSE Walls.* Austin, American Society for Civil Engineers, pp. 1-12.

Scotland, I. et al., 2014. *Measuring Deformation Performance of Geogrid Reinforced Structures Using a Terrestrial Laser Scanner.* Berlin, Loughborough University Institutional Repository.

Scotland, I. e. a., 2014. *Measuring Deformation Performance of Geogrid Reinforced Structures Using a Terrestrial Laser Scanner.* Berlin, Loughborough University Institutional Repository.

Shukla, S. K., 2012. *Handbook of Geosynthetic Engineering: Geosynthetics and their Applications.* London: ICE Publishing.

Skempton, A. W. & Jones, O. T., 1944. Notes on the Compressibility of Clays. *Journal of Geological Society,* pp. 100,199-135.

Staiger, R., 2011. *10 Years of Terrestrial Laser Scanning - Technology, Systems and Applications,* Bochum: University of Applied Sciences.

Stewart, D. P., Jewell, R. J. & Randolph, M. F., 1993. Numerical Modelling of Piled Bridge Abutments on Soft Ground. *Computers and Geotechnics,* pp. 21-46.

Stuedlein, A. W. et al., 2010. Design and Performance of a 46-m-High MSE Wall. *Journal of Geotechnical and Geoenvironmental Engineering,* p. American Society of Civil Engineers.

Tan, S. A. & Oo, K. K., 2005. *Stone Column FEM Modeling - 2D and 3D Considerations Illustrated by Case History.* Bangkok, Asian Centre for Soil Improvement and Geosynthetics, pp. 157-169.

Tan, S. A., Tijahyono, S. & Oo, K. K., 2008. Simplified Plane-Strain Modeling of Stone-Column Reinforced Ground. *Journal of Geotechnical and Geoenvironmental Engineering,* pp. 185-194.

Tice, P., 2017. *Five Things to Know for Better Targeted Point Cloud Registration.* [Online] Available at: https://www.spar3d.com/blogs/guest-blog/five-things-know-better-targeted-point-cloud-registration/

TREK Geotechnical Inc., 2017. *Rock Column Layout IFC,* Saskatoon: s.n.

TREK Geotechnical Inc., 2017. *Saskatoon Interchanges Project Geotechnical Design Report for McOrmond Interchange - REVISION 4,* Winnipeg: s.n.

TREK Geotechnical Inc., 2019. *Instrumentation Monitoring Report,* Winnipeg: s.n.

Truong-Hong, L. & Laefer, D., 2014. *Application of Terrestrial Laser Scanner in Bridge Inspection: Review and an Opportunity.* Madrid, s.n.

Van Helden, M. J., Blatz, J. A., Ferreira, N. J. & Skaftfeld, K., 2008. Numerical Modeling of Sand Drain Performance - A Case Study of the Salter Street Bridge Construction. *Canadian Geotechnical Journal,* pp. 751-767.

Vankavelarr, D. P. & Leshchinsky, D., 2002. *Inspection Guidelines for Construction and Post-Construction of Mechanically Stabilized Earth Wall,* Newark: Delaware Center for Transportation.

Washington State Department of Transportation, 2005. *Surveying Equipment, Measurements and Errors,* Washington: Washington State Department of Transportation.

Yang, H., Omidalizarandi, M., Xu, X. & Neumann, I., 2016. *Terrestrial Laser Scanning Technology for Deformation Monitoring and Surface Modeling of Arch Structures,* Hanover: Elsevier Ltd..

Yapage, N. N. S. et al., 2014. Numerical Modeling of an Embankment over Soft Ground Improved with Deep Cement Mixed Columns: Case History. *Journal of Geotechnical and Geoenvironmental Engineering,* 140(11), pp. 1-10.

Appendix A – Site Photos

Figure A-1 – Bridge Interchange Site as of May 9, 2018

Figure A-2 – North Approach Embankment Progress as of May 9, 2018

Figure A-3 – High-Strength Geogrid Shee

Figure A-4 – Back-Facing of North Abutment Wall Panels

Figure A-5 – Process of Wall Panel Placement

Figure A-6 – Front Facing of South Abutment Wall Panels

Figure A-7 – Front Facing of North Abutment Wall Panels (Centre Section)

Figure A-8 – North Wall Construction Progress as of May 25, 2018

Figure A-9 – Metallic Strip Reinforcement

Figure A-10 – South Wall Construction Progress as of June 2, 2018

Figure A-11 – North Wall Construction Progress as of June 2, 2018

Figure A-12 – Elevation of Compacted Granular Fill Behind North Wall on June 2, 2018

Figure A-13 – Construction of Embankment/Bridge Deck Construction on July 5, 2018

Figure A-14 – North Wall Construction Progress as of July 5, 2018

Figure A-15 – Profile View of South Abutment as of July 5, 2018

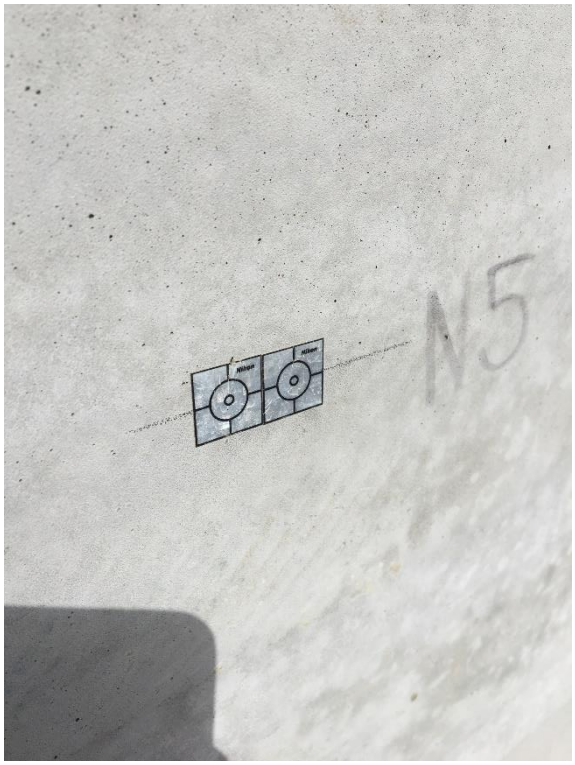

Figure A-16 – Survey Targets for Wall Measurements

Figure A-17 – North Wall Construction Progress as of August 28, 2018

Figure A-18 – Bridge Interchange Construction Progress as of August 28, 2018

Figure A-19 – North Embankment Elevation as of August 28, 2018

Figure A-20 – North Embankment Construction Progress as of August 28, 2018

Figure A-21 – Completed Bridge Interchange as of August 13, 2019

Figure A-22 – Profile View of South Abutment as of August 13, 2019

Figure A-23 – Middle Pier View Facing South Abutment as of August 13, 2019

Appendix B – Additional FEM Models

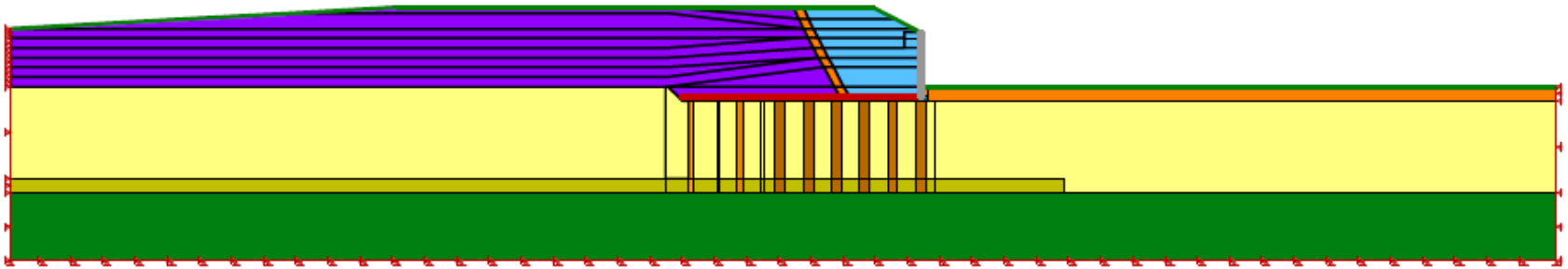

Figure A-24 – FEM South Abutment Profile Model with Horizontal Boundary Conditions

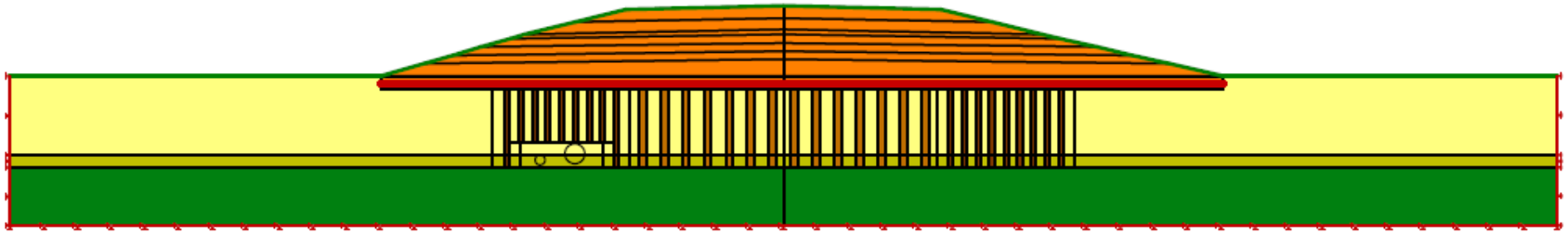

Figure A-25 – FEM South Abutment Cross-Section Model with Horizontal Boundary Conditions

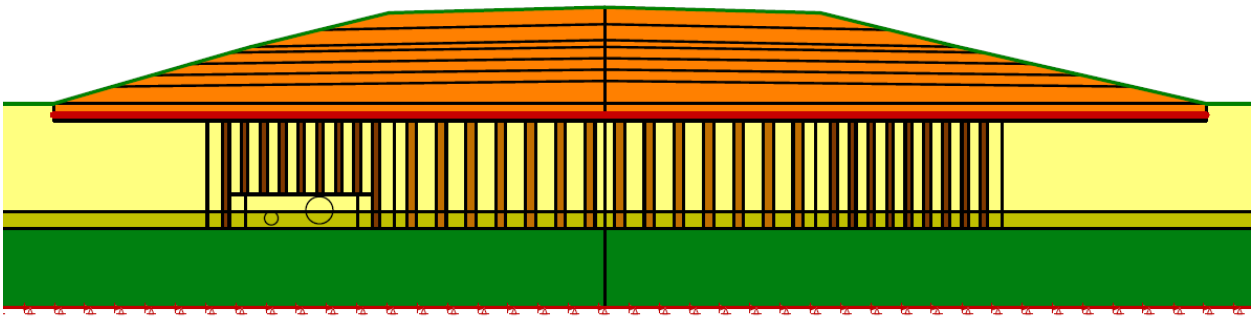

Figure A-26 – FEM South Abutment Cross-Section Model Case A

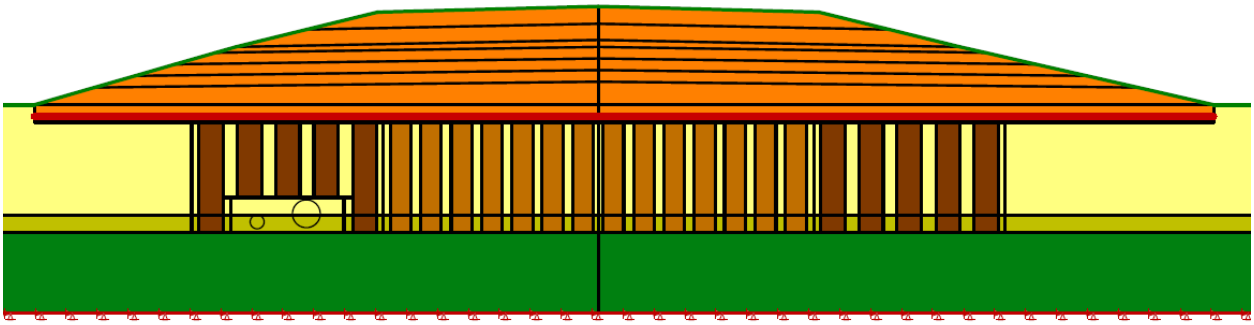

Figure A-27 – FEM South Abutment Cross-Section Model Case B

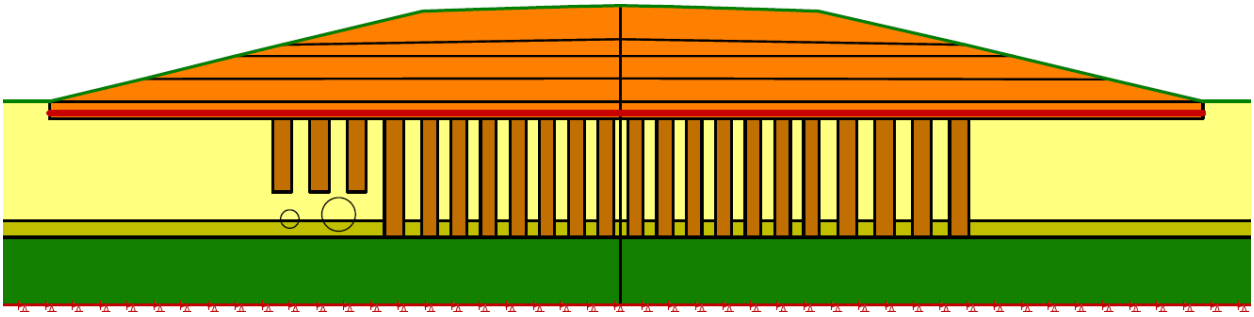

Figure A-28 – FEM South Abutment Cross-Section Model Case TREK

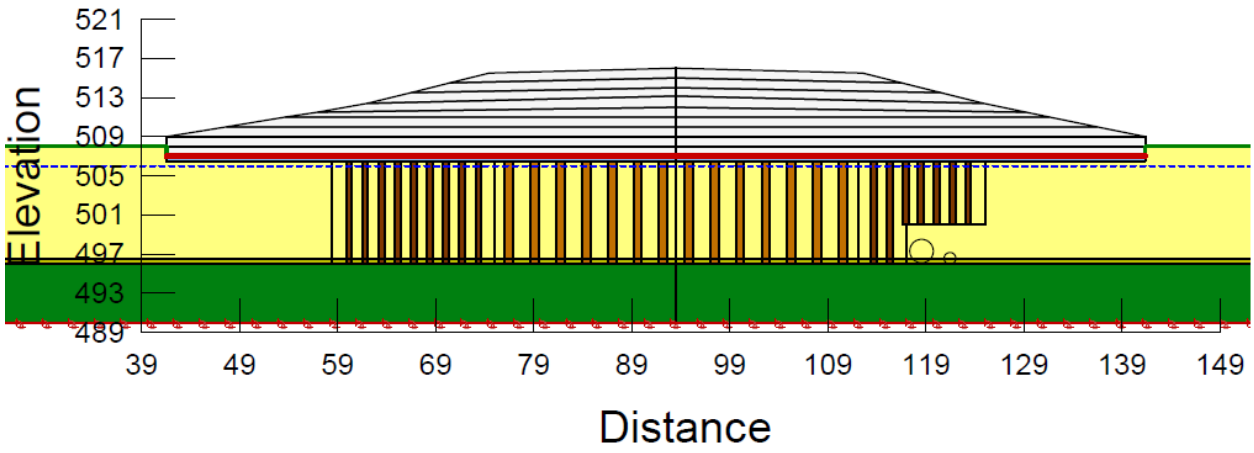

Figure A-29 – FEM North Abutment Cross-Section Model Insitu

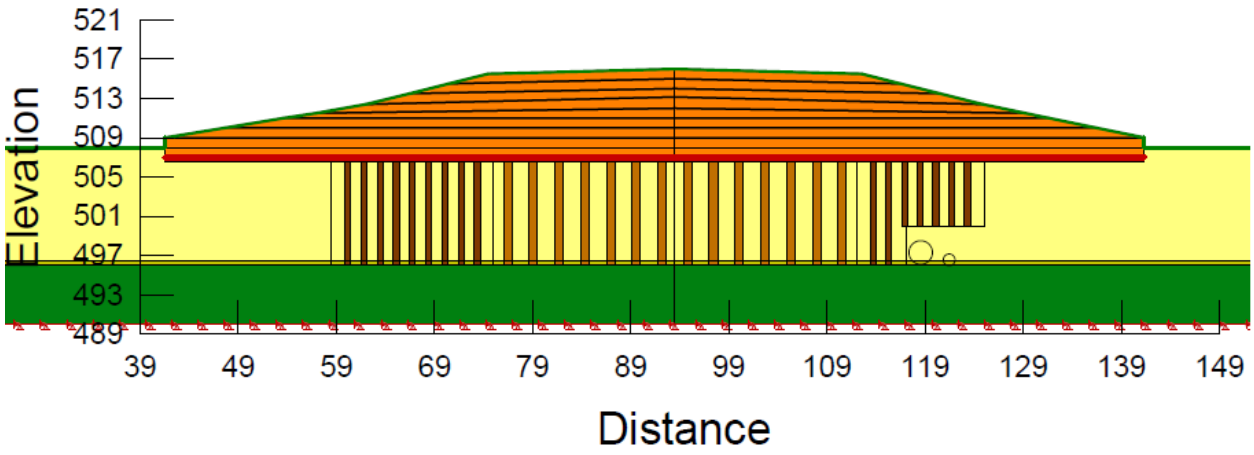

Figure A-30 – FEM North Abutment Cross-Section Model Completed Stage

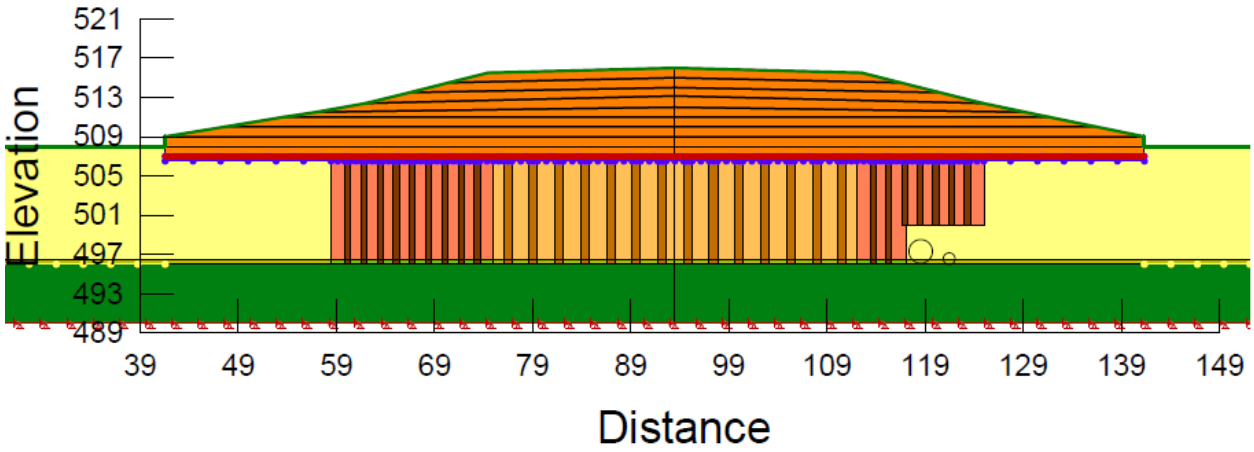

Figure A-31 – FEM North Abutment Cross-Section Model Completed Stage with Drainage Influenced Soil Zones

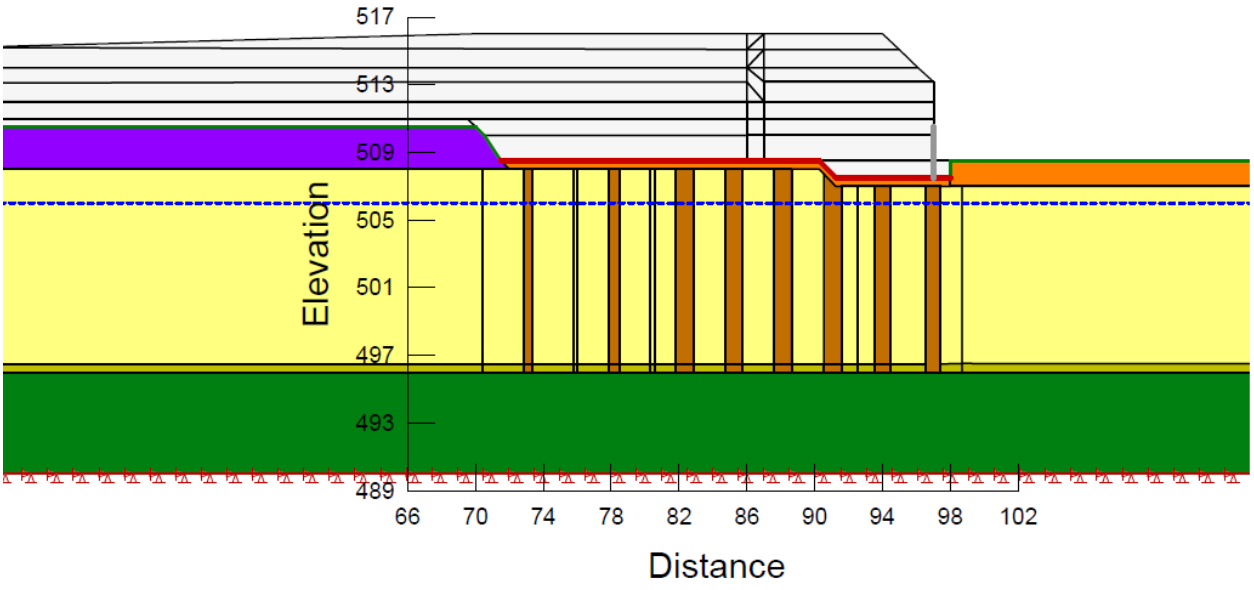

Figure A-32 – FEM North Abutment Profile Model Insitu Stage

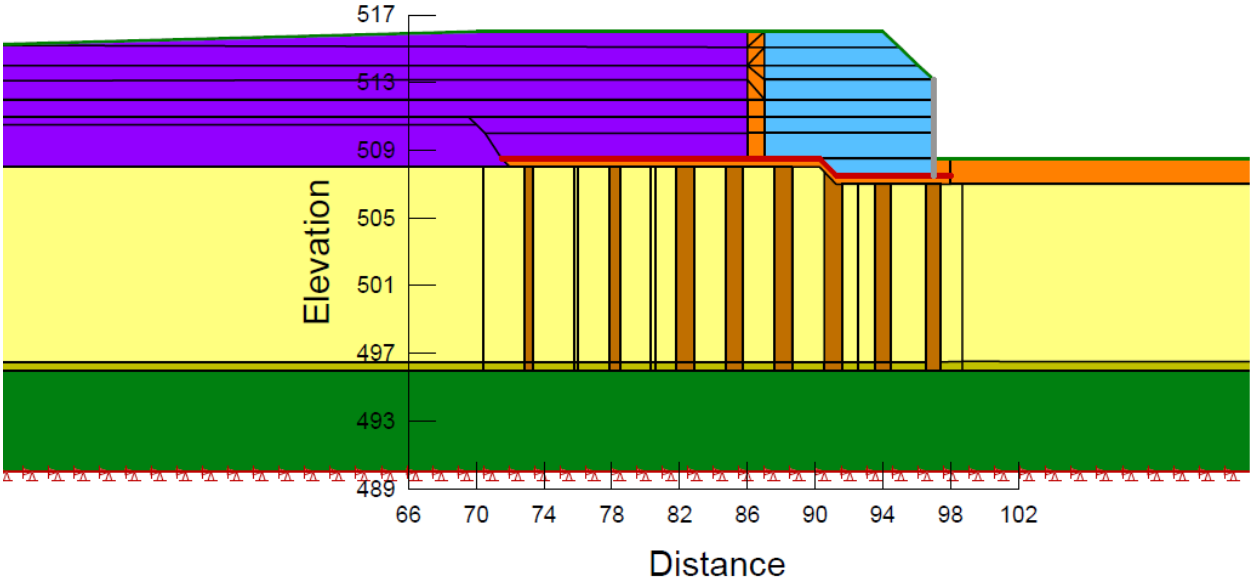

Figure A-33 – FEM North Abutment Profile Model Completed Stage

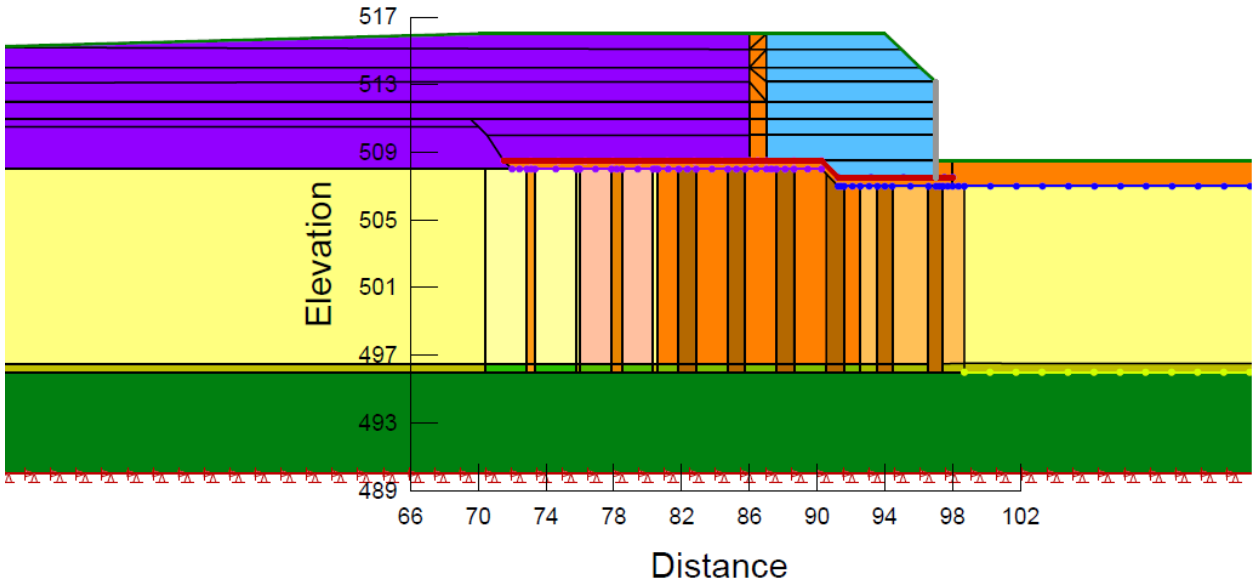

Figure A-34 – FEM North Abutment Profile Model Completed Stage with Drainage Influenced Soil Zones

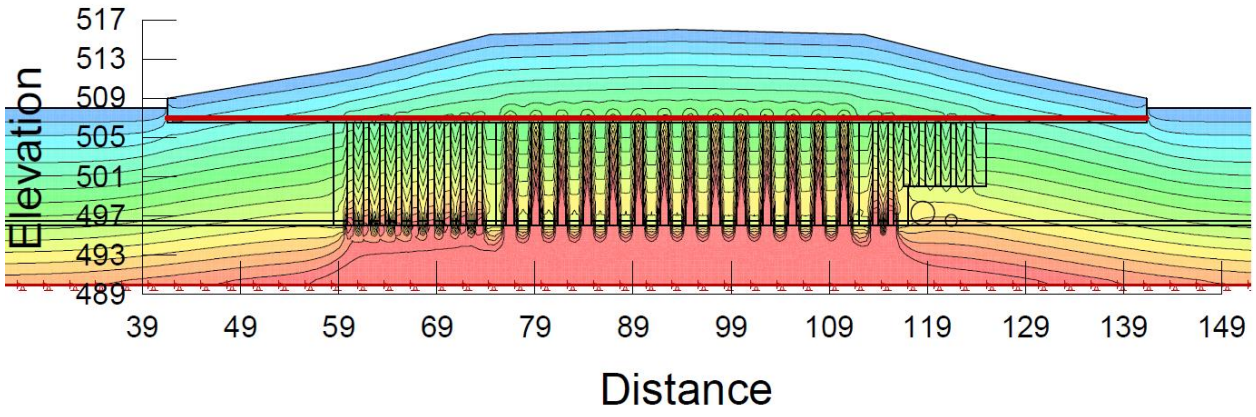

Figure A-35 – FEM North Abutment Cross-Section Model Y-Effective Stress Contour

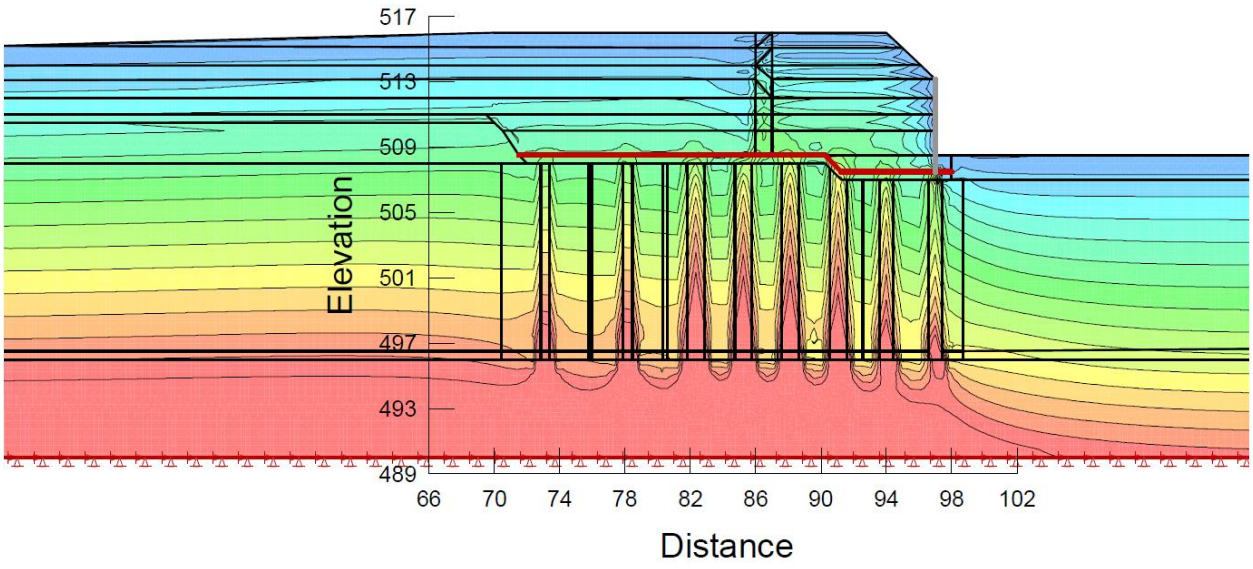

Figure A-36 – North Abutment Profile Model Y-Effective Stress Contour

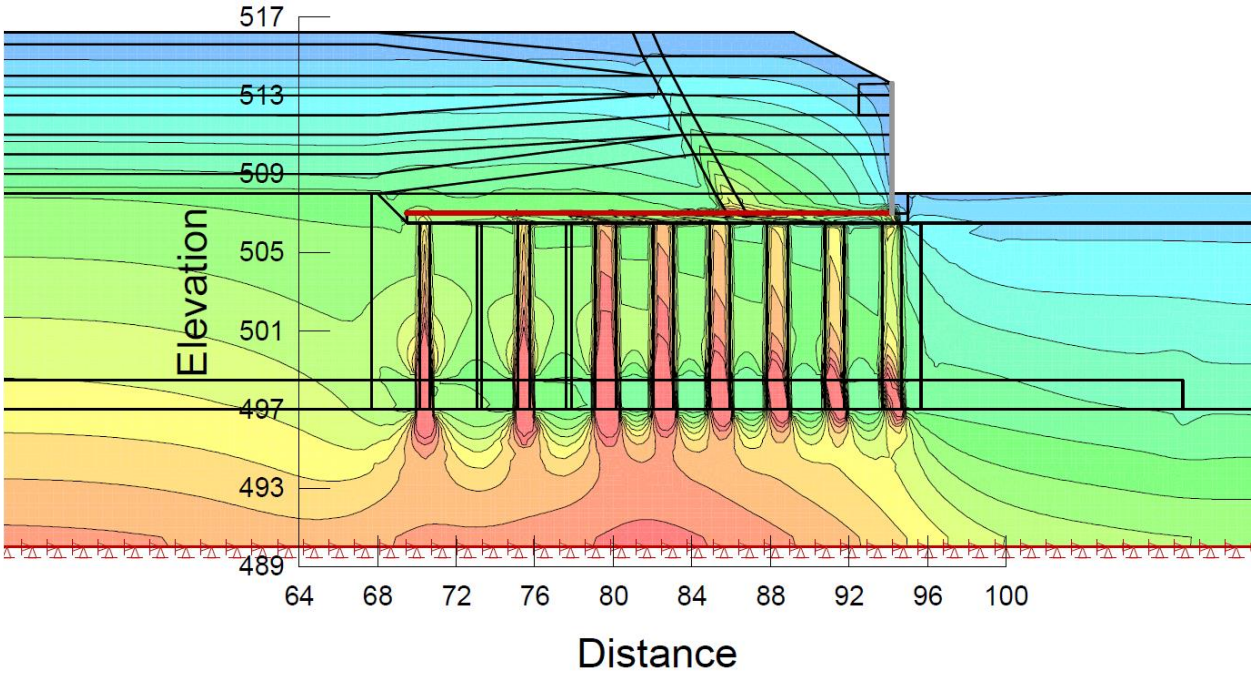

Figure A-37 – FEM South Abutment Profile Model Y-Effective Stress Contour

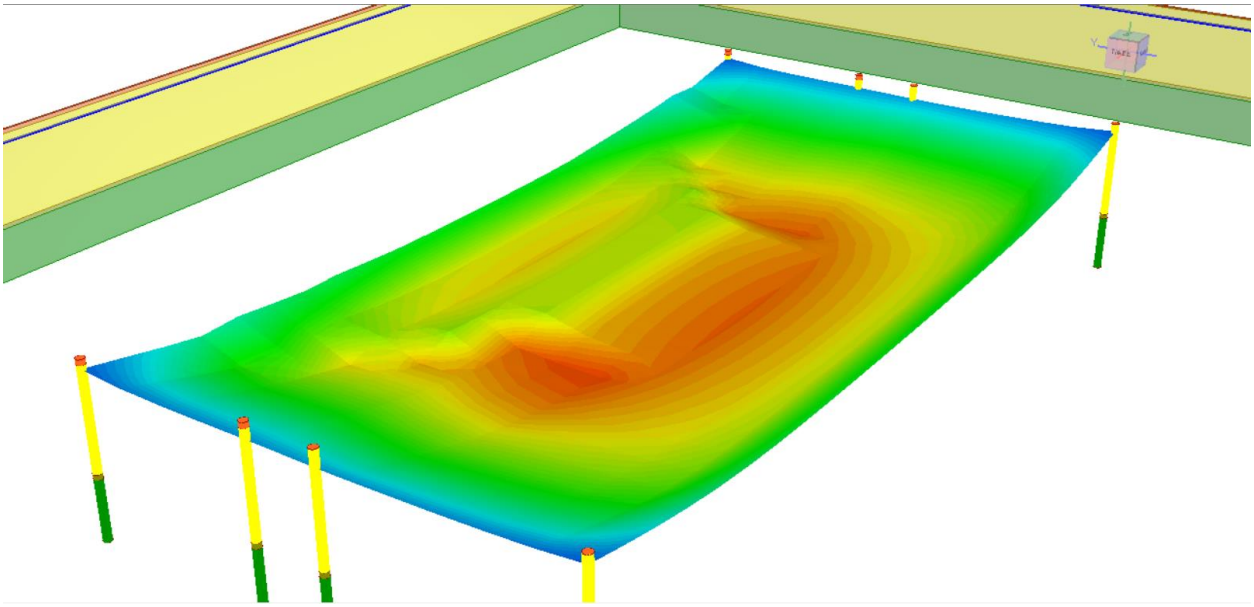

Figure A-38 – 1D Consolidation North Abutment 3D Deformed Grid Settlement Contour

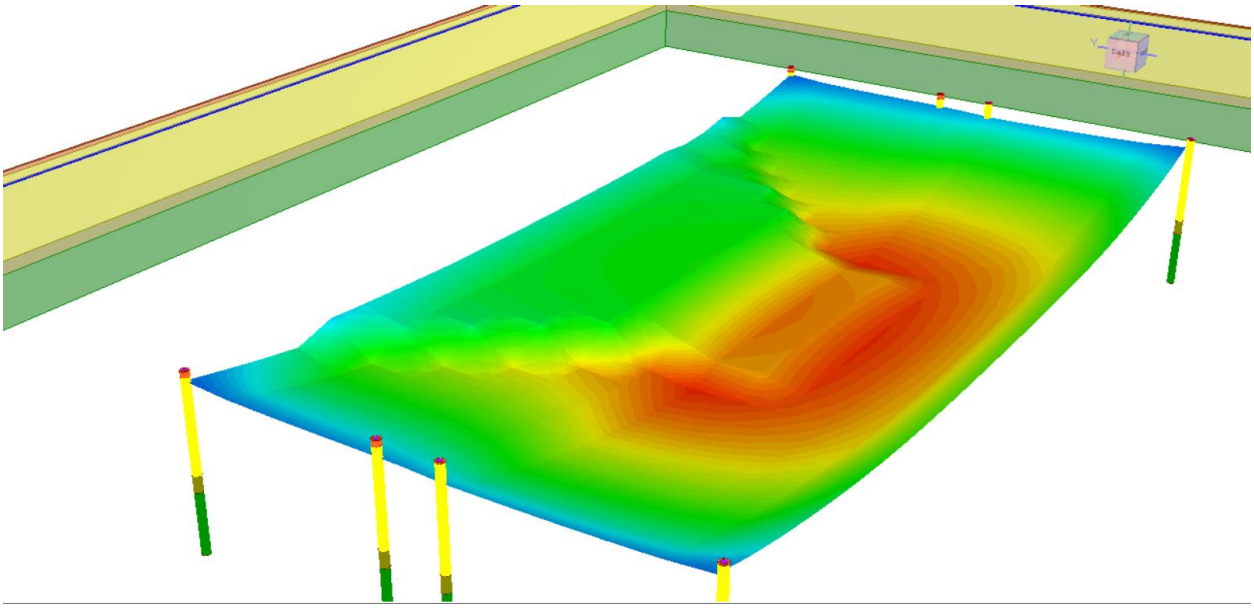

Figure A-39 – 1D Consolidation South Abutment 3D Deformed Grid Settlement Contour